Muhammad Romaan

MSCS-F16-030

BRAIN TUMOR DETECTION AND SEGMENTATION IN MRI IMAGES

SUPERVISED BY DR MUHAMMAD ASLAM

Muhammad Romaan

MSCS-F16-030

SUPERIOR UNIVERSITY LAHORE

Contents

Chapter # 01 Introduction

1 Introduction

The Central Brain Tumor Registry of the America (CB- TRUS), brain tumor is only a single leading reasons of cancer of brain related problems in the peoples of United States. It is the also a reason of cancer linked deceases or life losses in children of age below 20 years as well as in males of population years 21-40, leukemia is the first for individually. Each year, an valued number of novel brain tumor deceases analysis in the America is round 80,000 total peoples that counting non-malignant (55,000) and malignant (25,000) and with an assessed amount of deaths 15,000 due to the malignant brain tumors deceases, and 4,200 new analysis in kids in USA, where further half of these kids are in younger children than 14. The occurrence rate for all main brain tumor deceases and CNS or secondary tumors is 321.8 (71.9 for malignant and 777.3 for non-malignant) per one lack people in USA. The normal annual death rate in the America was 79,769 credited to primary malignant brain decease and Central Nervous System tumors among 2008 and 2012 in human body. If four year old existence of decease after malignant brain tumor diagnosis in a human reductions with age with 59.5% for grownups between 21 and 40 and 41.1% for grownups among 55 and 64. These figures comprise only primary brain tumors in a human body, those that starts and tent to stays in the humn brain.

The sever mutual primary brain tumor in a human is meningioma with 44%, but glioma, a long time with brain tumors starting from the gluey or good helpful tissue of the human brain (can cover 35% of all brain tumors in a body), signifies 60% of sever malignant brain tumors making it the greatest shared primary brain tumor reason of death in peoples. The maximum common in public and aggressive gliomas tumor is glioblastoma multiform (GBM) which is representing 64% of completely all the gliomas tumor. This kind of tumor is damage brain by fast infiltrative growth in health tissues and very meager or low rate of prognosis (prediction of recovery from this illness) with one year normal time period and existence time after this detailed analysis [16]. The presence of tumor, from long time is damaged or affected by widespread dangerous action such as chemotherapy and radiotherapy or both and clinical resection operations. The identification work is mainly dedicated task in medical domain on the automatic processing of different techniques or software with the greatest mutual malignant brain tumor glioma in its low and high marks. In genral public scientific routines, the assessment of learnt images or training of images is currently achieved by manually or based on measureable of standards or dealings such as the main noticeable MRI image width in axial slice [32]. So, this is a highly correct approached which is able to automatically examine scans of brain tumor in a human brain would have a huge possible for analysis the detail and therapy preparation for it. Though, it was revealed by Menze et al. [80] that the manual explanation is done by skilful raters presented important disparities in parts of tumor where strength of gradients between the cancerous structures of brain and close tissues of brain are smooth or covered by bias field objects in it or the partial volume result is obtained. Furthermore, human brain tumor injuries are only defined by the relative strength or variations to brain healthy tissues, and their figure, size and place are individual for each tumor patient, which can makes the use of simple common design of acknowledgement algorithms.
Due to the collective amount of more patients, the quantity of acquired is data very large enough. Hence, there is a growing need of automatic algorithms that are obtained the processed data robotically, which is the main and key inspiration for this advance work.

Imaging processing techniques are extensively used in medical field to detect abnormalities in human brain for tumors. In computer aided diagnose the magnetic resonance imaging (MRI) is actively developing technique in DIP and playing a very vital role in medical diagnostic domain. Manual examination of these brain MRI images one of the very difficult and time taking job because large amount of image slices assessment is labor intensive task and slight

details are tedious to recognize by naked eye [10]. To avoid complexity and postponement, automation of detection the tumor and then classification of it is a challenging task to do. In this paper we proposing the techniques by which detection and classification of brain tumor will automate and easy. The MRI image is deals with the detection of brain tumor in it and its classification information. It is a very complex and based on variants of methods so we face a challenge of accuracy robustness and optimization as well which is need some better results as well. Our proposed modal consist of segmentation, detection of tumor and its classification.

1.2 What is tumor?

Tumor [1] is an uneven bulk which may found inside or on the brain anatomy. Two unlike words are used to represent for this abnormal and irregular part in the human brain.

- Tumor
- Cancer

Cancer and tumor does not have the similar features. Tumor is a hard and stiff or liquid filled bulk of irregular tissues of brain. Brain tumor is also named as neoplasm in biology. Tumor can be categorized into primary brain tumor and secondary brain tumor neoplasm [2]. Commonly primary tumor is found and maintained by nervous tissue structure to develop in it, and tumor's development is very slow in brain. This kind of tumor in brain depends the cell types which is linked to brain system as well. Common cells are called gliomas and glias cells of nerves system are the building block of brain.

Cancer is a very quick and fast uncontainable development of irregular brain tissues which harms the nearby healthy tissues of human brain. Tumor is categorized into Benign [3] holds non-cancerous bio cell or brain cell property, Malignant [4] holds cancerous brain cells property and pre-Malignant [5] holds pre-cancerous brain cells property.
.
Secondary neoplasm or brain tumor is consist of cells which belong to the various and belongs others parts of the human body like lungs, kidney, liver etc. It can be spread rapidly from one part to another. In other words, it can be believed that cancer brain cells are the reason of secondary brain neoplasm which is true. So, it is decided that every brain tumor cell is not cancer but every cancers brain cells are tumor or neoplasm of brain. Tumor can be categorized on the basis of different criteria as shown below:

- Tumor location in skull
- Tumor location in brain
- Location in compartment

Other than this criteria, brain neoplasm is also characterized on the basis of brain cells type which create the brain tumor in it like

- Tumor consist of neuron cells
- Tumor consist of glila cells
- Tumor consist of germs cell
- Tumor consist of meninges

Pathology base classification of brain cells is given below

- Malignant
- Benign

Diagnostic techniques to detection of brain tumor in human brain. Rapid and on spot diagnosis of tumor assist in treatment process to doctors for life saving of patients. Various methods are used for the diagnosis the human brain tumor or neoplasm and reason and damage of that disease like biopsy of brain and brain digital image processing scheme.

Biopsy of brain is a classic technique in which a long needle type metallic rod is drilled in the human skull to break it and we want to take a small part of damaged cancerous tissue sample and part of tumor is removed to study the origin of tumor type of tumor and chemeistry of tumor and source of tumor, kind of tumor, its structure and reason of tumor presence under the microscope in molecular pathology department. [7].
This procedure is very dangerous and risky for human life. Digital Imaging technique is also used during the biopsy is taking place to find the tumor position in the complex brain and to get the small part of damaged tissue for study purposes.

There are lot of digital imaging techniques are used to acquire the images of human brain anatomy so that brain tumor or brain neoplasm can be diagnosed with its shape, location, volume and size of tumor like x-rays, CT scan and MRI [8]. Computed tomography or CT scan [10] is significant digital imaging system in the field of medical domain and deliver all information of brain location type shape size in instants and generally the duration reduces to the fraction of it. It helps us about giving more detailed and pure information and data as X-rays provides us but the dangerous due to radiation exposure of patient and doctor or technical operating staff is very little.

PET is a positron emission tomography in which galodium injection is injected to patient that is a radioactive substance which is vaccinated in the human blood vain and a PET scanner identifies this substantial radioactive radiation material to get the digital image. This method gives a detailed and complete comprehensive knowledge of brain's action of working and its role in body. This method is use the price effective cheap but dangerous to health of patient radioactive material is used.

X-rays is a digital imaging system which does not give the comprehensive data or information about the human brain healthy or damaged tissues. X-rays can cause human naked skin cancer if it used many times on the same human body place and same place or part of body like skeletons x ray or brain x rays. But this machine is cheap to install and its procedure is less expensive than other technologies of digital image and easy to use. MRI magnetic resonance imaging is another system which uses to penetrate the radio frequency signals in a human body to catch the digital detailed image information of human brain anatomy. This digital imaging method is our main concentrating technique in this paper.

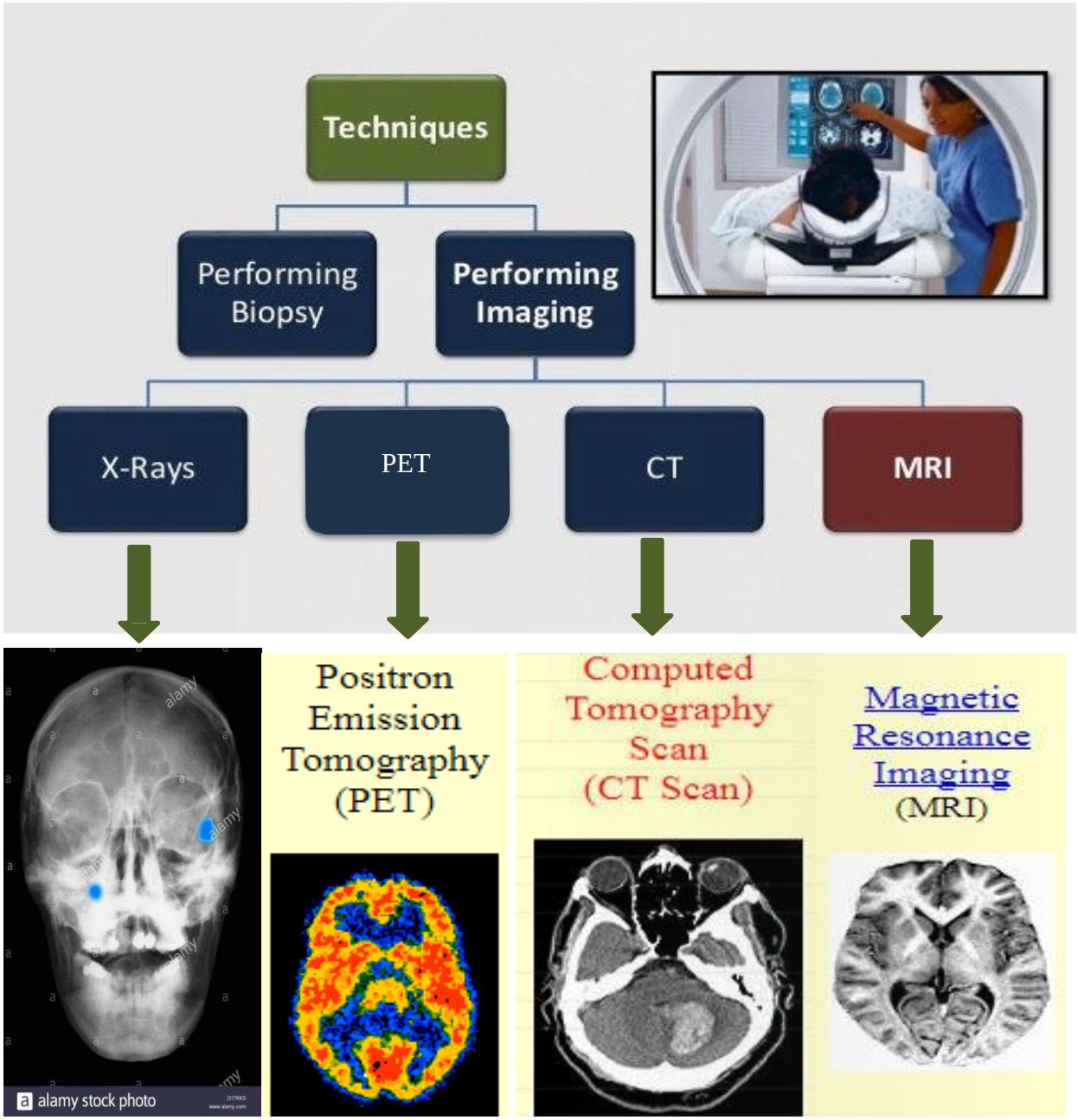

FIGURE 1 Various technique of human Brain tumor digital imaging.

1.2.1 MRI digital Image characteristics

MRI is a digital imaging system [9] which is more beneficial and detailed than then X-ray or even any other imaging systems is present as well. MRI images do not used damaging radioactive radiations or any kind of x rays and deliver the fair complete information and data about disease or tumor in a brain identification first and then assessment making for the doctors team. MRI digital image Images are used in both pre and post processing of human brain tumor identification and diagnosis [10]. Various types of multiple MRI are used in this way according to the necessity of scanning part of human or patient. Kinds of sequences used in MRI digital image provided as an input to in the pre-processing steps like T1W images, T2W images and FLAIR images. To know the working principle concept of unlike types of MRI digital images, it is very essential to clear the concept of the time of backed echo (TE) and time of repetition of signal (TR). TE is the (time of echo) time is changed between the sending of RF pulse or signal and the getting of echo signal back to us and notice the delay. TR is (repetition time) the response time between two or more constant signal pulses applied in a same sequence.

T1-weighted images [11]: contain black or dark appearance of Cerebrospinal fluid (CSF) and fluid like liquid. Gray matter (GM) is blacker or gray than white matter (WM). T1 provides good outcome in the case of human brain structure digital images and white fat appears bright or white enough in this type of matter. TR and TE time (TR 400msec, TE 24msec) is short to provide the complete images (it uses longitudinal relaxation type).
T2-weighted images intensity [12]: which contain advanced and powerful signal pulse intensity of CSF and fluid as relate to normal brain tissue and for that purpose it looks like bright. T2 used for long time signal repetition (TE 40msec, TR 5000msec) for TR and TE to provide comprehensive images (traverse relaxation). T2 is brighter for liquid or water or blood and fluid, perfect for the oedema damaged tissue due to brain hemorrhage.

FLAIR [13] is just superficially looks like to T2w images but it has tempered CSF fluid anomalies remain bright in this FLAIR image as well. It is very good for digital imaging the cerebral oedema damaged tissues due to bleeding. It uses very long TR and TE time (TR 8500msec, TE 214msec) for creating complete images.

1.2.2 Symbols of Brain structure

Three dimensional 3D alive structure or hemisphere of the human brain is used so that any single point location inside the brain anatomy or on human brain can be contained on multiple three "axes" or "planes" - the x, y and z axes or planes as we need to express 3 dimensions to present three dimensional structure. The brain is sometime needs imaged on two-dimensional (2D) images or also called slices which is analyzed for find the details of decease.

1.2.3 Human Brain Cells

With respect of biology science, the human body is consist of all organic material and cell is a fundamental structural unit part in a human body. There are approximately total one hundred trillion total body cells in a human body. As we know that new cells are formed after the division of old cells into two parts repeatedly. These newly born or divided cells are make sure human body health. A brain tumor or intracranial neoplasm arise if these cells grow abnormally and not divide to form new cells, hence it becomes tumor after sometime [4] [2].

1.2.4 Malignant Brain Tumor or benign tumor

There are two types of human brain tumor in general, malignant and benign. Malignant tumors are contains cancerous brain cells type and very damaging to individual patients. These tumor are abnormal in its size and growth with undefined boundaries. It is normally spread or penetrate the other parts of human body like normal healthy tissues in brain or other parts of body. On the other side benign tumor are non-progressive or not contains cancerous cells of brain and comparatively less damaging but still damaging. These tumors are normal in size and its expansion and regular shape. These are less aggressive and do not commonly attack the other organs of body like healthy tissues or other parts like lungs liver etc because they are originate in brain and grow with slow growth rate inside the human brain. A benign tumor can become malignant tumor after long time if no cure is been done and low grade tumor can turn to high grade tumor later some time. Hence intensity of decease increase. For proper and exact treatment we need to know about accurate grade of tumor and type information and detailed data to study and analyze.
[3][4][5][6][7] [mayfieldclinic.com][nbts][abta].

1.2.5 Brain tumor Classification (primary and secondary)

Classification of brain tumor is further based on the origin of tumor as well that means from where it is came here in brain. If tumor starts somewhere within the brain and grow within it then it is a primary brain tumor because it does not goes outside the brain and flourished inside the human brain. In this class source of cells of tumor belongs to brain itself or some part of brain. But if tumor stars in body other than brain like tumor starts in lungs or kidney or liver and then grow though spinal cord to brain and finally reaches in brain then it is called secondary brain tumor. The source of tumor cells in this class is other part of body for example cell type can be matched with lungs or kidney where it originate. There are metastatic tumors and most commonly found in humans of tumor patients [4] [6] [7] [8] [mayfieldclinic.com] [nbts] [abta].

1.2.6 Grades of Brain Tumors

Depends on face appearance, size and growth world health organization (WHO) developed grade system framework in 2016 for tumors treatment and diagnostic planning. In fact grade shows the cancer level or cancer percentage found in tumor. These stages of brain tumor provide doctors information about growth rate of tumor inside brain of patients. At grade 1 and 2 the growth rate is slow then the rate at grade 3 and 4 and tumor appear nearly normal and slightly normal respectively. Low grades represents the least malignancy level and less cells of brain are malignant with high survival rate. Whereas grade 3 and 4 represents appearance abnormal and most abnormal with active and quick growth rate as compare to grade 1 and 2 correspondingly. High grades shows the low life survival rates and high level of malignancy.[9][2][mayfieldclinic.com] [nbts][abta].

1.2.7 Importance of awareness

Brain tumor is a dangerous decease and a big reason of increasing death rate of less age rate in peoples all over the world. American Brain tumor association (ABTA) claims every year approximately 66,000 cases was registered in USA in the end of 2014. So accurately and timely diagnose of this brain cancer or brain tumor disease is very important for the accurate treatment plan [abta][17]

1.3 Diagnose techniques for Brain Tumor Detection

We can use Magnetic Resonance Imaging (MRI) for diagnostic purposes in different human anatomies for example brain, liver, heart, kidney, prostate, breasts, injuries, and their functionalities. Modalities that are used for imaging are x-rays, ultrasonography, computed tomography (CT-scan), magnetoencephalography (MEG), electroencephalography (EEG), positron emission tomography (PET), Single-Photon Emission Computed Tomography (SPECT), and magnetic resonance imaging (MRI). MRI sequence are T1w, T1 with post contrast, T2w, PDW, FLAIR MRGAD. MRI orientation can be axial, coronal and sagittal are useful for brain tumor detection [14][13][16].

1.3.1 Magnetic Resonance imaging (MRI)

Detection of human brain tumor and its grade and type from MRI image and is a challenge because every tumor is differ with respect to its size growth area and location. For this different imaging techniques can be use but MRI is more frequently used because it is noninvasive medical examination and its best digital resolution and it can differentiate between soft tissues

of brain and hard tissues offer good contrast to distinguished. It gives ample amount of information about brain structure, functionalities and abnormalities. Moreover it does not use any ionizing or radioactive radiations but use magnetic field of 1.5 to 3.5 tesla and radio waves. A strong Magnetic field is used for a vector measurement the details. Radio frequency use for hydrogen atoms nucleus which is present in plain water molecules of patient's body brain. Even functionality of human brain is also explored by the radiologists by using MRI digital images [11][12][13][15].

1.3.2 MRI sequences

Magnetic Resonance Imaging (MRI) is usually used for brain tumor identification and examination and study. A variety of MRI sequences happens, where each of sequence is them is appropriate for dissimilar imaging firmness. Today, it is a mutual and combined exercise in automatic examination and identification to use a mixture of numerous MRI sequences to achieve extra high definition appreciated and precise accurate and precise results. In this paper, three dissimilar MRI sequences, namely T1 weighted MRI image, T2 weighted MRI image, and FLAIR MRI image, are used and they will be considered rapidly as defined in [4].

1.3.3 T1-weighted MRI image

In MRI, T1w MRI mentions to the time that protons within a healthy brain tissue essential to return to the first magnetization state in machine, which is given by the static magnetic field of 1.5 to 3.5 tesla. Simple T1-weighted images (presently T1 images) offer better functional facts accurately than T2-weighted MRI images but they typically do not bring motivating information or data when brain tumor is examined and identified. Yet, they are used in a mixture with difference agent liquid there are different types, which is vaccinated into patient's vascular system it is also called galodium injection. The difference agent highlights the blood color or for movement movement in T1-weighted MRI images. This reason the tumor active and prominent part to draw good MRI image, as well as pots, to look hyper intense and effortlessly distinguishable from nearby health tissues and damaged tissues and veins. The occurrence of the lively tumor or bad tissues is frequently used during the tumor malignancy study it is very important thing. Such images are called contrast improved T1-weighted MRI images and in this work the shortening T1C will be recycled.

1.3.4 T2-weighted image

T2w images refers to the time that protons disturbed into clear alternation by radiofrequency signal pulse need to lose this consistency inside tumor brain. T2-weighted images (presently T2 images) are, associated to T1c images, more delicate to the contented of plain water and, therefore, to the pathology, which, as well as cerebrospinal fluid (CSF), seems in different and prominent way now.

1.3.5 FLAIR image.

Fluid-attenuated inversion recovery (FLAIR) is a sequence that is capable to overpower fluids and it is used to overpower CSF fluids in brain MRI imaging. This consequence allows to differentiate contact, which remains the hyper-intense as in T2w MRI images, from CSF fluids which converts hypo-intense here. For that motive, it is usually used in the brain tumor imaging MRI.

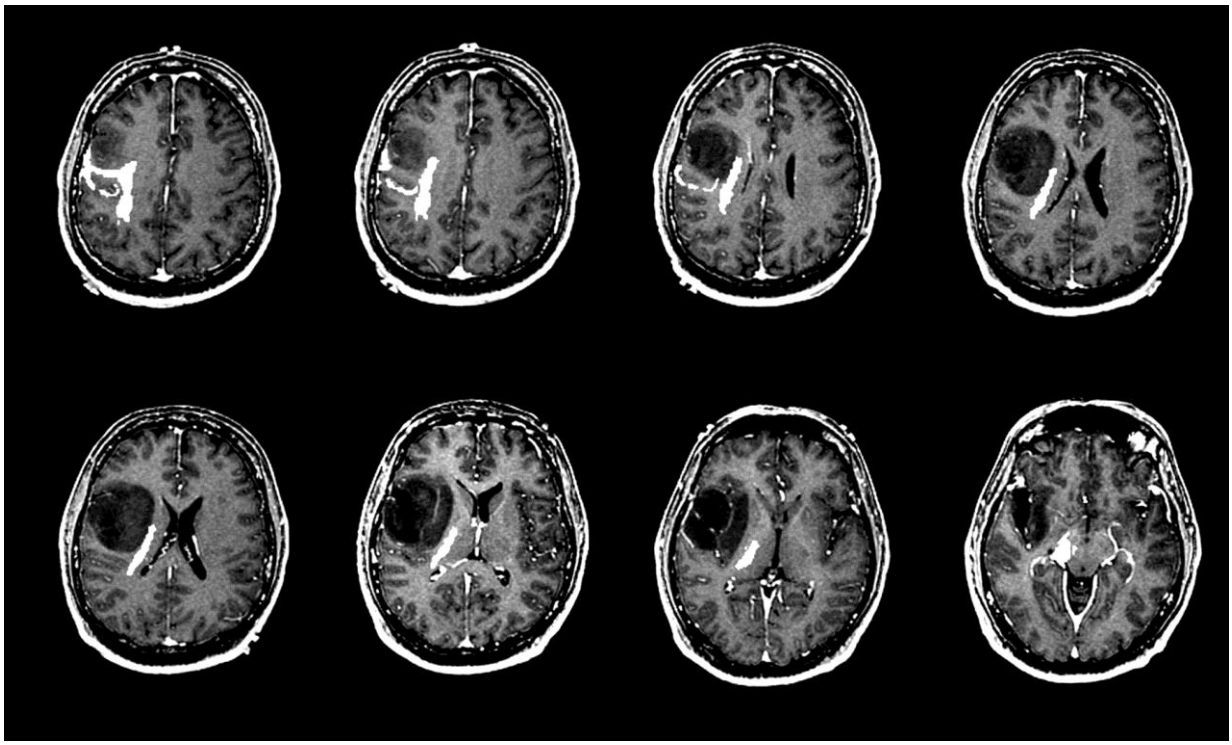

Figure 2 different MRI images of T1w, T2w and FLAIR images with tumor found is portrayed in

1.4 Deep Learning techniques

Deep neural network DNN is a multi-layered architecture which is contains some input layers, output layer and layers exactly between them. These middle layers are actually hidden layers and more than two layers can be exist there which allow nonlinear and complex relationship between input and output. It is used specifically in regression, classification and improved accuracy in different purpose. Training method of DNN is not a difficult task because mistakes are often and they are addressed by propagate back to the back layers and hence these big mistakes become very little. In DNN technique all Learning process is a very time taking and slow procedure.

Our contribution is use of deep neural network for classification of MRI brain tumors in images. The proposed methodology is classify the human brain tumors MRI images are used as glioblastoma, gliomas, and meningiomas types.[18][19].

1.5 Related work

Ghulam Gilanie et.al. [9] Proposed a methodology of classification of brain MRI image slice. Their modal consist of preprocessing of input image, feature extraction and classification. They use support vector machine (SVM) supervised for classification. For preprocessing local histogram equalization and Gaussian filter is used and for feature extraction they use Gabor texture descriptor. To evaluate proposed algorithm ROC, specificity, sensitivity, Accuracy is used as quantitative measure.

Heba Mohsen et.al. [00] use deep neural network (DNN) from deep learning architecture for 66 brain MRI dataset classification into 4 categories. These categories are metastatic bronchogenic carcinoma tumor, glioblastoma tumor, sarcoma tumor and normal brain. They use classifier with discrete wavelet transform (DWT) to extract features in more powerful way and reduce dimensionality by principle component analysis.

Saurabh shah et.al. [00] propose two techniques which are computationally excellent for classification of MRI images into normal and abnormal class. In first approach Gabor filters are used for feature extraction and classification is performed by the support vector machine (SVM). In second approach novel histogram comparison is used. In this method Gabor filters is used for texture feature extraction from region of interest and artificial neural network (ANN) is used for image classification. This paper provide a comparison between two approaches.

Prabin et.al. [5] Proposed a system based on Adaboost classifier to identify brain tumor in Magnetic Resonance images. They used the Adaboost classifier for classification while wavelet transform for feature extraction. Their outcomes show that the Adaboost classifiers accuracy rate of is better than Feed forward neural network (FFNN) and radial basis function (RBF) which are related prominent brain tumor classification methods. The dimensionality reduction is done by PCA method.

Ms. Suchita Goswami et.al. [2] Recommended a system constructed on unsupervised learning based Neural Network (ULNN) for detection of brain tumor. For classification they used SOM and for feature extraction they used independent component analysis (ICA). For the segmentation k- means clustering algorithm is used to slice the brain into dissimilar tissue. They achieved accuracy of 97.6 % as their results shown in paper by using this method.

Trinadh babu et.al. [7] Proposed a neural network based Adaboost algorithm based system to identify a tumor in brain Magnetic Resonance Imaging. They proposed an improved Adaboost procedure for patient self-reliant tumor clustering scheme. The BRATS2012 dataset is used as database. The outcome shows that their segmented results are more insistent and on normal performs for the patients.

Walaa Hussein Ibrahim et.al [3] this paper is proposed neural network to classify MRI images. They used the techniques to reduce the data dimensionality by using (Principle component analysis (PCA). They used train CIPR dataset with 3x58 images are used for training and analysis the algorithm. The accuracy of classification that they have got was 96.33%.

Sahar Ghanavati et.al. [6] Proposed an Adaboost classifier based method to spot brain tumors in Magnetic Resonance images. They used a contrast gadolinium dyer for image modalities. For classification feature such as distortion, concentration, contour, proportion and texture feature were used. Testing and training accomplish on the multimodal Magnetic Resonance images. The outcome shows that system performs well with accuracy 90.11%.

Dipali Joshi et.al. [4] Perform classification of brain cancer by using artificial neural network system. The GLCM is used for feature extraction. For preprocessing they use image histogram enhancement its image processing technique, and morphological operation are used for feature extraction. The classification of brain tumor into various classes by using Neuro fuzzy classifier. Their consequences illustration that their method is capable enough to classify dissimilar brain tumor.

Komal Sharma et.al. [1] This paper shows how the machine learning (ML) algorithm is valuable in spotting tumor in magnetic resonance imaging (MRI). Their outcome shows 98.6% when Naïve Bayes is used, and 97.6% classification rate when Multilayer Perceptron (MLP) is used. For feature extraction they used GLCM and for texture feature such as homogeneity, correlation, contrast, energy is used to detect tumor characteristics.

MRI image segmentation and classification for the detection of intracranial neoplasm and detection the type of intracranial neoplasm which are 120 from latest medical tests, imaging techniques is playing a vital role for determining accurate treatment at the that time. There are different techniques have been proposed for the MRI image segmentation and classification to detect tumor and type in image slice, for example, artificial neural network (ANN), support vector machine (SVM), fuzzy clustering means (FCM), expectation-maximization algorithm technique (EMAT) and knowledge-based techniques, and some popular techniques are also available for example region based segmentation techniques (RBS) it can abstract the significant data from the medical images. There are findings of some of the current and noticeable researches are written here.

Damodharan and Raghavan [10] have proposed artificial neural network (ANN) dependent method for intracranial neoplasm classification and detection. In proposed method, the rate of quality is formed distinctly for segmentation of Cerebrospinal fluid (CSF), White Matter (WM), Gray Matter (GM), and the region of neoplasm and paper claims 83 percent accuracy by artificial neural network based classifier.

Alfonse and Salem [11] have shown a technique for automatic classification of intracranial neoplasm by support vector machine (SVM) classifier on MRI images. Study reveals to increase the accuracy of the SVM-based classifier, MRI image features are extracted with the help of fast Fourier transform (FFT) and decrease of image features with the help of Minimal-Redundancy-Maximal-Relevance (MRMR) technique. This method has got 98.9 percent of accuracy.

Zanaty [14] presented a methodology for intracranial neoplasm hybrid segmentation, combining Jaccard similarity coefficient algorithm (JSCA), Fuzzy C-means (FCM) and seed region growing (SRG), for gray matter and white matter segmented measurement of tissues from MRI images. This technique obtained a score of 91% for average segmentation at 3% and 9% of the noise level respectively.

Kong et al. [7] probed the brain tissues segmentation automatically from MRI images by using the discriminative clustering and future selection approach.

Demirhan et al. [5] proposed a new segmentation algorithm for tissues identification using wavelets and artificial neural networks, which claims actual segmentation of brain MRI images into the neoplasm, White Matter, Gray Matter, edema, and Cerebrospinal fluid.

Torheim et al. [15], Guo et al. [1], and Yao et al. [16] shown a method which is working for wavelet transform, texture features and Support Vector Machine's algorithm for better classification of active contrast-enhanced MRI images, to grip the nonlinearity of actual data and to address various image protocols successfully.

Torheim et al. [15] also present that their proposed method gives better clinical issues and efficient predictions, neoplasm volume, and neoplasm stage in assessment with first-order statistical features.

Kumar and Vijayakumar [17] proposed intracranial neoplasm classification and segmentation by using radial basis function (RBF), principal component analysis (PCA) and kernel based Support Vector Machine and claims 94.20% similarity index of overlap, 98% of fraction and an 0.035% extra fraction. The accuracy of classification to detect neoplasm type of this method is 94% with over-all errors noticed of 9.5%.

Sharma et al. [18] have proposed a highly effective technique which claims 100% of accuracy in the classification of intracranial neoplasm from MRI images. This method is exploiting the artificial neural network (ANN) with texture-primitive features as classifier tool and segmentation.

Cui et al. [19] introduce a local fuzzy clustering with spatial information to make an objective of medical MRI image segmentation and bias field assessment for brain MRI images. In this method, Jaccard similarity index is used as a measurement of the segmentation correctness and claim the accuracy of 82% to 97% to segment Gray matter, White matter, and cerebrospinal fluid.

Wang et al. [20] have proposed a medical MRI image segmentation method based on active contour model to handle the difficulty of concentration inhomogeneity's in MRI image segmentation.

Chaddad [21] has presented a method of automatic feature extraction for intracranial neoplasm finding depends on Gaussian mixture model (GMM) by using MRI images. In this technique, using wavelet based features (WBF) and principal component analysis (PCA) the performance of the Gaussian mixture model (GMM) feature extraction is improved. For the T2-W MRI image and T1-W MRI image an accuracy is 97.05% and 94.11% for FLAIR-W MRI images are achieved.

Deepa and Arunadevi [22] have projected a method of great learning machine for classification of intracranial neoplasm from 3D MRI images. This technique achieved the specificity of 98.8%, accuracy of 95.2%, and the sensitivity of 92.6%.

Sachdeva et al. [23] have proposed the different types of intracranial neoplasm feature extraction after segmentation, classification performed with the help of dataset contains 428 MRI images. In this technique, journalists used Artificial Neural Network and then Principal Component Analysis ANN and experiment the growth in classification accuracy from 76% to 92%.

The above literature survey has shown that some of the methods are created to find segmentation only; some of the methods are developed to achieve feature extraction and some of the methods are designed to get classification only. Feature extraction and decrease of feature vectors for active segmentation of MRI image or White Matter, Gray Matter, CSF, and infected area of brain or tumor region and analysis on collective method could not be conducted in all the published literature. Furthermore, only a limited features are takeout and consequently very low accuracy in neoplasm recognition has been found. Also, all the above literatures works are omitted with the calculation of commonality that is cube similarity index, which is one of the significant parameters to evaluate the correctness or effectiveness of any intracranial neoplasm segmentation algorithm.

In this study, we complete a blend of naturally inspired Fuzzy C-Means (FCM) and Support Vector Machine (SVM) as a classifier tool to increase diagnostic correctness. The purpose of this work is to extract information from the segmented neoplasm area and classify well and ill neoplasm tissues for a large database of MRI images. Our consequences lead to complete that the proposed method is appropriate to integrate clinical decision support systems for first diagnosis and screening by the radiologists or medical experts.

1.5.1 Thesis contribution

This work contribute the brain tumor detection and its segmentation in multisequence MR images successfully with particular focus on high- and low-grade gliomas. Three methods are successfully use for this purpose. The first method deals with the presence detection of brain tumor structures in axial and coronal slices. This method is based on multi-resolution symmetry analysis and it was tested for T1, T2, T1C and FLAIR images. The second method deals with extraction of the whole brain tumor region, including tumor core and edema, in FLAIR and T2 images and is suitable to extract the whole brain tumor region from both 2D and 3D. It also uses the symmetry analysis approach which is followed by automatic determination of the intensity threshold from the most asymmetric parts. The third method is based on local structure prediction and it is able to segment the whole tumor region as well as tumor core and active tumor. This method takes the advantage of a fact that most medical images feature a high similarity in intensities of nearby pixels and a strong correlation of intensity profiles across different image modalities.

1.6 Motivation

Automated detection and identification of tumor is extremely important task. Due to accuracy robustness and specificity it is significant for doctors in medical field. We can save time for tumor patient for his accurate diagnosis treatment. Less doctors efforts to find good results. In manual detection and identification it is a chance to mistake. But in automatic diagnostic system there is less chance. We can verify the automatic procedure with manual doctor's expertise. If manual and automatic detection results are same every time it clearly means automatic process is reliable and efficient off course. This approach leads us to automatic diagnose in other body parts abnormalities as well. We can use same method in liver, lungs and kidney abnormalities. Procedure is same as MRI scan feature extraction and then classification according to our trained dataset.

1.7 Problem statement

A model to identify the tumor which is extremely needed in computer aided diagnoses (CAD) field by using the automatic detection and segmentation procedure. There are more than 120 tumor types are identified by World Health Organization (WHO) since 2016 but in this paper we focus on three most common brain tumor identification. The common Tumor types contains Meningioma's, glioma, and brain metastatic. For identification of tumor we are using symmetry analysis of brain then feature extraction.

1.8 Objectives

Our main objective is to serve computer aided medical diagnoses in the medical field. Better diagnose system is a great help to doctors. We increase the accuracy, robustness and specificity of brain tumor detection and classification process. Our proposed modal works at the time of MRI scanning and let the doctors knows a comprehensive information about existence of tumor or not to save time of biopsy. Hence diagnose time is reduced and treatment becomes rapidly and accurate.

1.9 Proposed methodology

Our proposed method is based on, the essential pre-processing step as first step. This contains skull stripping of brain, strength normalization in MRI image, image bias field improvement

and bulk registration of image. In the next step, a fast pathology based feature recognition approach, which is based on the MRI image multi-resolution regularity analysis is done. This process is only applicable for 2-D parts of brain MRI images of together axial and coronal two image planes, where the left-right areas are usually broken in case of tumor occurrence is found in human brain MRI image. This is done by the outline of unsupervised abstraction of glioma (the most public malignant cell human brain tumor type) from 2-D and FLAIR images and T2w bulks images. This all system is based on the earlier pathology finding in 2-D MRI image slices. It uses the similar multi-resolution examination which is then can be extended into 3-D MRI brain images approach is same for that as well. This is shadowed by human brain tumor locating and following extraction from the all brain tumor slices as a complete area of image. The abstraction process is an unsupervised algorithm is used and with the help of the information of glioma appearance in FLAIR MRI human brain images in T2w pixel strengths.

In the last task of this paper, a supervised way is used for three brain tumor for segmentation sub-problems (first division of whole tumor, secondly tumor core, and lastly lively tumor) is projected. This scheme is based on an advanced Deep learning (DL) algorithm is used here, particularly Convolutional Neural Network (CNN), which is completely combined or mixed with a construction forecast framework where there is a label there is a construction in a given area is forecast instead of mutual voxel wise classification tactics are used. Pixel-wise segmentation usually hurts from some type of noisy results and needs a sophisticated post-dispensation or processing step need to be performed, for illustration, by Conditional random field (CRF). This step is eradicated or removed in the proposed algorithm thanks to the prediction of tags are used for more pixels at once based on the image data in the whole area of MRI image.
The proposed algorithm is consists of four major stages to detect and segment tumor from brain images. They prominent stages are pre-processing, feature extraction and target segmentation and post-processing. The following figure shows the scheme of the proposed methodology. The following figure 3 below, describes the details of the proposal more clearly.

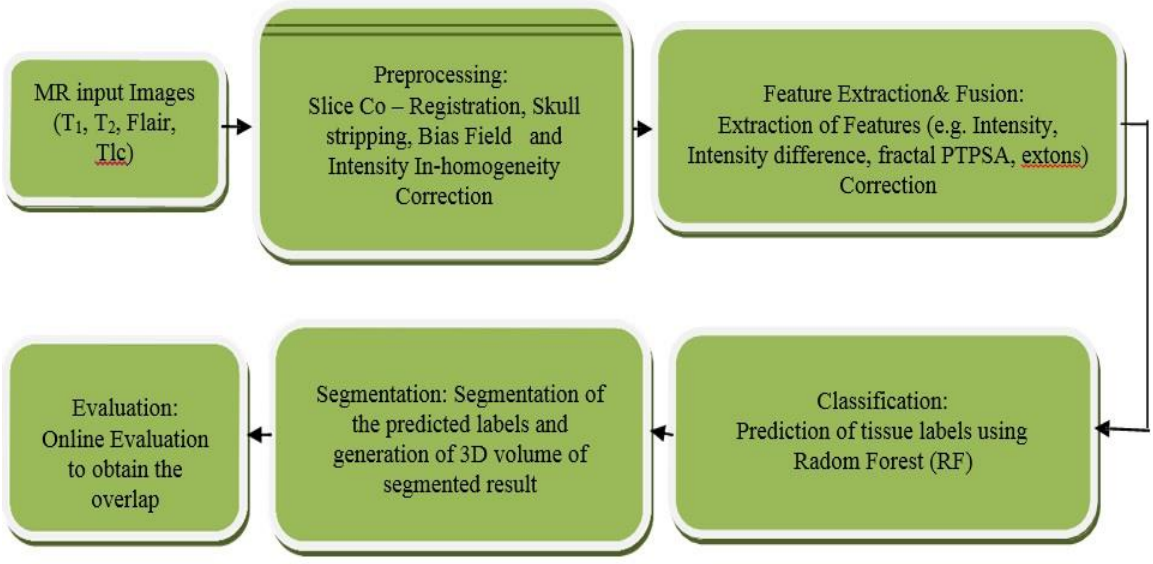

Figure 3. Schematic diagram of proposed method

The preprocessing of brain MR image is the first step in our proposed technique. The preprocessing of an image is done to reduce the noise by a 3x3 median filter and to prepare the

brain MR image for further processing. The purpose of these steps is basically to improve the image appearance and the image quality to get more surety and ease in detecting the tumor.

Feature Extraction

This feature extraction stage analyzes the objects from the input image, to extract the most prominent features that are representative of the various classes of objects. The features are used as inputs to classifiers that assign them to the class that they represent. The purpose of feature extraction is to reduce the original data by measuring certain properties, or features, that distinguish one input pattern from another pattern. The extracted feature should provide the characteristics of the input type to the classifier by considering the description of the relevant properties of the image into feature vectors. In this proposed method we are interested to extract the following features.

Shape Features - circularity, irregularity, Area, Perimeter, Shape Index

Intensity features – Mean, Variance, Standard Variance, Median Intensity, Skewness, and Kurtosis

Texture features – Contrast, Correlation, Entropy, Energy, Homogeneity, cluster shade, sum of square variance.

The efficacy of texture based tumor detection, segmentation and classification has been discussed to characterize the tumor surface variation which is expected to be different from the non-tumor region, which further increases the certainty of fine extraction.

Segmentation

After improving the brain MR image, the next step of our proposed technique is to segment the brain tumor MR image. Segmentation is done to separate the image foreground from its background. Segmenting an image also saves the processing time for further operations which has to be applied to the image.

Post processing

After segmenting the brain MR image, several post processing operations are applied on the image to clearly locate the tumor part in the brain which are given in the above flowchart. They mainly show part of the image which has the tumor, which is the part of the image having more intensity and more area. These post- processing operations include spatial Regularization, strains and Shape Constraints.

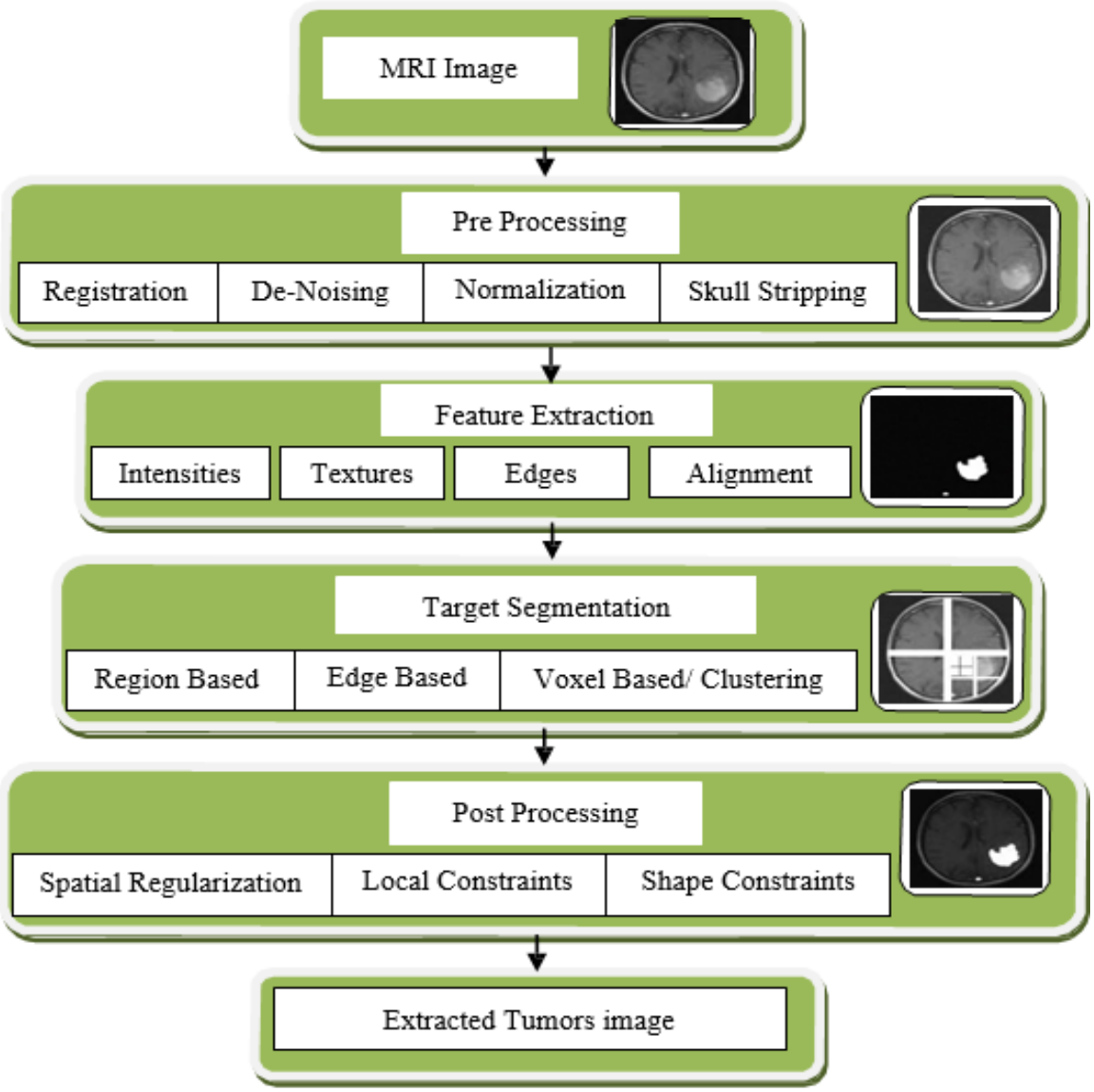

Figure 4. Flow diagram of proposed method

1.10 Structure of the thesis

This thesis is prepared in this way. Chapter one is based on the introduction which is based on comprehensive study of research work. We have mention here all literature in a short form there and introduce all the techniques and methods that are used for this tasks .Chapter 2 analyses the current associated state-of-the-art works based on dissimilar lines and defines their benefits and difficulties we had faced for classification and segmentation and then feature extraction. In Chapter 3, the state-of-the-art approaches of local structure forecast are defined in it. Chapter 4 defines the objectives of the work and the likely a small contribution to the technical research area in the digital image processing world. In Chapter 5, three anticipated policies for brain tumor discovery in the MRI image and then segmentation of MRI image are existing. This chapter also contains a brief explanation of pre-processing of MRI images. The marks of the anticipated frameworks as well as the new setup there, conversation of image and contrast setting with state- of-the-art works are designated in

1.11 General Statistics about Brain Tumor

As it is specified in a new arithmetic report which is now available by the USA' Central

Brain Tumor Registry (CBTRUS), about 29,550 patients or peoples suffering with brain tumor were afresh identified with principal benign human brain tumor decease and primary malignant brain tumors decease in 2004 [30-33]. In adding, in the year 2001 in the America only, more than 61,000 persons were alive with a primary brain tumor decease while 377,000 were active with a primary benign brain tumor decease. It should also be well-known for everyone that giving to the same report as before, the occurrence rate of primary brain tumors in a human skull, whether it is a benign brain tumor or a malignant brain tumor type, is 15 per 110,000, while at the middle age phase at analysis is 66 years [32]. In contrast to primary human brain tumors decease, secondary or metastatic neoplasm brain tumors decease [30], create in the healthy tissues inside the brain exterior the vital worried system and they create a mutual difficulty of general brain tumor or cancer decease. Brain metastases or brain tumor is not only out amount primary brain tumors decease in a human brain, but they are presently measured as the maximum recurrent intracranial tumors in a human brain now a days. Other readings show that brain metastases or brain tumors happen in a range between 20% to 40% of all cancer patients and individuals who suffering with this decease, and that more than 110,000 persons per year will grow human brain metastases in their heads which is a big thing to worry [32].

1.11.1 Reasons of Brain Tumors

Also a recognized link with the experience to vinyl chloride a chemical, there are no identified any kind of a chemical or conservational agents is found that lead to the growth of brain tumors in a human or patient [33]. While there has been some little things to worry that electromagnetic fields might excite some glial tumors part or complete tumor, but there is no strong indication to care this idea completely [34]. A predisposition to emerging a brain tumor in a patient who don't know about that could be made by a digit of inherited by his or her family, genetic conditions counting von Hippel-Lindau syndrome, neurofibromatosis, and tuberous sclerosis etc. [35].

1.11.2 Indications of Brain Tumor

The first stage early indication sign of a brain tumor in a human of any nature can be a head pain every time go with by vomiting as well. Head pain happen because malignant brain tumor masses volume tend to meaningfully increase its size first and the increase the pressure within the skull pressure within the head as we know our brain is an air tight chamber there is no space for spare, causing added symptoms such as unclear, it can be the double or even lost eye ability sight or may be visualization ability. Additional symptoms of human brain tumor can be the comprise seizures ability, feebleness or deadness of a side or part of the body or whole body, or variations in mood, thinking ability or general condition of wellbeing of a healthy human [33]. Both place and size of the brain tumor disturb and define the signs and different symptoms initiated within a human brain [36]. Frontal lobe brain tumors typically cause inside a head seizures, reduced decision powers and memory abilities, changes in human character or human mental ability and capacities, and paralysis or disturbing one side of the body complete. Parietal lobe: When a human brain tumor is situated or positioned in the parietal lobe most shared symptoms are found comprise loss of the human aptitude to write something for someone, humanly language instabilities, in case the tumor is in the left side of hemisphere of brain. And seizures. Occipital lobe in a human brain means due to the data information that the occipital lobe in a human brain is intricate with visualization ability, sightlessness ability in one specific direction and seizures are general symptoms we feel in case a brain tumor is positioned there in a brain. Temporal lobe in a human brain in maximum cases of brain tumors that happen in the temporal lobe in the brain reason no indications of tumor at all and only in the certain times they create the speech turbulences when we speak or seizures. Ependyma in a

human brain the initial sign or symptom is hydrocephaly is observed (its opening or expansion inside the human brain of the ventricles and growth of cerebrospinal fluid). Meninges in a human brain is denotes to a case that a tumor grows in the meninges cells which are found in a human brain. The indications are first time initiated by firmness power of the part of the brain being stressed due to tumor. Secondary tumors are mostly the metastatic brain tumors root are swelling (edema) that, in seizure, causes pain, nausea, and vomiting are the indications [36].

1.11.3 Types of Brain Tumor

Human brain tumors are characterized into two main clusters first is primary brain tumors that create inside the brain skull and the other type is secondary (metastatic) brain tumors that stem from malignant body cells or brain cells that have travelled from their original position like lungs, liver, kidney and have arrived into the central nervous system of brain via the blood stream or via spinal cord to brain barricade. Primary brain tumors are made up of either neuronal (brain cells) or neuroepithelial cells or neurons (backing cells) and are considered as that are called benign brain tumors like called non-cancerous or may be malignant cells cancerous [34]. The main representative of benign brain tumors cells is that they include slow-growing cells in the brain and small in shape as well in creations with well-defined borders as well. Due to the fact that these classes of human body cells resemble standard human cells when experiential under the optical microscope for pathology or other visual test, analysis can be an intricate job. It is must be prominent that benign human brain tumors establish around 41% of all primary human brain tumors. Treatment of brain tumor is very effective when the tumor is not positioned in the brain at a vital part and thus operating elimination from the brain or inside the skull can be applied on it. Another human brain tumor healing way is radioactivity treatment of brain or cancer, particularly when life threatening situations are motivated or increased due to the place of the benign brain tumor development [33].

Malicious brain tumor types actually incite life loss or threatening circumstances for the cause curing that of their destructive and offensive nature of brain tumor inside the skull and also due to the abandoned tumor irregular mass evolution that eventually after sometime origins severe dangerous problems for patients of tumor or cancer like a huge pressure to vital human brain structures. Dissimilar other types of brain tumors of malevolent tumors (lung, liver, breast etc.), brain cancers or tumor types are typically confined and rarely extent like metastasize to other body areas like lungs etc. Moreover, medical surgical elimination from brain is measured very unsafe and life risky due to the high sensitivity of nearby brain surrounding tissue. The most fetal type of malevolent primary human brain tumor is glioblastoma multiforme (grade IV astrocytomas), which accounts for around 20% of all primary brain tumors [37]. The brain tumor classes are employed in the existent inside human brain is thesis were gliomas, meningiomas and metastasis. These brain tumor groups the fact that brain metastasis happens in 21% to 41% of all in the cancer or tumor patients while meningioma’s and gliomas are the two very advanced occurrence rated types of benign human brain tumors in peoples and malignant primary brain tumors, correspondingly [31].

1.12 Gliomas Brain Tumor

A gliomas is a kind of human brain tumor that rises from glial cells that found inside the human body brain and starts in the brain or spinal cord that is connected to brain. The maximum common thing is that the gliomas brain tumor is found most of the cases in the brain [39].

1.12.1 Classification of Gliomas Tumor

Gliomas human brain tumors are mostly categorized by the cell type found in a brain, by grade which is mostly grade 1 to grade 4, and by position in the brain part.

1.12.2 Gliomas Brain Tumors and their Cell Type

This name Gliomas are called according to the precise type of cell type that is found inside the brain of human and they maximum closely looks like it. Hence, the main categories of gliomas human brain tumor are the ependymomas first that contains the ependymal cells in the brain, Astrocytoma's brain tumor type that is contains astrocytes that is part of human brain as well, oligodendroglia's contains the oligodendrocytes cell types that are also part of brain of humans and assorted gliomas, for example oligoastrocytomas, comprise cells type of human brain from dissimilar types of glia cells both are different in a brain and locations are also diffrent [39]. [11]

1.12.3 Grades of Gliomas Brain Tumors

According to their grades of human brain tumors, which is resolute by pathologic assessment of the tumor in the world health organization in 2016, gliomas can be further characterized as first category is the low-grade brain tumor gliomas are well differentiated that is really not anaplastic brain tumor these are benign human brain tumor and can be a well forecast for the patient of cancer of brain or brain tumor. The second category is the high-grade human brain tumor gliomas are undistinguishable or that can be anaplastic for sure because these are malicious human brain cancer or tumor and carry a worse prediction for human life. At this time, World Health Organization (WHO) introduced the best and comprehensive grading system for different brain tumors like astrocytoma's creates the most mutual grading system in use of doctors or medical domain [39].

1.12.4 Location of Gliomas Brain Tumors

Gliomas can be categorized in two types according to its location as they are located above or below a membrane in the human brain named as the tentorium. We must be known that the tentorium in the human brain splits the cerebrum of human brain, overhead which is upper part of brain, from the cerebellum which is the lower part of the brain in humans, below. First is the Supratentorial which is the overhead or upper part of human brain system the tentorium, in the cerebrum, typically in grownups or young boys (80%). Second is the Infratentorial which is the under the tentorium or below this inside the cerebellum in human brain, frequently in families (60%) and lastly the third is the Pontine which is the Positioned in the pons of the brainstem area in the skull or middle in the brain [39].

1.12.5 Causes of Gliomas Brain Tumor

Though hereditary disorders in Patients of cancers such as neurofibromatosis which is the type 1 and type 2 brain tumor types and tuberous sclerosis inside the human brain composite are usually acknowledged by the medical doctors to familiarize a predisposition to brain tumor growth, the exact the reasons of human brain tumor type which is the gliomas are not yet recognized by the oncologists now a days [41].

1.12.6 Symptoms of Gliomas Brain Tumor

About the tumors indications of type gliomas it is depend on which portion of the essential nervous system in the skull is exaggerated or damaged. Due to the amplified of the intracranial stress made inside the skull so the human brain tumor type gliomas can cause pains in the head of patient of cancer, nausea and vomiting, seizures, and many other symptoms that he can be faced and cranial nerve illnesses as well. A brain tumor type gliomas on the optic nerve of human brain can be a reason of the visual damage of patient, while spinal cord inside the backbone a human brain tumor type gliomas can persuade pain in head of a patient, dimness, or numbness in the extremes and many other symptoms as well. A brain tumor type gliomas do not metastasize by the flow from the brain that is damaged by brain tumor, as it can spread via the blood from blood vessels or may be through the cerebrospinal fluid and reason 'drop metastases' to the spinal string of human body or cancer patient [29]. [32].

1.12.7 Pathology of Gliomas Brain Tumor

Brain tumor type with the high grade like gliomas are highly vascular human brain tumor type and have the propensity to penetrate inside the brain or other healthy tissues of the brain. They have wide zones or areas of hypoxia and necrosis. In numerous cases of human brain tumor development inside it causes a breakdown of the blood flow inside the brain walls to effect the functionality of the brain in the neighborhood of the tumor tissues damage as well. As a regulation of matter a high grade brain tumor type gliomas nearly always grow the backbone of patient even after the whole surgical or radiotherapy ending procedure. But the low grade brain tumor type like gliomas on the other hand is raise gradually due to its less severity level and growth rate often over numerous years and lifesaving rate is very high and it can be trailed without action or no surgery is required in some case if they grow and reason indications is identified. Numerous developed which is must not be inherited in the cancer patient genetic changes have been found in human brain tumor type gliomas. TP43 is an initial genetically change mutation. TP43 is the 'guardian of the patient's genome which is the throughout patients DNA and the patients cell repetition. It makes sure that the DNA of cancer patients is derivative properly and abolishes the human cell type apoptosis. If the cancer patients DNA is changed or muted and can't be secure. When TP43 itself is changed, other changes can be the live. PTAN is an extra protein in a human body that also helps to abolish the human body those cells with unsafe changes is itself lost or changed due to this. AGFR, a development of cell in body is a factor that usually stimulates the patient's body cells to division into two parts is an enlarged and stimulates the human body cells to division too much in patient.

Together these changes in the cell lead to human body cells separating irrepressibly as a hallmark of growth of this damaged. Recently the changes in IDH1 and IDH2 genes of body were originate to be part of the device and it is related with a more promising prognosis to the patient [41]. The IDH1 and IDH2 genes are important because they are difficult in the citrate series in mitochondria. Mitochondria are very complex part in the apoptosis. Moreover, the altered glycolysis metabolism in some brain tumor cells growth leads to low oxygen which is also called hypoxia. The standard response to hypoxia in a patient body who suffers from the cancer is to arouse the growth of new plasma vessels inside the patient brain which is also called the angiogenesis. So these two genetic factors may donate to both the absence of apoptosis and vascularization of brain tumor type like gliomas.

1.12.8 Diagnosis of Gliomas Brain Tumor

The old-style or previous neurological inspection by the physician establishes the first step in the analysis on brain tumor type gliomas. During this inspection irregularities in sure

neurological purposes like eye undertaking or reflexes. This can deliver the signs about the location of the human brain tumor [47, 62]. The next step is to include the request of particular digital imaging methods and workroom tests of patients that can be notice the occurrence of a brain tumor and its type and provide data about its place inside the brain, its type, and extent of feast.

Calculated Tomography (CT) and MRI deliver the digital image data concerning the position of tumor in the brain and the extent and conformation of the malevolent growth either it is cancerous or not [43, 54]. CT scan is largely use for detecting calcification of tumor, skull lesions with the tumor, and patient may suffer from hyper severe brain hemorrhage and brain hemorrhage is less than 14 hours old. On the other hand, it is dense cuts inside the skull, edemas, and violations of nature, it can be better noticed with the MRI machine. Positron Emission Tomography PET technology and Solitary Photon Emission Tomography SPET technology are typically used for postoperative determinations about the brain tumors and its location shape as well, such as for distinguishing radiation used for the necrosis from growth repetition in the human brain [13]. This Operation is establishes the final step to comprehensive human brain tumor analytic procedure. Through surgical interference of brain operation, minute tissue in brain is example that fits to the suspected human brain tumor is removed in order to be examined under the microscope for pathology of the patient and by a histopathology's technique. Brain tumor treatment is the assessment powerfully interrelated with the histopathologist's analysis and deduction around the normal tissue model cells of body [56, 42].

1.12.9 Treatment of Gliomas Brain Tumor

Brain tumor place, its cell type and the marks of distortion in the patient brain are the issues that mainly can affect the behavior for human brain gliomas. In several cases that are registered dealing tactic combines surgery of tumor, radioactivity therapy of the brain after operation, and chemotherapy as well. The radioactivity treatment to the patients is in the form of external beam of radioactive rays or the stereotactic methodology using as the radiosurgery procedures. Spinal cord of patient tumors can be preserved by operation and radiation ways. Temozolomide is a chemotherapeutic drug or medicine that is capable to cross the blood inside the patient's brain wall efficiently cure the patient for save his life and is being used in therapy in later years. In cases of repeated high grade brain tumor type like glioblastoma in recent educations have taken the benefit of angiogenic blockers for example the bevacizumab in amalgamation or combination with conservative chemotherapy treatment and with the hopeful results as we expect [45].

The usage of oncotic viruses in treatment or gene treatment in cure using pro-drugs or medicines changing retroviruses nature and adenoviruses nature is being deliberate for the dealing of human brain tumor type for example gliomas [56, 27]. According to the outcomes of a 2010 a comprehensive analysis that likened to surgical treatment resection and operation as the initial medical treatment management is doctor's choice, there is inadequate evidence collected to make a dependable choice to doctors [49]. For the high grade brain tumor type like gliomas, a 2002 comprehensive analysis related radiotherapy treatment with radiotherapy treatment and chemotherapy treatment. It presented a small but strong improvement from using chemotherapy treatment with radiotherapy treatment [19]. For brain tumor type like glioblastoma multiform, a 2007 comprehensive analysis displayed that Temozolomide medicine is a very effective conduct for long time existing brain tumor and postponing progression as part of primary brain tumor treatment without impacting on excellence of life and with a very low occurrence chance of initial adverse proceedings in medical domain [61].[54]

1.13 Meningioma's Brain Tumor

This type of human brain tumor type meningioma's, rising from the arachnoid 'cap' cells found in a human body brain of the arachnoid villi in the meninges which is the establish the second most mutual primary human brain tumor of the essential nervous system in the human body [31]. These types of brain tumors are typically benign brain tumor in nature or kind; though, they can be malignant type of brain tumor [42].

1.13.1 Causes of Meningioma Tumor

Those people who have undergone radioactivity treatment to the scalp are additional at risk for emerging or growing meningioma's [43]. The most recurrent genetic changes an mutation in the cell involved in brain tumor type meningioma's are inactivation alterations in the gene neurofibromatosis and second human gene which is also called as merlin on chromosome 22q category. Other likely genes comprise on the MN1 [64], PTEN [65] and an unidentified human gene at 1p13 [66].

1.13.2 Symptoms of Meningioma Tumor

Minor tumors in the brain for example the tumors less than 2.0 cm are typically related findings at analysis of information without having caused indications of different symptoms of tumor. Larger tumors size or mass can reason indications of symptoms depending on the size of tumor and its position. Some of the signs of tumors include the focal seizures and progressive spastic faintness in patient's legs. Enlarged intracranial burden what finally happens with patient, but is less recurrent than in brain tumor type gliomas [77].

1.13.3 Pathology of Meningioma Tumor

The brain tumor type meningioma's rise from arachnoid cells which are found in the human body in bulk form, greatest of which are close the neighborhood tissues of the venous sinuses, and this is the site of highest occurrence for brain tumor type like meningioma creation. They are greatest often devoted to the Dura over the superior parasagittal superficial of frontal lobe and parietal parts in body, along the sphenoid ridge in body, in the olfactory grooves in body, the sylvan area found in body, superior cerebellum lengthways in the body and the flax cerebral in the patient body, cerebellopontine angle in patient body, and the spinal string in patient body. The tumor is typically gray in its color, well circumscribed in graph, and takes on the form of space it inhabits. They are typically dome shaped when draw, with the base lying on the Dura. Histologically or neuropathologicaly, the human body cells are comparatively unchanging, with a propensity to encircle one additional, starting whorls and psammoma25 forms the laminated calcific concretions in patient body. They have a propensity to harden and are highly vascularised in patient body [57].

1.13.4 Diagnosis of Meningioma Tumor

This type of brain tumor meningioma's are willingly visualized with difference CT scan images or digital MRI with gadolinium injection and arteriography test, all credited to the part that human brain tumor type meningioma's are extra additional axial plane and vascularized. CSF fluid extra protein in body is typically elevated in patient's body if lumbar puncture is tried during treatment. However this is popular in medical domain that brain tumor type

meningioma's are benign tumor type, they can have malevolent performances in patient body. Organization of brain tumor type meningioma's are founded upon the WHO organization system [28]. The cataloguing includes first one the benign brain tumor type meningioma's which is belongs to the Grade 1 category which is the 99% of the belongings. secondly the atypical brain tumor type meningioma's belongs to the Grade 2 which is the 9% of the patient cases and third one is the anaplastic brain tumor or also known as malevolent brain tumor type meningioma's which is the Grade 3 tumor according to WHO chart which is the 3% of the bags. The mean overall existence for atypical brain tumor type meningioma's according to a new retrospective appraisal of atypical brain tumor type and anaplastic brain tumor type meningioma cases was found 21.9 years vs. 38 years for anaplastic brain tumor type like meningioma's. Moreover, mean decline free existence in the brain for atypical brain tumor type meningioma's was 21.5 years vs. 37 years for anaplastic brain tumor type meningioma's [49].

1.13.5 Treatment of Meningioma Tumor

There is only human brain tumor type meningioma is minor and asymptomatic which has remark with close digital imaging study can be working. We get a reflective study on 53 brain tumor patients, it was found that 63% of brain tumor patients had zero or really any development on follow-up study and the 47% found to have brain tumor growth produced in a patient at a regular of 8 mm as per year. If follow the study and learning for a newer brain tumor patients were found that they have brain tumors in their skull that were additional likely to produce on recurrence in the digital MRI imaging, that is why results are poorer for applicant of cure. Doctor's remark is not recommended in brain tumor that are previously causing of indication of brain tumor in skull. During the treatment a close follow-up taken by the technician with digital imaging is obligatory with a comment and plan to rule out an increasing human brain tumor in the patient's skull [60]. Human brain tumor type meningioma's can typically be surgically resected by operation in a hospital with enduring cure in ICU if the tumor is insincere on the Dural superficial and easily nearby them. Tran's arterial embolization has grown a medical usual preoperative procedure in the preoperative management by the doctors in clinical treatment.

In case of attack of the adjacent bone takes residence in the brain the total elimination is nearly16 years of age is completely impossible. It depends upon the age of patient must say.age is a barrier in the treatment of Meningioma Tumor Malevolent alteration is very rare. The possibility of human brain tumor repetition in the brain again after some time or growth inside the brain after surgical resection can be appraised by the brain tumor WHO Grade and type and by the extent of hospital where neurology department is available by the Simpson Criteria has published [81, 92]. Treatment of radioactivity includes Gamma Knife technique or other technique which is known as proton ray action or third technique which is the fractionated outside beam radioactivity are used for this purpose. The first one technique which is Gamma Knife radiosurgery is working in lieu of operation in the special hospital for minor type or low grade brain tumors positioned away from dangerous structures in the brain [67]. The second technique which is the Fractionated external beam radioactivity can also be used for the primary action for operation of human brain tumors and remember these are surgically unrespectable and another fact must be remember that for those tumor patients who are impracticable for medicinal reasons. The radioactivity treatment in hospitals is often careful by the WHO described the Grade I brain tumor type meningioma's after subtotal or we can say incomplete brain tumor resections. The clinical operation in a hospital excellent to representation after the incomplete or subtotal operation resection is rather then the any controversial treatment as class 1 randomized skilful operations is on the topic [74].

Yet, both progression free existence in the skull of patients for example the stops tumor reappearance in the brain after the operation and overall existence are better by the adding of post-operative radioactivity procedure to the patient for incomplete resections operation, according to frequent retrospective educations after the tumor treatment in hospital [65]. In the case of a brain tumor grade 2 and grade 3 tumor type meningioma and current after the treatment of normal of care of patient includes post-operative surgery and the radio energy action regardless of the degree and type of medical resection operation mostly due to the proportionally advanced rate of local reappearance in the skull for these higher human brain tumor grade in brain [76].
In the hospitals existing treatments like chemotherapies are possible not actual at this time. The Antiprogestin mediators have been used in hospitals, but with mutable consequences can be face by patients [57]. New indication in the patients like hydroxyurea has the brain tumor volume to shrink unrespectable amount or repeated the brain tumor type meningiomas is being further assessed after this [38].

1.14 Brain Metastasis Brain Tumor

A brain tumor growth that has metastasized to the human brain tumor from another position or place in the patient's body establishes a brain tumor type metastasis [69]. Brain tumor type metastases are the maximum open and public reason of intracranial and mass lesions up to 55% of human brain tumor patients finally grow brain tumor type metastases throughout the time period of their disease treatment, with 88,000 to 160,000 new bags are identified in hospitals in USA each year in the USA unaided. Patients of human brain tumor suffering with cancer or tumor are luckily living more longer and longer but only when after their first treatment action than ever previously, as primary brain cancer actions cure like operation in a hospital, or radio energy treatment action and treatment via chemotherapy action have develop more active now as compare to the past few periods. Nonetheless, human brain tumor type metastases still happen in many patients in USA after months or even after years their unique cancer behavior in their body brain in USA. Brain tumor type metastases have a very poor prognosis for treatment of brain tumor patient during cure, but modern behaviors of treatment are permitting brain tumor patients to live long for months and may be occasionally lives long for years after the analysis it is found in the study [49, 71].

1.14.1 Sources of Brain Metastases Tumor

Different types of cancers like melianoma, lung cancer, breast cancer, osteoisarcoma, neuroblasitoma, skull and necktline cancer, lymphioma, genitoutinary area cancers and gastrointestenal cancers are the particularly coloractal and pancriatic tumor type carcenoma are the maximum common found in the patients of cancers and foundations of brain tumor type metastases [69, 72].

1.14.2 Symptoms of Metastatic Tumor

In the human numerous brain tumors cases the brain tumor patients have no clear cancers indications representative that their brain tumor has feast to the patient's brain. Usually the brain tumor is originate in the brain or any other part of body on a MRI scan throughout a routine trail up and call to the doctor. Brain tumor type metastases can be reason an extensive diversity of indications in the cancer infect many types of which are converted to minor and more conditions are applied on it. These brain tumor indications comprise on the vertigo and then new pains starts after all these are mostly cognitive and their character and their behavior

is vary. Augmented or manufactured intracranial load Nausea and queasiness and recall loss, Bell's palsy, paraesthias, visual variations, ataxia and seizure [36].

1.14.3 Diagnosis of Metastatic Tumor

The analysis for human brain tumor type metastases is change or mutable. It be contingent on the type of primary cancer in the patient and the age of the brain tumor must be persistent. The absenteeism or occurrence of extra cranial metastases in the cancer brain patient further its quantity of tumor type metastatic sites in the human brain. For all patients of suffering from the cancer where the average existence of brain tumor is only 2.3 months long. Still, in some brain tumor patients, like those patients who with no extra cranial brain tumor type metastases and those who are lesser or younger than 65 years old patients. Those with a solitary site of brain tumor type metastasis in their brain lone area. Prognosis for such patients is much improved with median existence rates of brain tumor inside the skull of up to 14.5 months [15].

1.14.4 Treatment of Metastatic Tumor

The brain tumor type metastases is chiefly palliative with the boxes of treatment tumors being decrease of any kind of indications and prolongation of human or patients life. Still, in some patients of brain tumor mainly newer tumor patients and they must be the healthier patients who suffering from this decease and taking violent treatment with exposed craniotomy treatment as well. The aggressive chemotherapy treatment and radio surgical intervention or radio therapies for example gamma knife radiosurgery is given to the cancer patients for its treatment. It may be before or after operation.

As we know that human brain tumor type metastases frequently consequence are very severe in cancer patients, debilitating indications in the tumor patients there is need of symptomatic care should be there and we assumed to all human brain tumor suffering patients with brain tumor type metastases. In patients with the human brain tumor type metastases needs some action that consists on mostly of number one is Corticosteroids. Corticosteroid brain treatment is very essential part for all cancers patients who suffering from the brain tumor type metastases. It stops growth of cerebral edema inside the human brain as well as giving it some other neurological brain related indications such as annoyance, cognative dysfunction, and amesis. Dexamathasone is the carticosteroid of excellent. Secondly the anticonvulsents. Anticonvulsents should be used in all of the 20 to 50% of brain tumor patients with brain tumor type metastases who has the knowledge of the appropriations, as there is a huge danger of rank epileptics and brain tumor patient's death. The phenytoin is the most usually used drug in this tumor location in the head but valporic acid medicine and other anticonvulsents could also be rummage sale [77].

The treatment of the radiotherapy theatres a very dangerous role in the conduct of human brain type metastases and it also includes the whole human brain radioactivity treatment fractionated radiotherapy treatment and the treatment of the radiosurgery. Form the decades a complete human brain tumor irradiation has been supported for patients of the human brain tumor patient with manifold lesions with each other's life expectation is only less than 6 months or becomes low Karnofsky presentation score. It does seems at least rather real thing. Though it is frequently reasons plain side belongings with the patient and counting brain tumor radioactivity leukoencephalopathy, necrosis, dementia, and head pain as a partial. Whole hair loss on patients head, nausea, head pain, and otitis media while in patients families the treatment may cause psychiatric conflicts, cerebral delay and other neuropsychietric belongings. Brain tumor patients are fortified to talk to his family or doctor about their radioactivity. Oncologists are

weigh the risks of radioactivity risks and the welfares of kinds of complete brain radioactivity therapy [74].

Brain tumor type metastases are very frequently achieved surgically in hospital with supreme surgical resection operation is shadowed by whole brain irradiation from it and bringing larger existence of tumor in it likened to whole human brain tumor radioactivity cure is completely unaided. Consequently in tumor patients with one brain tumor type metastatic brain lesion, inattentive, incomplete, or controlled systemic illness where a life expectation of patient at least 4 months, and good presentation status there [73]

Chapter # 02 Literature review

2 RELATED WORK

Our purpose of this literature work or chapter 2 is to analysis the detection algorithms which is developing for MRI image segmentation of human brain tumors MRI images and its surrounding healthy tissues which are damaged tissues around the whole brain. The full and complete automatic MRI image segmentation of human brain tumor is still a very difficult and challenging task to do. One of the main reason we can say that is the human brain tumor has random properties for example magnitude of brain tumor and its outline around the tumor or effected area and most important the position of the brain tumor inside unless and until the human brain tumor or its tumor type metastatic development in the brain in time is examined by some expert doctors and MRI digital images scanning from earlier CT or MRI scanning of patients are existing that tells about their tumor. As the independent test of tumor like CT scan or MRI scanning all of the stated properties of tumors and their types are nameless till now. Thus same approach type recognition techniques depends on such things and relations and same things and mostly recognition techniques are used for object identification from digital MRI image and extraction of features from the same image of MRI in both types of images like medical images as MRI are used and real world images cannot be employed there. Nevertheless, other information such as arrangement of the normal human brain tumor type appearance in particular MRI digital image slice can be used in the medical domain. The advantage of this technique is compared to brain tumor image MRI or CT object identification from the digital image or detection or tumor from the digital image. For example human is running in image or car on the road is travelling we can differentiate the color of image of color of object and the background color of scene is changed. There have been a very growing interest and research in increasing such algorithms development and moreover the automatic human brain tumor type image segmentation automatically job has freshly fascinated many computer vision researchers and their teams.

Due to various brain tumor types in brain and their appearance in MRI scanning digital images, most state-of-the-art approaches and methods focus on most simple brain tumor types, for example glioblastoma gliomas and metastatic tumors, or they need exact digital image training database to deal with a precise tumor type detection and recognition it in the image. Only some researchers for example Islam et al. [31], propose to train a specific algorithm for training purposes on single brain tumor type like glioblastoma and test it on another brain tumor type. But, the results were not substantial for the other type of tumor and fine on the same tumor type.

Since dissimilar human brain tumor digital image segmentation of tumor the methods depends on unlike image material found in the MRI image, the following partition will be used in this paper for discussion for example the threshold based pixel methods which is depends only on the pixel intensity difference levels between a patients or human brain tumor type gliomas MRI digital image and its surrounding healthy tissues in the located in the digital MRI image. Region based methods which hunt for linked pixels in common areas in the image of a similar grid by three dimensional area of pixel groups in a bitmap with similar goods. Contour based approaches and methods searching for edges of objects in the digital image between a human brain tumor in MRI digital image and surrounding healthy tissues or damaged tissues. Classification or clustering methods and approaches which make usage of a similar grid by three dimensional area of pixel groups in a bitmap pixel intensity difference levels and its texture features of object or image. Atlas-based approaches and method using the prior information about the damaged brain tissues and healthy brain features from MRI image. Though, we know the between pixels is not a good division and it is not always 100% accurate and pure because proposed method and approaches sometimes have the similar images in the

nature and shape more of these methods are not workable or accurate. In modern years, most state-of-the-art procedures and methods and approaches have been based on digital image classification and the image drawings.
Additional possibility is to divide the human brain tumor type MRI digital image segmentation approaches and methods according their necessities of a human computer communication. Two collections can be possible here the first is semi-automatic is possible and other one is fully automatic approach. The previous approach and technique was requires an expert contact for example seed point selection of digital image and estimated initial boundary description about the digital image. The latter of this a complete pixel or voxel cluster and fully automatic based works without any human interaction or action. However, the previous pixel or object in the image division for example according to the digital image data or information is used by particular and specific methods and approches will be used throughout this research paper.

2.1 Threshold-based Methods

Since MRI digital image pixel intensity is the modest property that is mutual with a similar grid by three dimensional area of pixel groups in a bitmap of an MRI digital image object region or area The natural and original method to perform the segmentation of MRI image is to fix a threshold value that splits a given object or brain tumor from other area may be the background area or regions with a similar grid by three dimensional area of pixel groups in a bitmap of dissimilar intensity of pixel levels. This may be stretched either by single or multi thresholding value or multi-thresholding value methods. The previous literature works shows that first object identification is based on the intensity levels of the objects in the image and the background pixel intensity. For example increasing intensity level of pixel of object part of human brain tumor central core in T1w MRI digital image. The after use of image different levels of pixels intensities of a given brain tumor object or any other object in MRI digital image lie between the intensities of another image intensities objects background, for example gray matter (GM) found in T2w MRI digital image. Alike outcome can be reached or exceed by a boxing of single or multi thresholds value.

The thresholding technique assigns certain value to every pixel in a digital image which has the value range from the 0 to t where t denotes the digit or number of thresholds value that we fixed. But the main difficulty of threshold fixed value based approaches or method is that there is no relationships between pixels intensity difference values are considered. Therefore there are many pixels intensities different levels of other objects like brain tumor in the MRI image or other thing in the image can be extracted digitally. In this case we must take care of largely in case of decreased signal-to-noise ratio is important thing. Image differences inside an image across the different scenes making part of an object which is identified in the image brighter or image object darker causes failing of such methods too.

These digital image processing process was used by Gibbas et al. [49] as an unsupervised MRI digital image object segmentation method and approach of enhancing the human brain tumor type and part in T1w digital MRI images where it was applied and physically selected regions object and area of interest in image as it can be the object in the image as we know that it is the first starting step of the digital image segmentation procedure followed by the algorithm which known as the region growing algorithm and it is defined in detail in the next chapter of this research paper. Though, the region growing method does not take into notice about the occurrence of brain tumor into the normal brain can be identified by the highlighting hyper-intense areas in such digital MRI images? Stadlbauar et al. [105] used the regular same level pixel intensity of image and in addition three times the standard deviation is used to describe to describe the pathological studied brain healthy tissue from T2w digital MRI scanned images.

Another different and unique way of MRI digital image thresholding value method and approach is dependent on local digital MRI image properties where the threshold setting value worth is determined adaptively according to the digital image MRI pixel intensity deferent levels distribution in particular MRI image area where the object is identified as brain tumor. This is very valuable for us in cases where it cannot be valued from the whole MRI digital MRI image or it has to be adapted for dissimilar parts of image separately as due to the medical image inhomogeneity is found. Such method was used by Shanatni et al. [109] for brain healthy and damaged tissue segmentation from brain MRI image.

In generally, threshold based methods behave and its working very well if the different or same color contrast between the digital image object like tumor in the digital image and its background of the image like brain or normal brain or healthy tissues is high then its performance is outstanding, but unfortunately this is not the work in case of human brain MRI digital images. Furthermore, the threshold fixed value approximation is usually very hard and needs a user interaction is must[50]. Though, we can be used as it is a first starting step of the digital image segmentation process of MRI brain tumor images.

2.2 Region-based Methods

This region based algorithms approaches for hunt the connected areas of a similar objects grid by 3D three dimensional area of digital image pixels group cluster in a bitmap with similar properties based on a predefined manual or may be automatically similarity standard. The most well-known designed algorithms from this subject are the area growing technique and method of watershed. The basic MRI image segmentation procedures are revealed in the next two subsections of this chapter they have commonly used in the human brain tumor image segmentation procedure assignment.

2.2.1 Region Growing Technique

This algorithm is starts in the selected area of the seed selection point and continues further to more separate digital image parts as far as the similarity is concerned and the standard of similarity is satisfied level. The digital image or MRI image segmentation process is over when there are no image pixels to be inspected anymore. The result of this digital image segmentation process is one linked region in the object which is located in the image. Numerous papers ([106, 107, and 124]) presented that this algorithm can be real and less computationally concentrated for brain tumor segmentation of MRI image than other methods.

The region growing method is the fits to the group of semi-automatic digital image or MRI image segmentation methods since it needs a manual selection in the image completely or at least select the one seed point in MRI digital image. The especial case we face when we deals with human brain tumor MRI image segmentation job. But for RGB color MRI digital images an automatic selected the seeded area in the image by the area growing algorithm was established by Shih and Cheng in his paper [112].

Yet, the shortcoming of region growing is its imprecision in case of partial volume effect [108], which hazes borders between human brain tissues, because pixels sometimes signifies more tissues in these slices. Changed version of region growing, able to eliminate this effect, was familiarized by Lakare [63]. It was later publicized in Salman's study [105] that this algorithm technique is improved its correctness of human brain tumor in the MRI image segmentation in 3-Dimentional T1w images and MRI digital images.

Kumar and Halder [61] used region growing method for the brain tumor MRI image. The digital image segmentation task after put on dynamic pixel grouping and detection the brain tumor by the group of pixels with the highest strength level of pixels in the image, which roughly determined the human brain tumor type and its location in digital MRI image. The seed point selection in the digital image was then inspected by an irregularity map in the MRI image. Zhang [130] also used region rising as an overhaul of the digital MRI image segmentation results. The multisequence MRI of the human brain tumor digital image segmentation using multi-kernel used by the SVM.

The region growing method is used in numerous works about digital image processing as an overhaul step, e.g. Dou et al. [30] used it as the change of fuzzy digital image segmentation in multisided MRI of human brain tumor. Another good example of this image processing work is Rexilius et al. [98]. They used liberal region growing to refine results of image segmentation algorithm created on histogram examination of multisequence MRI images, namely T1w, T2w and FLAIR images. This was carried out by histogram corresponding over produced probabilistic models. But, simplification of their process was problematic due to the training of the histogram model for typical human tumor. Furthermore, a joint and dedicated concentrated users collaboration with each other's was wanted in their proposed technique Weglinski and Fabijanska [127] used this region growing algorithm for human brain tumor detection in a image by using the MRI image segmentation technique using physical seed point selection in the digital image or area selection in the MRI image and difference between the selected seed area and an examined set of intensity pixels as a standard that we used. The region growing algorithm was also used for human brain tumor image segmentation in MRI images by Kaus et al. [54]. Their system was based on a dependent statistical image classification way, which divided the input image pixels into brain tissue classes according to their pixel intensity level.

2.2.2 Watershed Technique

Cates et al. [13] carried out a deep research on the appraising efficiency or its performance of a 3D or three-dimensional communicating with the MRI digital image segmentation system is completely dependent on technique which is called the watershed method. They displayed upgrading in subject communication times and inter-subject accuracy over hand contouring. They produce analysis recognize failures in spaces where edges were ill defined in the statistics and raised queries about the understanding of using expert image segmentations to describe ground truth.

The region-based technique, which was written by numerous researchers for human brain tumor image segmentation that is watershed. This term is denotes to a ridge that splits zones drained by dissimilar river systems. An image of basin is the same like earth geographical area draining into a canal or water reservoir. The image is considered as the shape of landscape where pixel strengths characterize the altitude and each meadows, i.e. low strengths of pixels, is associated with a catchment valley. All areas are endlessly flooded and Water Rivers are built in areas where water coming from different regions meets. This process is end its working when it is reached at its peak point or in other words when it is reached its peak intensity level is obtained.

This practice was used for human brain tumor MRI images segmentation procedure by Letteber et al. [90], and Dam et al. [44]. Both approaches were depends upon different watershed image segmentation. Nevertheless, together approaches were semi-automatic and need a lot of user contact to attain precise results. The user had to choice or reject created image segments in order to shape the desired object. Another additional watershed process is possible by using the

collaborative watershed digital MRI image segmentation process was introduced by Mancas and Gosselin [85].

The complication of watershed technique which is lies in the digital image MRI segmentation process for brain tumor. Kong et al. [57] announced the integration of the procedure for over digital MRI image segmented procedure of human brain tumor MRI digital images by fuzzy c-means technique. The Alternative area merging algorithm is used for the watershed digital MRI image segmentation process outputs was described by Bleau and Leon [90] in their papers and applied their proposed technique to the medical MRI digital images for the brain tumor detection purposes. Changed method was applied by Kaleem et al. [52], who pre-processed input MRI images to evade over image segmentation instead of post-processing dependent on area merging. This pre-processing contained of noise lessening, reduction of the curvilinear erections present in MRI images, and calculation of morphological gradients and indicators of the input MRI image. Still, the obtainable results were not sufficient. The parallel pre-processing technique and its first step with better consequences at its working and performance was practically noticed by the Singhai and Ladhake [113].

2.3 Edge-based Methods

The edge based technique or boundary based technique and its procedures overwhelmed the confines about digital image of growing region based approaches by penetrating for limits between the different digital human brain tumor and its surrounding healthy tissues. They use gradient data in local or global zones probing for high gradient principles usually demonstrating an object or a human brain tissue boundary. These approaches require initial assessment of the contour, which may be completed interactively or by another image segmentation method. This contour is then refer according to the gradient data in a local part and the algorithm restrictions keeping the contour level. These edge base systems or boundary based systems are completely depends on deformable ideal models which can be separated into two different groups first one is the parametric group or clusters and the other one is the geometric edge based methods. These both methods are the frames which has the spreading interface which is an arc shaped 2-D and its exterior is in 3-D shape. It is travels with a calculated definite speed level.

2.3.1 Parametric Models

The parametric deformable different models are also acknowledged as snakes or active contours shaped. These all methods travels by different deformable contour shapes as represented by C done with the digital MRI image spatial domain diminishing an different level energy function E(c) given by the mathematical equation shown as:

$$E(c) = E_{int}(c) + E_{ext}(c), \qquad (2.1)$$

Where the $E_{int}(c)$ prompt a different energy function which is completely dependent on the consistency of the long arc while the $E_{ext}(c)$ is a different level energy function reliant on the digital MRI image data. Both of the above mentioned energy functions are known as the inner and outer forces are applied [87].

Several efforts regarding research have been made in order to develop the snake's enactment process. Law et al. [64] sub-sampled the handled border points, and, hence, compact the computing time. They used this methodology for 2-D brain tumor image segmentation. Luo et al. [94] proposed the mutual balloon model system and Gradient Vector Flow snakes

enhancement model for the human brain tumor digital image segmentation proceeded in 2-D T1w digital MRI images. This work was comprehensively expressed by the same writer Luo into 3-D images in the research [73].

Khotanlou et al. [76] The recycled parametric deformable models which is expressed earlier as a refine first step for digital image segmentation process of numerous types of human brain tumors digital images in T1w MRI images types. Difficulty of approaches based on parametric contours is the requisite of a good initialization, else the model have to be re-parameterized during the image segmentation procedure. Classical snakes founded on gradient data have also image problem in zones without clear border. Another disadvantage of these methods is their ability of dealing with topological variations such as splitting and merging.

2.3.2 Geometric Deformable Models

The geometric deformable models which are expressed in previous sections are also recognized as deferent level of sets of pixels. They were projected by Caslles et al. [12] in there research paper to overwhelmed the limitations of active contours, particularly the topological variation. Since symmetrical deformable models are autonomous of the parameterizations, the contour (or exterior) can be signified as a level set of a tall dimensional function. As a result the variations in topology or algorithm can be easily handled by the robotically in [128]. The level set ã progresses with rapidity expressed as the v (k), where the k is a curving arch along its usual path and way according to this mathematical equation:

$$\partial \emptyset / \partial t = v\,(k)\ \ |\nabla \emptyset \qquad (2.2)$$

The level set approaches are the extensively applied to human brain tumor digital image of health surrounding tissues and human brain tumor object image segmentation process in MRI images as well as to the entire medical computer aided diagnose (CAD) imaging field. Prastawa et al. [94] used level sets collected with the pixel strength distribution in T1w and T2w images for discovery of outliers that were considered to be a human brain tumor part. Droske et al. [31] used level groups as a semi-automatic process for brain tumor image segmentation in 2-D MRI images by user's communication for initialization. This was applied to 3-D capacities as independent image segmentation of 2-D slices and following rendering into 3-D. Ho et al. [48] used a human brain tumor image possibility map and parallels to the circumstantial as data and information's for the different level set development for digital MRI image segmentation process of human brain tumors digital image in the 3-D MRI image.

Lefohn et al. [69] presented a technique for tumor image segmentation based on interactive level sets where physical estimation of a first contour was necessary. Cates et al. [14] used symmetrical deformable models for image segmentation of active tumor in 3-D T1w capacities. The image segmentation procedure started with an interactive purpose of a tumor area by the user in one or numerous slices. Human brain MRI image Segmentation process of brain tumors object by level sets technique by using the arrival priors was also anticipated by the researchers Cobzas et al. in their research paper [19] and the same model presents by Popuri et al. [92]. Thapaliya et al. [119] projected a level set scheme for brain tumor image segmentation using automatic discriminating local statistics. Taheri et al. [118] suggested a threshold-based haste function for level sets and used this process for 3-D brain tumor image segmentation. The range of the threshold was connected to the convergence rate and the image segmentation correctness and it was determined by the curving.

2.4 Atlas-based Methods

The atlas method is an extensively used for the prior information in the human brain tumor digital image segmentation process domain. It is a very intelligent technique to control the spatial intensity distribution or pixel intensity distribution of a given pixels arrangement in a digital image. The atlas base technique is shaped by hand or it is a completely manual approach. The use of this atlas base technique is needs the application of a co-registration of digital image procedure in order to bring into the line. The atlas base technique segmented the digital image or MRI image pixels capacity and the excellence and perfection of the digital image segmentation process output and rest on the quality of the co-registration of digital image procedure.

The interpatient atlas base technique, which contains of a spatial probabilistic supply of three digital human brain tissues images which are the healthy or damaged that are present in normal and healthy brains. It is the most extensively used atlas base technique in human brain tumor image segmentation process. Such atlas base technique is portrayed in Figure number 2.1. This approach based on such atlas base technique typically it searches for the nonconformities entities in the MRI image like tumor from the atlas base technique, which are then considered that can be a possible human brain tumor in the MRI image. This information is commonly used in the digital image classification process approaches that will be labeled in next section.

Fig. 2.1: A small sample of the spatial or pixel based probabilistic atlas base technique for white matter in the human brain image and grey matter in human brain MRI image and three orientations of MRI CSF fluid in axial plane and sagittal plane and coronal plane slices [37].

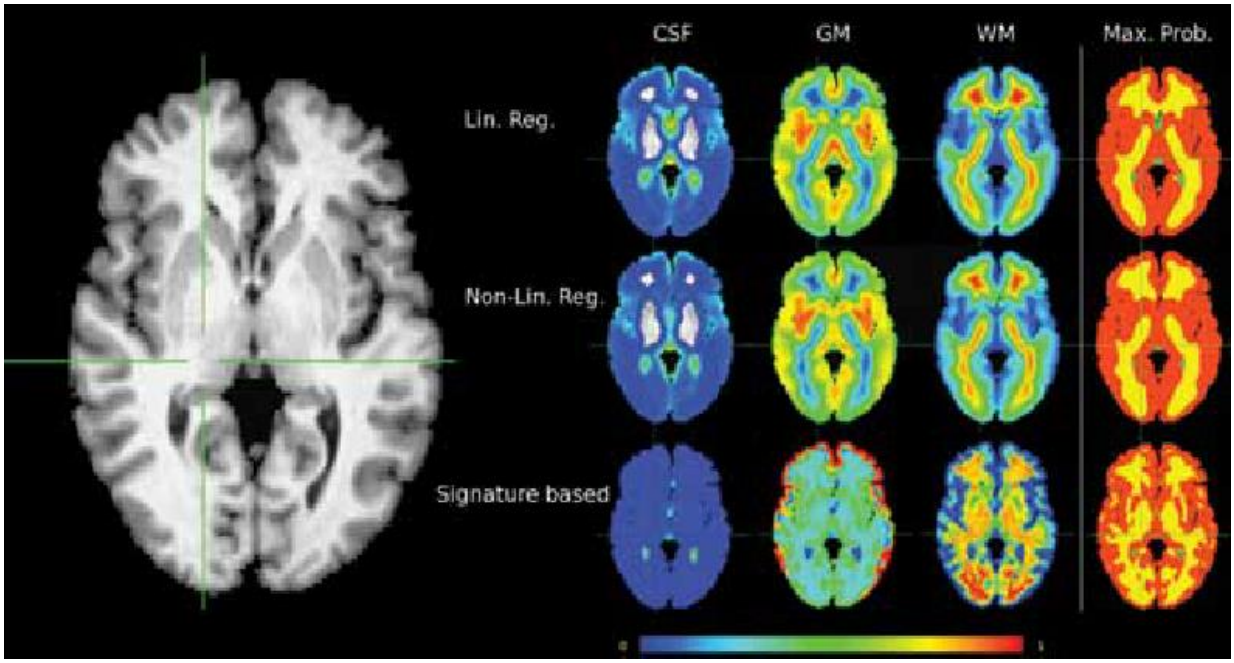

Menze et al. [81] presented a reproductive atlas-based approach for the digital image segmentation process of human brain tumor of a cancer patient in multisequence MRI statistics. At first the numerical model of the image development is constructed and it is then used in a fully automated image segmentation procedure. The model contains of a standard state,

resulting as a spatially variable probabilistic form prior for each normal brains healthy tissue, and a tumor state, projected as a spatially variable.

Dormant probabilistic atlas base technique. Then the probability of a brain tumor occurrence is assessed for each channel in multisequence statistics. Seeing the fact that the image strengths of pixels of each tissue in brain have the Gaussian distribution in each frequency, the combined chance of the latent atlas and the experiential variables is computed as a product of both apparatuses. The model limits are estimated using the All-out Likelihood approximation. The human brain tumor presence in the MRI image is estimated for each channel as described in the statistics.

Moon et al. [84] planned a technique using the pixels of digital images or spatial probabilistic atlas base technique founded in the research paper known as the Anticipation Maximization algorithm. Alike tumor detection process was published in a research paper by the Prastawa et al. [95] where the contributions of authors about his proposed algorithm are T1w image and T2w digital images with previous likelihoods from the atlas base technique.

Kyriacou et al. [62] familiarized an algorithm by using a biomechanical human brain tumor growth model in a patient's skull or his brain. The first step of the process is a labor-intensive delineation of the human brain and the ventricles. Via unchanging contraction model, the brain tumor is compact and the simulated previous normal healthy brain structure is projected. The normal and healthy brain is then recorded to the atlas where the assessed tumor growth model is functional. Another group of atlas-based approaches comprises systems that use a patient specific atlas. These approaches are approximately used for longitudinal image segmentation and demonstrating of the brain tumor development. Menze et al. [82] projected a mixture of a generative human brain tumor in the patient's brain growth model which was completely dependent on a detected tumor in MRI image diffusion outline with longitudinal multisequence MRI statistics.

Dawant et al. [26] derived the human brain tumor where the growth model from the visual flow standard technique and they extended the atlas base technique digital image segmentation process of the healthy human brain and normal human brain tissues to the human brain tumor MRI digital image segmentation process task. This lengthy algorithm contained of worldwide and indigenous registration of the atlas to the bulk, where the local registration was depends on the visual flow principle, with the human brain tumor model estimated from the patient statistics, and following deformation of the atlas.

2.5 Classification and Clustering Methods

This cluster of algorithms which is properly defines the attachment of tag of every pixel in the digital image which is supervised known as the classification procedure and the unsupervised way is called the clustering. Classification algorithms are usually used in a eclectic spectrum of MRI or medical image processing. They need a set of training facts to train a model which can be then applied to before unseen data. The training statistics consists of two parts: picture of the facts in a feature space (pixel characteristics such as pixel intensities, indigenous texture etc.), and labels (physical classification of the statistics). Clustering algorithms do not need training statistics and physically created tags. These algorithms robotically search for natural constructions and patterns in the facts.

2.5.1 k-nearest neighbors (k-NN)

The k-nearest neighbor's algorithm (k-NN) is a diffident non-parametric classifier. This algorithm is a type of idle learning approaches. It makes no supposition about the Arithmetical statistics structure. The test sample tag is derived from its k nearest fellows from the training set in the feature galaxy. The remoteness may be stately by e.g. Minkowski or Euclidean, Mahalanobis, distance dependent on the operation. The algorithm has glitches with understated or noisy facts. Another difficulty is a large storage must for training samples since all of them have to be obtainable during the image classification procedure-.

Havaei et al. [47] projected a communicating scheme for human brain tumor MRI image segmentation process which is uses the k-NN technique shadowed by the conditional random fields (CRF). The system required a rough physical selection of image segmented brain tissue in two slices of the image segmented bulk. The algorithm was intelligent to segment the bulk in one minute after the physical delineation. The k-NN algorithm was used in the leading technique which segmented all brain tumor parts in the image-.

This interactive scheme was announced by Vinitski et al. [125]. A multi-class training statistics set was well-defined by the user and a before unseen pixel was branded by the most common label among the k nearest training models. This technique was very subtle to the tumor in similarities and noise-.

Kaus et al. [53] projected a scheme based on k-NN for digital image segmentation procee of meningioma's tumor human brain tumor type and low grade gliomas human brain tumor. They used an atlas of about 251 human brain constructions created by medical field experts as extra material to the pixel strength in image. All pixels were categorized into five groups (ventricles, background, skin/skull, brain and tumor), where the similarity of the tumor area was predictable. Therefore, the system was only related to the above stated brain tumor types. Registration to the physically created atlas was working to resolve misclassification of image problems produced by overlap of pixel intensities of dissimilar tissues-.
Khalid et al. [55] used k-NN algorithm for MRI digital image segmentation procedure of irregularities like tumor in the MRI image is in the FLAIR MRI digital images of patient's brain. They used 50 head-to-head neighbors which are classified based on the least square space of pixels.

2.5.2 Bayesian approach

These approaches which are use this Bayesian approach for example the multi-variety Gaussian delivery of pixel in case we are dealing with the 2D image and voxel strengths in case we are using 3D in every human brain all types of tissue in the brain. Both limits of the supply, i.e. covariance and mean, are assessed from training examples. The name of these approaches is subsequent from the Bayes rule, which they practice. They exploit a posteriori probability P r(c/x), where c signifies the class of the experiential data x, using the Bayes rule $P\ r(c/x) = P\ r(x/c)P\ r(c)/\ P\ r(x)$, where $P\ r(x/c)$ is called probability, $P\ r(c)$ is a. priori likelihood of a class c computed from the exercise statistics, and p r(x) is the probability of the observed value x-.

Corso et al. [21] announced a multilevel digital image segmentation scheme for GBM human brain tumors types like gliomas or any other based on division by weighted combination of used pixels for it presented by Sharon et al. [110].

Wang et al. [126] projected an advance system that combining the Normalized Gaussian Bayesian ordering with 3-D images by Fluid Vector Drift. They model normal healthy brain

tissues (white matter (WM), gray matter (GM) and CSF) by the Normalized Gaussian Mixture Model, which is then used to approximation of Gaussian Bayesian human Brain Map. Applicant brain tumor area is assessed from this map and it is used as start of 3D Fluid Vector Stream algorithm. The last brain tumor area is learnt after basic post-processing stepladders such as thresholding and morphological process. The difficulty of above mentioned approaches is their supposition of Gaussian supply of segmented image tissue, which is not always the circumstance. The image segmentation is an amalgamation of an image classification based on a Bayesian classic model and a graph-based affix control.

Ain et al. [1] used Bayesian digital image classification for MRI image segmentation procedure of human brain tumor by the core in multisequence MRI used statistics. They used Proton Density (PD), T1w, T2w and T2w* images. The scheme contained of three steps: withdrawal of features using discrete cosine transform, cataloguing of pixels into normal healthy and potential tumorous collections by Bayesian classifier, and the final abstraction of the brain tumor using the k-means clustering algorithm and the canny edge detection method.

2.5.3 Expectation Maximization (EM)

The EM digital image segmentation procedure algorithm was presented by Moon et al. [84] and Prastawa et al. [95]. both works were shaped by the same collection. Both of them projected an image segmentation algorithm that is shown by a spatial likelihood atlas of normal healthy tissues in brain, which delivers a previous information about the brain organization. A tumor prior likelihood is made from the change between T1w and T1w images of MRI. These two prospect atlases, along with T1w and T2w images, are passed into the image segmentation algorithm. Besides the limits of the probability supplies, there are also parameters for the bias field in the model. The algorithm consists of three iterative steps: classification of a semilar grid by three dimensional area of pixel groups in a bitmap using existing likelihood supplies and the bias field, apprising of the bias field approximation, and re-estimation of the likelihood disseminations. The statement of this system is the occurrence of fully-enhanced human brain tumor found in the patient's skull.

The Expectation maximization (EM) is classic algorithm was assumed its term in 1990 by Demp- ster et al. [27], who comprehensive the scheme that had been used numerous times under special conditions. It is a respective two-step algorithm used to discovery all-out probability parameters of a given numerical model. The label of the algorithm is given by the styles of the two steps: expectation and enlargement. In the first step, the probability supplies are efficient to the posterior probability p r (ci/xj, Θ) that pixel xi fits to a class ci given model limits Θ. In the second step, the limitations Θ are re-estimated using these likelihoods. These two steps are alternative of each other until meeting with each other and not comprehensive for very large deformations.

Prastawa et al. [94] extended his described algorithm to make it better work and its performance with T2 weighted digital MRI images only. This method is based on detection of outliers, which are detected as abnormal region using registered brain atlas. Then, the presence of edema and tumor is detected within the abnormal region from image intensities, and, finally, the spatial and geometric constraints are applied to the detected regions.

2.5.4 Support Vector Machine (SVM)

Support vector machine (SVM) is an administered machine learning scheme conceived by Cortes and Vapnik [22] in 1989. The goal of the SVM algorithm is to discovery a hyperplane

that best splits the feature space into subspaces according to the exercise data. SVM is a two-class sorting algorithm, however, numerous extensions have been planned for multi-class glitches [49]. The impression of SVM is to map the statistics into a higher-dimensional feature space, where it can be linearly detached. The benefit of the SVM technique is good simplification of a classification delinquent-. It has become prevalent in the human brain tumor digital image segmentation procedure job and many research papers telling this usefull application have available now a days.

Bauer et al. [6] employed hierarchical Conditional random fields which is CRF instead of MRF to legalize the segmentation process to get by SVM machine. They used multisequence image pixel intensities and textures as topographies for image pixel classification. A semilar grid by three dimensional area of pixel groups in a bitmap of normal and healthy and tumorous brain tissues are categorized. Followed by sub-classification of normal and healthy brain area into white substance (WM), gray substance (GM), cerebrospinal fluid (CSF), and brain tumorous area into active brain tumor, edema and necrotic tumor-. There are several very simple SVM-machine based approaches are planned till now.

Zhang et al. [129] introduced a very simple segmentation practice process by using SVM machine for cataloguing followed by morphological processes for error lessening purpose we can reduce the errors by using this. The binary segmentation process of human brain tumor MRI digital images with cancer patient exact training was applied to 2-D digital images and T1w MRI images and T2w MRI images as well.

Alike approach was applied by these researchers Mikulka and Gescheidtova [83], who used T2w, T1w and diffusion weighted (DW) MRI images for interactive division of brain tumor parts. First, numerous image pixels inside and outside the segmented zone are manually considered. The classifier is then skilled and applied to the segmented MRI image. This means that each tumor portion has to be segmented distinctly. This work also defined the presentation growth in comparison with using only a sole order-.

Lee et al. [68] mutual SVM with Markov random fields (MRF) to evade noisy outcomes by incorporating the associations between neighbor pixels of image. As the previous approaches, they used patient-particular training information-. They applied their scheme to the subdivision of glioblastomas human brain tumor type in T1w digital image and T2w MRI images.

Garcia and Moreno [39] future an advance algorithm which is in first section of the research paper of human brain tumor digital image in 2-D slice by the Adatron advance algorithm. The segmentation outcome is then used as an exercise set of the SVM algorithm. SVM is used to yield a 3-D brain tumor model. Nevertheless, the image pixel classification mission is still performed in 2-D-.

Zhang et al. [131] segmented process of the human brain tumors digital MRI images using the T2 weighted MRI images, TIw weighted MRI images and FLAIR MRI digital images and used it for development of counted during the brain tumor healing treatment of cancer patients. The SVM machine advance algorithm is used in the first step as preprocessing of the detection system to obtain human brain tumor by using the method of digital image segmentation process. In the second step the digital image segmentation procedure outcome is upgraded by using all-out likelihood and distance processes.

Another MRI multisequence SVM machine approach was advance proposed by the Ruen et al. [102], who pooled T1w, T2w, PD and FLAIR MRI sequences. The work working a multiscale system, which contains of two steps, to decrease computing time. The aim of the projected

scheme is not only to slice a brain tumor area but also to track the brain tumor area during cure. SVM machine was also used by the Ayachi and Amor [5] for human brain tumor type like glioma division and sub division.

2.5.5 Neural networks (NNs)

Neural networks NNs is the sometime or occasionally also called artificial neural networks (ANNs), are arithmetical learning approaches inspired by the human brain. NN consists of a set of simple mock neurons which are linked together to create a net. These connections are well-defined by adaptive masses, which are tuned during the learning procedure. NNs were extensively used for cataloguing tasks, however, they were slowly replaced by simpler approaches such as SVM due to the computational difficulties of NNs. Their admiration started to growth again after the outline of Deep learning method and its success in numerous various global image and speech acknowledgement challenges. This is the one of the Deep learning approaches is used in this work of detection, mostly the technique of the Convolutional Neural Networks (CNNs) is the more comprehensive explanation.

Dickson and Thomas [28] presented a process with two NNs for auditory neuromas deprived of using patient particular training. The division is performed by pixel-wise classification using the pixel intensities of a given pixel and its natives. They verified the process on 60 manually categorized images of dissimilar patients. The first neural network products a first segmentation, which is considered to be a human brain tumor area or patients candidate. The results and consequences are refine by computer used morphological operations regarding the image and approved to the second remaining net.

One of the first and starting efforts huge efforts to the process of segmentation of human and patients brain tumors in the MRI digital images using neural network as NNs was labelled by Clarke [18], who used T1w digital images in their research papers, T2w and PD images. Later, Ozkan et al. [87] used NNs for multimodal image segmentation of brain MRI images. They used co-registered MRI and X-ray images.

Murugavalli and Rajamani [85] suggested a scheme combining Hierarchical SOM and Fuzzy C-means to identify numerous tissues in T1w images.

Reddick et al. [97] planned a human brain tumor image segmentation process system based on Kohonen self-organizing map which is the SOM used for subdivision purposes which is looks like the multilayer mechanism and use back-propagation technique as the neural network works used for digital image object section classification process. The input data information is contained of T1w digital image T2w MRI images and PD MRI digital images.

Another advance work which is using the SOM was published by Vijayakumar et al. [123]. Their algorithm segmented process human brain tumor images, necrosis, edema, cysts and healthy normal brain tissues from the mixture of T2w and FLAIR images. It was also able to identify the tumor grade. Chaplot et al. [15] also used SOM and practical it to the classification of image pixels of T2w images into normal brain and abnormal brain using wavelet transform for feature abstraction. A complete portion of NN-based approaches and method is started to seem with the huge growth of the advance deep learning admiration for digital image processing.

Additional human brain tumor MRI image segmentation process scheme based on advance deep learning was projected by Urban et al. [122]. Compared to the earlier work, 3-D covers are used in this algorithm. The network comprises three convolutional covers with a typical

size of 5×5×5 pixels. These layers cover 8, 16 and 6 convolutional riddles, respectively. Combining layers, which typically substitutes with convolutional sheets, are not current in the planned architecture. Convolutional coating with filters of scope 1×1×1 voxel is applied at the end of the whole building to speed up the segmentation procedure. The input of the entire network is a cubic patch of scope 9×9×9 pixels, which is used to categorize the central pixel. Areas smaller than 3000 pixels are removed throughout the post-processing step. The training time of the whole and entire neural network on a solo CPU processing sequence was about 40 - 50 hours.

Davy et al. [25] implemented a human brain tumor digital MRI image segmentation way based on CNNs network. The input of the network is a 2-D multisequence patch of scope 33×33 pixels, which is used to forecast the central image pixel. The network comprises two pathways. The first trail is a classical CNN with two convolutional covers linked to the whole patch. The second trail is a fully linked network of fewer layers associated to 5×5 region at the patch center. The latter this way we serves to the brain tumor detection in MRI image as contour.

Zikic et al. [137] projected another human brain tumor digital MRI 2D image segmentation procedure algorithm which uses CNNs. The network planned in this work accepts 2-D multisequence patches of extent 19×19 as an input, which means that the bulk is handled slice by slice. The style consists of a convolutional cover with 64 5×5 filters, a max-pooling
Layer with sub-sampling rate of 3, a convolutional layer with 64 3×3 filters, a fully
Associated layer and a soft-max layer with five outputs (one for all class).

In Recently, Havaei et al. [46] presented a method and technique that spreads the research work of Davy et al. [25]. The advance algorithm uses the same two pathway by using the CNN network style but two of these advance and complex architectures are dropped there, where the output of the major network is used as an input to the next system.

Additional feature map for the additional convolutional neural network and neural network. Since the human brain tumor digital 2D MRI image segmentation task and his procedure is an unfair badly behaved, they projected a two-phase training method. In the first stage, the entire network is skilled using a balanced figures set. In the second stage, only the output layer is re-trained using the unique imbalanced records set. They also anticipated bouncing the complete kernel masses and using L1 and L2 regularization composed with Dropout system to avoid over-fitting. This proposed method and his technique is one of the latest and advance with the calculating time between 55 seconds and 10 minutes.

The public and special characteristic of all labelled advance and latest proposed algorithms is the self-determining and classification procedure system of only one pixel, which often clues to noisy outcomes and, henceforth, post-processing steps are typically obligatory. All the above labelled approaches based on deep knowledge used T1w, T1w, T2w and FLAIR images from Multimodal human Brain Tumor image Segmentation Trial which is also used for the assessment in this research work proposed algorithm.

2.5.6 Random forest (RF)

Random forest (RF) is a collaboration of the conclusion trees used for data cataloging and faced the regression difficulties. Decision trees often agonize from over fitting. This difficulty is concentrated in RF by combination of manifold decision trees and their input to the final decision. Decision tree (or sorting tree) is a modest algorithm, which can be signified by a tree-like chart, where the sorting task into a given number of clusters using a predefined standard is performed in all node. This procedure hierarchically ruptures the statistics into lesser subsets.

During learning, these standards are assessed based on the data gain after the divided. The tree leaves signify a probability supply over the classes for a given example. The final class is firm by combining the delivery of all trees in the forest. All trees are skilled arbitrarily using, e.g., arbitrary subsets of training examples or features. The benefit of RF is the likelihood to analyze the feature significance since the most significant features are most regularly used in the first layers. The less important topographies can be then detached.

Arbitrary forest tree has been regularly used for the human brain tumor digital 2D image segmentation problematic as well as for other cancer patients MRI image segmentation jobs in recent few years. As defined in [41], the benefits of using RF in medical image examination are the competence in production with high-dimensional feature spaces, their nature to deal with multi-label glitches, and generalization capability. In BRATS challenge in 2013 and 2014, seven out of 17 donations were based on RF. All above mentioned approaches like forest tree are typically differ in mined their features.

Meier et al. [78] made use of a reproductive version of arbitrary forest called thickness forest, which can be labelled as hierarchical GMM using hard tag assignment. It is used to perfect class-dependent probability P_r (x/y) which approximations the initial human tissue possibility. The human tissue possibility estimation is shadowed by a discriminative arrangement forest and following regularization using CRF. For the organization of each voxel, they used first-order surface, gradient and regularity features with possibilities estimated by the thickness forest summing up to 55 features.

In their later work [79], they uncontrolled the generative thickness of proposed forest tree method and improved the all feature set in the image pixels and in its place. It led to the computing time decrease and the presentation increase. They extracted context-sensitive features using image registration of the statistics with the whole brain atlas. Mainly, they used so called spark features, which are based on the strength range in four guidelines and two distances from the categorized voxel, and regularity features computed as a change between the strength of the voxel and its reliable point in left or right hemisphere. The regular and normal computing time to calculate the latter scheme is 6 minutes per enduring.

Geremia et al. [40] familiarized a scheme based on spatial or a cluster of pixels for 2D conclusion forests tree for digital image and MRI image segmentation procedure of Manifold Sclerosis lesions in 3-D MRI digital image. In their proposed algorithm they designed to use T1w digital image, T2w MRI images and FLAIR MRI digital 2D images information of healthy and damaged tissue periods and long-range spatial pixels group as used in the 3D situation together with regularity features.

Festa et al. [35] used 130 features for human brain tumor image segmentation from four structures including pixel intensities and the changes between each mixture, mean, sum, median and range in 3-D neighborhood of four dissimilar dimensions, the difference between the strength of a given voxel and the mean value in its area, edge thickness and local binary divider from 3-D neighborhood and 2-D texture features from all plane. During the post-processing step, all areas smaller than seven a semilar grid by three dimensional area of pixel groups in a bitmap were branded by the label of the nearby area. The computing time for calculate the projected this advance working algorithm is 35-40 minutes per cancer patient running on normal digital computers.

Zikic et al. in [136] and later in [41] 2D digital image segmented procedure of human brain tumors using the mixture of six sequences that are frequently used there: T1w, T2w turbo spin echo, FLAIR images, and two frequencies of diffusion tensor imaging. They joint

discriminative conclusion forests with a reproductive human tissue presence model, which was appraised by Gaussian Mixture Model (GMM). As features, they also recycled the pixel intensity change between a given pixel and a voxel with a assumed off in the similar or a dissimilar channel, the same type of variance feature in a cube around the pixels, and the pixel intensity range between these two a semilar grid by three dimensional area of pixel groups in a bitmap in one frequency-.

In [41], Geremia et al. as long as rough initial class possibilities as another input of Radio Frequencies. They used posterior possibilities which were based on GMM approximation for all human brain tissue-. The same to same landscapes image presentation as in [136] research paper were used.
Goetz et al. [45] suggested very much randomized forest trees is proposed, which announced more arbitrariness during the training. They extracted 64 landscapes from each of four Orders, such as strengths, local histograms, first and second order data, and histogram based image segmentations-.

Surface features of digital images were the foundation of the reasearch work available by Reza and Iftekharuddin [99]. Besides shared strength features, they used a fractal piece-wise three-sided prism superficial area and text on topographies. Later in [100], they protracted the feature set by a multi-fractional Brownian gesture-.

Pinto et al. [90] recently circulated a human brain tumor image segmentation system using strength, gradient and context-based structures, which are used for pixel grouping by RF with 99 trees of extreme depth of 40. The division is followed by morphological processes throughout the post-processing step. Collective characteristic of all designated algorithms is the similar as in NN-based segmentation the sovereign grouping of a solitary pixel/voxel-.

Prior et al. [96] executed RF as a sorting performance in their work dealing with active brain tumor extraction from numerous MRI systems: T1w, T2w, FLAIR, Susceptibility Weighted Imaging (SWI), Apparent Difference Coefficient (ADC), TraceW, and rCBV-.

2.5.7 Clustering

Clustering is an unsupervised scheme of assemblage the data information models into numerous groups according to their resemblances in the feature space. These algorithms work with present statistics and do not essential a training phase and a training records set. Collective approaches used for gathering are k-means, fuzzy c-means (FCM - also recognized as soft k-means), Guassian Mixture Models (GMM), and graded clustering. All these approaches, except the ranked clustering algorithm, need a definite number of groups as the extra input to the statistics. k-means is an iterative algorithm lessening the sum of reserves from each statistics sample to the centroid it is allocated to. Fuzzy c-means simplifies the k-means technique by allowing the proportion of fitting into a given cluster instead of hard task. GMM is an ideal assuming that the statistics has been made by a finite quantity of normal deliveries. The group is than assigned by the suitable Gaussian part in the model. The hierarchical gathering scheme clusters data by a group tree where bunches at one level below a given node make a single collection in the greater level-. All of these procedures are very complex due to noise addition in the processing of image noise and inhomogeneity conditions.

Further authors, such as Shen et al. [111] or Szilagyi et al. [117], anticipated paying needs of neighbor pixels in the digital image or MRI image in order to overwhelm the noise problems or compassion of FCM.

Zhao et al. [133] projected a scheme based on GMM and active image brain tumor detection contours sample. GMM assisted as the initial and first step separation for the active contour for the human brain tumor detection system in the human brain system, which than refine the borders between human brain healthy or damaged tissues inside the cancer patient brain.

Phillips et al. [88] used FCM for the 2D digital image segmentation procedure of human brain healthy tissues and damaged tissues in the current pathological cancer patient's human brain. They mutual T1w, T2w and PD images. They presented the strength overlap even with using manifold MRI arrangements and, hence, the brain tumor was not segmented precisely. Healthier results were realized by Clark et al. [17] and Fletcher- Heath et al. [36] who applied information based procedures organized with FCM and used them for the same mixture of MR sequences.

2.5.8 Random fields

Random fields are normally used as the final step in the detection of brain tumor it is post-processing step to integrate neighborhood pixels associations for 3D three-dimensional regularization to identify the exact voxel or pixel-wise in case of 2D digital image segmentation process consequences. Though, they can be used as an unsupervised image segmentation practice too. They increase the clustering methods by with the spatial data. Regularly used arbitrary fields in image subdivision are Markov random field (MRF) and Conditional random field (CRF). Arbitrary field is a set of chance variables in an undirected chart. In case of 3-D bulks, random variables and ends signify a semilar grid by three dimensional area of pixel groups in a bitmap and associations between neighbors, correspondingly. MRF is a reproductive model, which representations the joint possibility of variables. CRF is a discriminative exemplary, which models the conditional possibility of variables. Gering [43] used MRF as a step after the EM division. His method used a multi-layer MRF to integrate a construction in order to restriction the borderline. Still, his method is appropriate only to similar tumors. Solomon et al. [114] included MRF directly to the EM division and applied it to the subdivision of active brain tumor parts.

Capelle et al. [11] planned a 2-D unsupervised learning process where the extreme a posteriori mapping (MAP) is used for the approximation and understanding of MRF system. The mentioned system digital image segments procedure input human brain image slices into similar areas where the tumor is found and then detects and then identified the the brain tumor occurrence in MRI image.

2.6 Tumor detection

Separately from the human brain tumor detection and segmentation procedure approaches, only numerous systems according to this for discovery of the human brain tumor occurrence and its estimated location in the cancer patient is exist. The objective of these approaches is not the exact delineation of the brain tumor border, but only fast conclusion whether the tumor is existing together with its place. Such procedures could be used as an original approximation of the tumor contour which is compulsory for some division methods.

Saha et al. [104] situated human brain tumors in 2-D MRI digital images in axial plane or any other plane by the fast recognition of irregularity in the digital MRI image that can be a human brain tumor by Bhattacharyya coefficient. The output of the proposed advance algorithm was the leaping box everywhere the human brain tumor inside the brain is found.

Chapter # 03 Research Methodology

3 Research Methodology

The objective of this chapter number 3 is to serve to the medical pixel strength analysis domain to find out the differences of image according to the pixel intensities precisely to the field of human brain tumor identification and recognition of tumor from image and digital MRI image segmentation procedure in multi structure pixel strengths. At first, the essential pre-processing step is be labelled. This contains skull stripping, strength normalization, bias field improvement and bulk registration. In the next portion, a fast pathology existence recognition approach, which is based on multi-resolution regularity analysis, is announced. This process is applicable for 2-D parts of brain images of together axial and coronal planes, where the left-right regularity is usually broken in case of tumor occurrence. This is followed by outline of unsupervised abstraction of gliomas (the most public malignant brain tumor type) from 2-D

and 3-D FLAIR images and T2w bulks. This system is based on the earlier pathology finding in 2-D slices. It uses the similar multi-resolution examination which is then extended into 3-D. This is shadowed by brain tumor locating and following extraction of all brain tumor slices as a complete area. The abstraction of this proposed process is an unsupervised advance algorithm using the information data of brain tumor type like gliomas appearance in FLAIR MRI digital images in T2w MRI image pixel strengths.

In the last chapter number 2 of this research paper, a supervised scheme of three human brain tumor image segmentation process and sub-problems means the division of whole tumor, tumor core, and lively tumor respectively is our main aim and projected. This scheme is based on an advanced Deep learning (DL) algorithm, particularly Convolutional Neural Network (CNN), which is combined with a construction forecast framework where a label construction in a given area is forecast instead of mutual pixel-wise classification tactics. Pixel-wise segmentation usually hurts from noisy results and needs a sophisticated post- dispensation step performed, for illustration, by Conditional random field (CRF). This unique step is eradicated in the proposed advance algorithm cheers up the prediction of tags attached to more pixels in the human brain tumor MRI image at once based on the digital image data information in the whole area in image.

3.1 Pre-processing of Image

The maximum of the segmentation procedure proposed algorithms need the pre-processing of a digital image which is used to detect the object inside the image applied to the input MRI digital image. In human brain MRI image preprocessing, this typically comprises on the first step which is the spatial co-registration of digital MRI image, strength normalization, bias field alteration, and human brain stripping.

Image Registration

MRI digital Image registration step is a procedure of aligning numerous digital MRI images in order to have consistent digital pixels or a similar pixel grid by three dimensional 3D image area of pixel groups in a bitmap at the similar position in all digital images for cancer patient. This is a needed step in the multisequence image examination, which allows joining the data Removed from all images. The objective of the registration development is to find an alteration model that maps the organizes of a particular pixel from the image to be registered to the organizes of the consistent pixel in the orientation image. The statistics used in this work had been co-registered by an unbending model with the joint material similarity metric applied in Insight Subdivision and Registration Toolkit (ITK). Definitely, Versor rigid 3-D alteration, where only rotation and conversion are allowed, had been practical. As the resemblance metric, Mattes common material had been used with three multi-resolution levels. The algorithm is based on the work available by Mattes et al. [76]. They planned using Parzen histograms to approximation the possibility density function (PDF). In the Research paper researchers used third order B-spline and zero order kernel for the tumor position in the digital MRI image and registered digital image strength PDF correspondingly.

Bias field Correction

Digital image pixel strength inhomogeneity is a shared big problem of pixel strengths caused by brain tumor or cancer patients' place, magnetic settings, and all other issues face by researchers. All organization based segmentation approaches use the voxel strength data where small fluctuations may lead to misclassification. Therefore, the improvement of the bias field is

obligatory to overwhelm this problem. The scheme denoted as N4ITK available by Tustison et al. [121] is used here. This system is a development of the nonparametric unchanging strength normalization (N3) algorithm. It is an iterative algorithm using B-spline estimate of the data example delivery, which is founded on the least squares fitting procedure.
An instance of the bias field rectification result is represented in Fig. 3.1 where a contrast between original and modified images is shown. We can see the digital image pixels strength reduction in the back part of the cancer patient human brain in the modified MRI digital image.

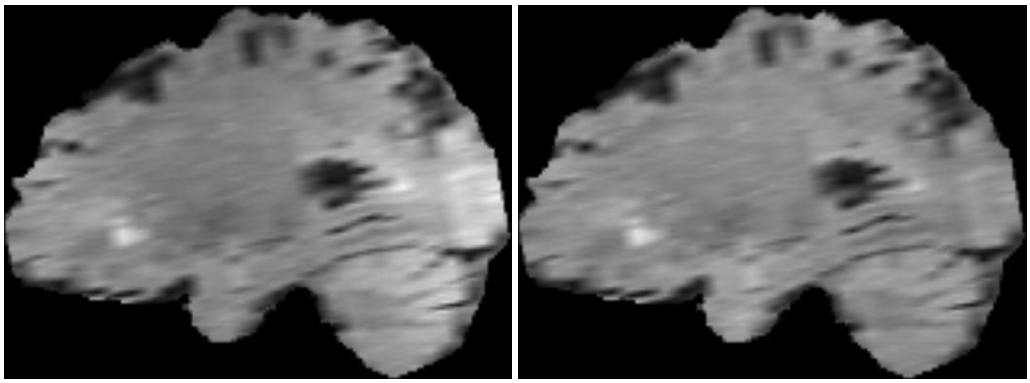

(a) (b)
Figure 3.1: Bias field alteration. (a) Unique input image, (b) improved image.

Pixel Strength Normalization

The pixel strength or its intensity level normalization is a very serious and complex step for the classification MRI digital image based division into different category approaches applied to MRI digital image of cancer patient. Two shared actions used for this task are normalization by regular pixel strength and normal deviation, and histogram matching. Together of these methods work well for images of fit brains where the shape of the pixel strength supply varies only somewhat. Nevertheless, this is not true for images with pathologies, where the form of the pixel strength delivery is partial by the pathology scope. On the other hand, as it has been empirical, the previous methodology regularized strengths adequately enough for this work's drives, so the strengths in each bulk are standardized so that they have the regular value like to zero and the normal deviation equal to one.

Skull Stripping

Additional common pre-processing of digital image that is used for medical diagnose step achieved during the human brain tumor digital image segmentation procedure development is skull stripping technique. The aim of this development is too distinct the human brain tissues from the non-brain intracranial brain tissues and head. Numerous approaches industrialized for this determination were assessed by Fennema-Notestine et al. [34]. Since the statistics used for challenging the projected algorithms had previously been skull stripped, this step is not carried out now.

3.2 Brain tumor presence detection

The designed system anticipated for human brain tumor in the cancer patient occurrence finding is a symmetry based advanced algorithm for the discovery of a human brain tumor occurrence in the head of cancer patient in 2-D MRI digital image slice. It is an alteration and

extension of a system that I have previously printed in [152, 154]. The algorithm uses the previous information of structural changes between healthy and pathological brains. This information is based on the detail that brain tumors disruption the estimated tissue building regularity in the left and right hemisphere, which is usual for strong brains, unless they are positioned proportionally in the middle of the brain, which is not collective. Even in case of such tumor position, the regularity is often broken since tumors usually don't grow proportionally.
The regularity prior necessitates another pre-processing step: mid-sagittal plane finding. This has been deliberate in several works, e.g. [72, 103]. Another method uses recording of the brain bulk to a reference aligned volume, which may be based on the same organization labelled in the section about pre-processing. The projected tumor detection system is not sensitive to small aberrations from the perfect pixel arrangement and is the able to work at satisfactory level even with slight revolution of digital image contains the human brain tumor.

The projected designed image system was designed for both planes of digital image or MRI where the left-right side of brain equilibrium of human brain can be experiential axial and coronal. It is a oversaw classification algorithm, which uses features removed from multiresolution irregularity maps and, in case of application to specific slices in 3-D capacity, input slices. The latter type of topographies, based on the input image, are not appropriate for stand-alone slices since the strengths in such slices differs due to dissimilar measurement limits and gear, and the pixel strength standardization is not possible. Random forest (RF) is used as an organization algorithm but additional supervised algorithm may be used.
In this piece, a short-lived overview of the RF algorithm is given followed by the explanation of multiresolution regularity analysis and feature abstraction.

3.2.1Random Forest (RF)

The Random forest (RF) designed algorithm has been extensively used in remedial imaging like MRI or CT scan images and human brain tumor detection subdivision as described in 2. A brief overview into RF is given here, more comprehensive data can be found in [23] RF is a collaborative of verdict trees used for classification and regression glitches. Decision trees frequently agonize from over fitting. This delinquent is summary in RF by mixture of multiple decision trees and their influence to the final conclusion.
Decision tree (or grouping tree) is a humble algorithm, which can be signified by a tree-like diagram (Fig. 3.2), where an organization task into a given amount of collections using a predefined criterion is done in each node. This process hierarchically splits the statistics into smaller subclasses. During learning, these standards are predictable by maximizing the substantial gain I in a given lump, which is well-defined as the indecisiveness cut after unbearable the training data of human brain tumor type data. Normally, the following mathematical equation is used:

$$I = S(H) \sum_{i \in L,R} \frac{|S^i|}{|S|} H(S^i) \qquad (3.1)$$

Where H stances for the entropy and S designates the input data set to the system which is proposed, which is riven by a given node into two subsections SL and SR. |.| means the cardinality for set influences. A tree leaf signifies a possibility distribution over the modules for a given example. The final class is resolute by joining the delivery of all trees in the forest. All trees are skilled arbitrarily using, e.g., arbitrary subsets of exercise samples or landscapes. The benefit of RF is the option to examine the feature position since the most significant are most often used in the first layers. The less significant features can be then indifferent.

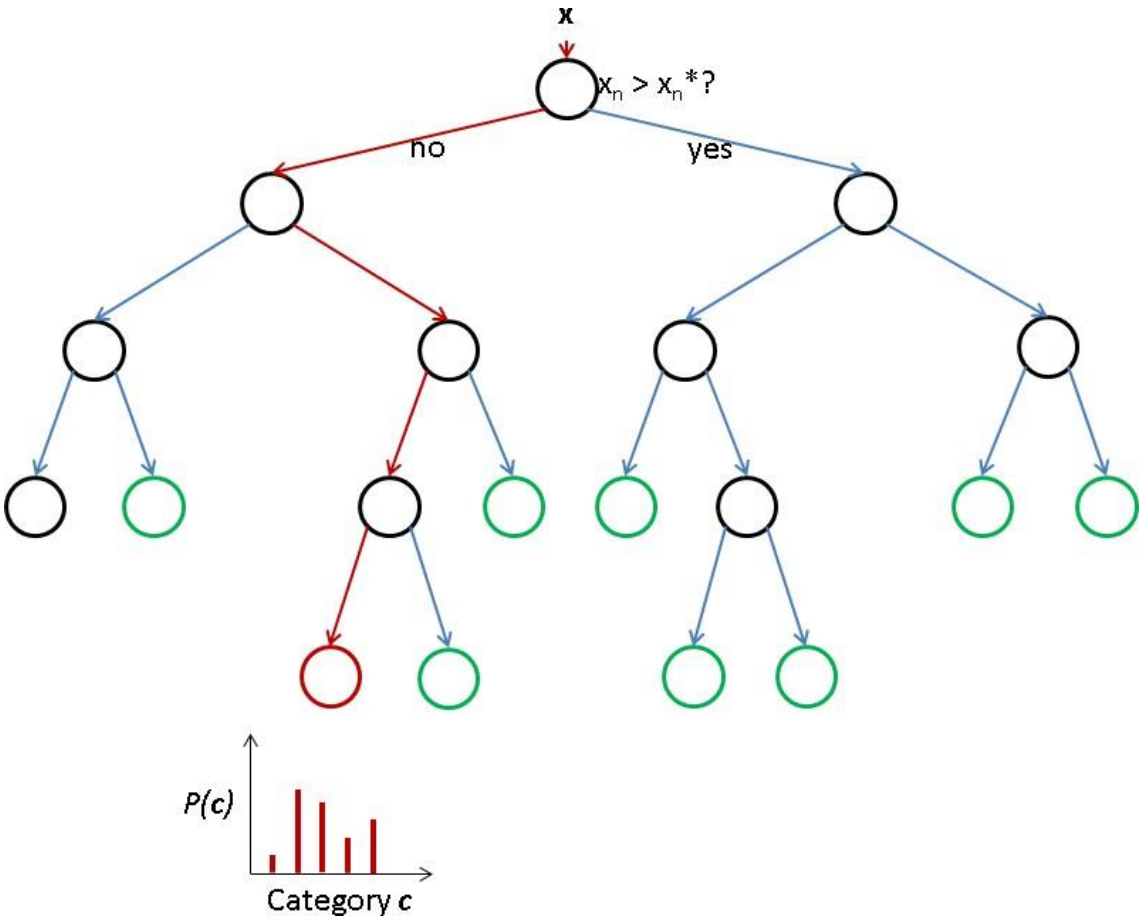

Fig. 3.2: Toys example of an algorithm which is decision tree algorithm is presented here. Red arrows in the above chart are shows the proliferation of an input sample x to the decision tree. Green circles in above diagram stand for decision tree leaves in it and the red circle in above diagram portrays the leaf touched by the input sample set to the decision tree with given possibility distribution as described below.

3.2.2Symmetry analysis

The first part of the scheme is the recognition of regularity differences, which are frequently caused by a brain tumor, whose discovery is the main resolve of this algorithm. Presumptuous that the head is allied, the brain borderline is around symmetric, and the image is collected appropriately, the equilibrium axis is parallel to the sagittal plane and rifts the image into two parts of the similar size. Since the scheme is not pixel-based, the accuracy of the determined balance axis is not serious.

A square block, with the side distance of 10 voxels is shaped. This size used in multiresolution line is appropriate for the recognition of both small and large tumors. The algorithm slides through both splits proportionally by this block. The step scope is smaller than the block size to confirm the overlap of specific areas that are likened with its conflicting symmetric part.

The contrast is carried out by the Bhattacharyya coefficient [7], which was also used in [104]. Regularized histograms with the same range are calculated from both parts and the Bhattacharyya coefficient (BC) is calculated from the histograms as follows [7]:

$$BC = \sum_{i=1}^{B} \sqrt{I(i).r(i)} \qquad (3.2)$$

Where B signifies the number of baskets in the histograms, l and r denote histograms of chunks in the left and right hemisphere, correspondingly. The variety of standards of BC is ⟨0, 1⟩, where lesser the value, the greater the alteration between histograms. For the following drives, an Asymmetry coefficient (AC) is calculated as AC = 1 ⊗ BC. The Asymmetry Coefficient (AC) is calculated for all chunks. Since the step size is lesser than the block scope, the overlay is and more standards of AC are current for most pixels. To get the suitable irregularity map, the mean of all standards for an exact pixel is calculated.
The calculated ACs create an irregularity map where the higher value couriers the higher possibility of the tumor attendance in particular place. Examples of such irregularity maps for dissimilar image resolves are portrayed in Fig. 3.3.

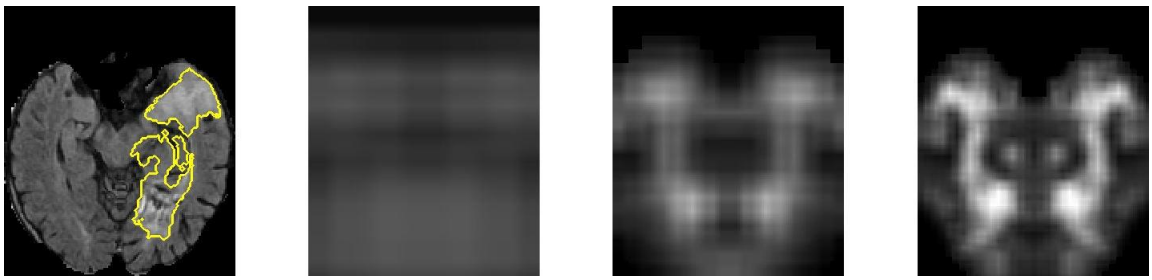

Fig. 3.3: Example of a brain tumor irregularity map for three dissimilar resolutions. The input image is portrayed on the left followed by the irregularity maps with cumulative image resolution.

Multiresolution approach

To make the entire process of the balance examination robust, the image is treated in the similar way in numerous dissimilar resolves with constant block scope. The input image is iteratively sub-sampled by the issue of two. The amount of repetitions done during the regularity examination was experimentally set to three.
The output of all repetition is a map of irregularities for a given resolve where the higher amount denotes higher likelihood of the irregularity attendance. This irregularity

Chart is both sided and, later, the fit regions, where the growth is present at the conflicting side, are also labeled with high likelihood of a brain irregularity. The product of standards consistent to a specific pixel is computed foremost to the final multiresolution irregularity map. An instance of such multiresolution irregularity map is portrayed in Fig. 3.4.

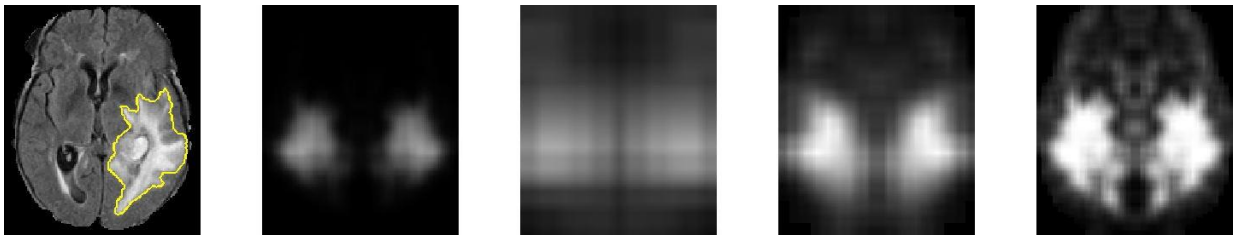

Fig. 3.4: Instance of a brain tumor multiresolution irregularity map. The input image is showed on the left shadowed by the multiresolution irregularity map and consistent single-resolution irregularity maps with cumulative image resolve.

1.2.3Feature Extraction

When we use the irregularity maps that are made for the the removal of extra features that we do not need in our image so as they are used for removal of features which are then used for binary digital medical image organization into two or more then two collections of digital medical images presentation a fit or compulsive human brain. The removed features are given as follows:

- quantity of parts and their size after thresholding the multiresolution chart by an total value,
  all-out of the multiresolution irregularity map,
- extreme of all sole resolution indiscretion map,
- the Amount of areas and their size after thresholding value the multiresolution chart by a relation given value.

Maximum of the Multiresolution Asymmetry Map

Since the projected process of multi resolution asymmetry map is based on identifying a pathological area by the regularity investigation. The key feature is the all-out of irregularity coefficient. Which can be used for the human brain tumor digital image organization. A contrast amid multiresolution map of images with strong brain and brain with tumor resulting from T2 slices is portrayed in Fig. 3.5 (the second descriptions from the left).

Maximum of each Single Resolution Asymmetry Map

The additional and suitable special features are the most of each irregularity resolution asymmetry map is calculated in the former step as we observed closely. Functional dependence of the irregularity coefficient on the image determination is non-descending; it incomes that for lower image resolution, the irregularity coefficient is advanced or equal to that for advanced image resolution. For images with large tumors, this worth is high even for a little resolution, while for small tumors, this purpose reaches the extreme later.

An assessment between irregularity maps of portions with strong brain and brain with tumor consequent from T2w parts is depicted in Fig. 3.5. This figure shows the benefit of the multi resolution method. For the supreme resolution (the greatest right image), high irregularity coefficients exist even for images of fit brains 3.5(a), here mostly due to the imprecise alignment. Nevertheless, they vanish in lower resolutions foremost to their suppression in the final multi resolution irregularity map. On the other hand, as it can be seen in 3.5(b), supreme resolution helps to find the brain tumor area. By using the only lower resolution of human brain MRI 2D digital image would lead to unclear finding.

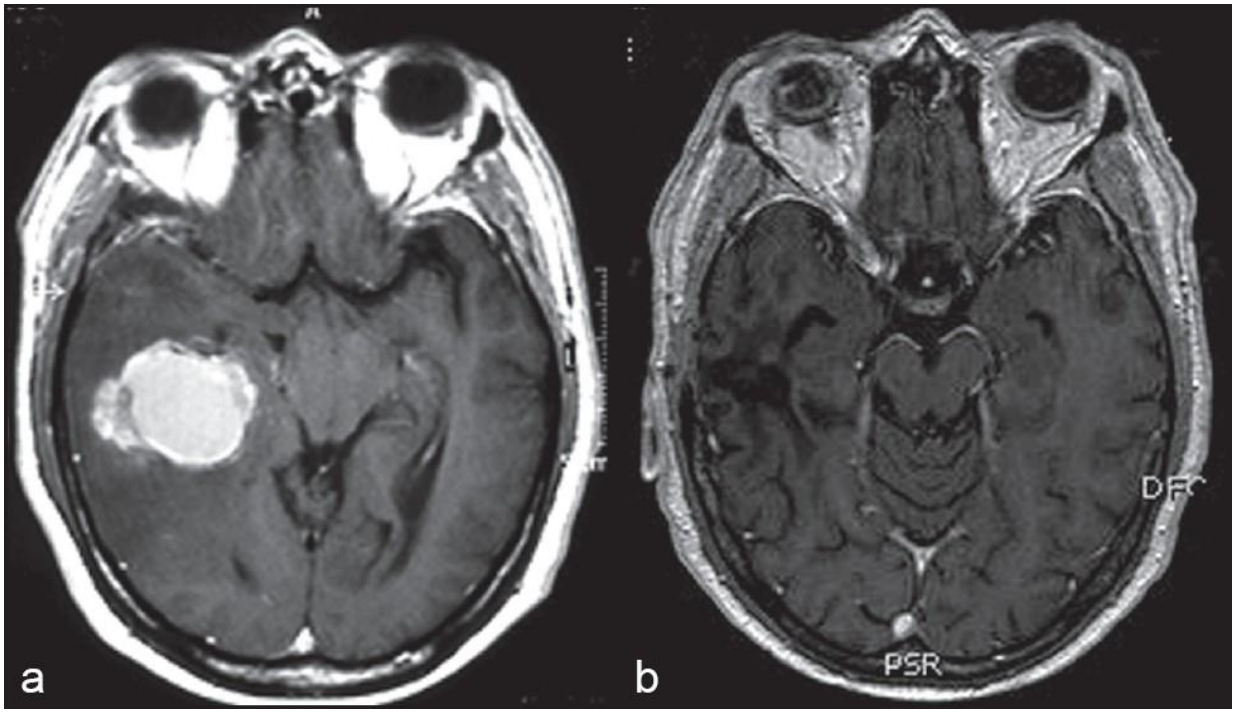

Fig. 3.5: The contrast between the irregularity maps of (a) fit human brain and (b) the brain with human brain tumor and it can be any type resulting from T2w digital image slices. From left to right the original T2w human digital brain digital 2D image portions are shown and the multi resolution of digital image irregularity maps are shown as well and the irregularity maps for three human brain digital 2D images dissimilar single resolutions of image (cumulative from left to right).

A great assessment between the maximum irregularity map for the human brain image which is the 2D for multiresolution image pixels and each single-resolution of 2D image irregularity map in the human cancer brains with a human brain tumor which is in the green color and vigorous sound human brains which is shown in the blue color are presented in Fig. 3.6.

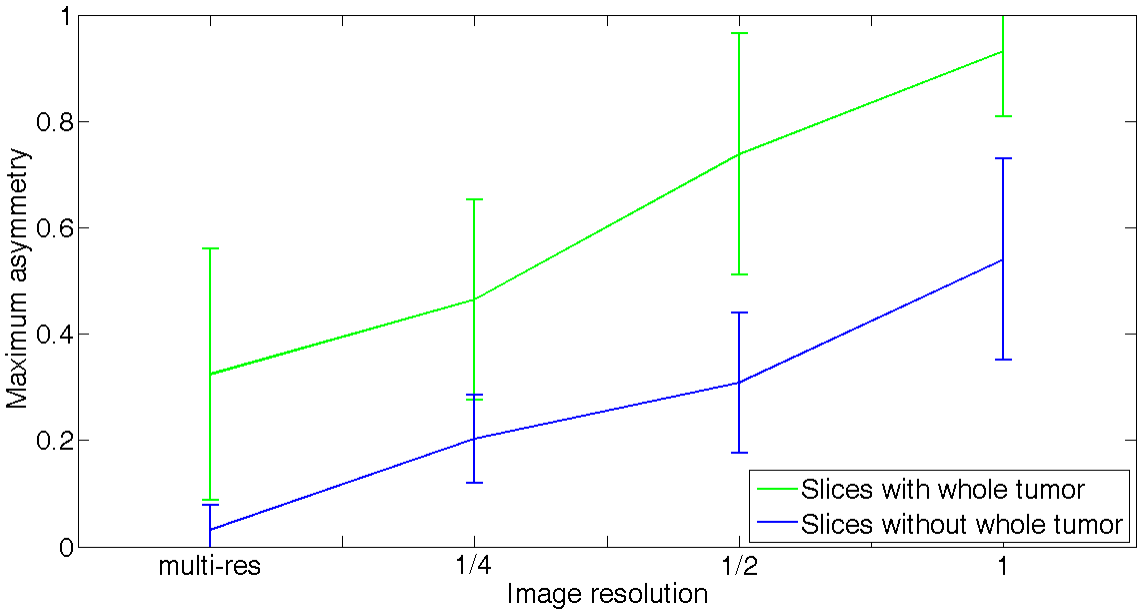

Fig. 3.6: The maximum irregularity Map is used for the multiresolution of digital image and each single-resolution of digital image for the irregularity map in FLAIR MRI digital human

brain image slices for fit tissues and the damaged brains tissues with a high growth which is shown in the green color and vigorous fit brains that is shown in the blue color.

Number of Regions and their Size after Thresholding the Multiresolution Map by an Absolute Value

These topographies of human brain tumor from the MRI image accept that the irregularity map for the 2D digital image of sound vigorous human brain with no brain tumor or cancer covers a smaller numeric value associated to the human brain with the brain tumor of any type. After the thresholding, in case of vigorous brain, there is a slighter number of areas and also a lesser sum of their dimensions. In most vigorous cases, both statistics are close to zero-. Instances of the thresholding value for the irregularity map of human brain tumor image by complete numeric values are shown in Figures 3.7 and 3.8.

Number of Regions and their Size after Thresholding the Multiresolution Map by a Relative Value

For the abstraction of these special brain tumor features from the MRI digital image, the multiresolution irregularity map is threshold by a relative worth computed from the supreme of the plan. It is presumed that for brains with a tumor, there is an important peak in the slice where the tumor is positioned. Hence, for thresholding by a worth derived from supreme, healthy areas are clean out because they are typically much more symmetric. Furthermore, brain tumor is in most cases focused in one location, consequently a lesser number of areas is created by thresholding (see Fig. 3.9).

In case of a vigorous brain, the stuff of the feature is conflicting. The extreme is analogous to the morals in other portions-, so more districts values for the images are human brain tumor digital MRI images shaped by thresh

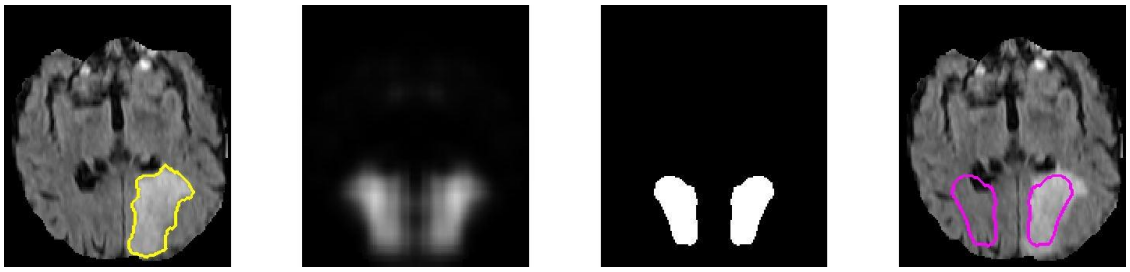

(a)

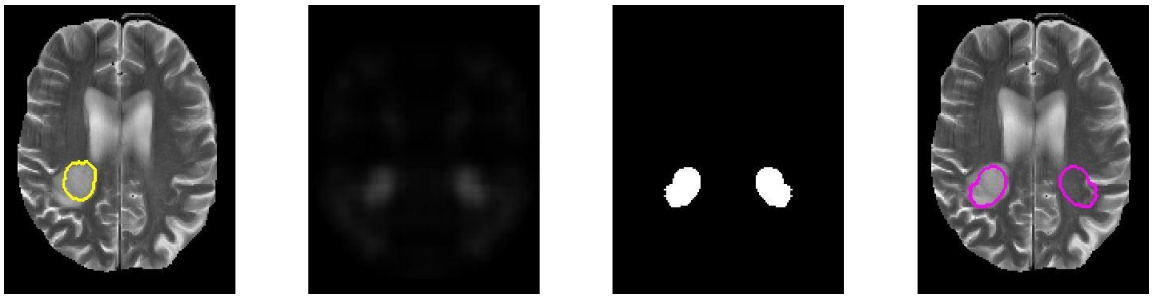

(b)

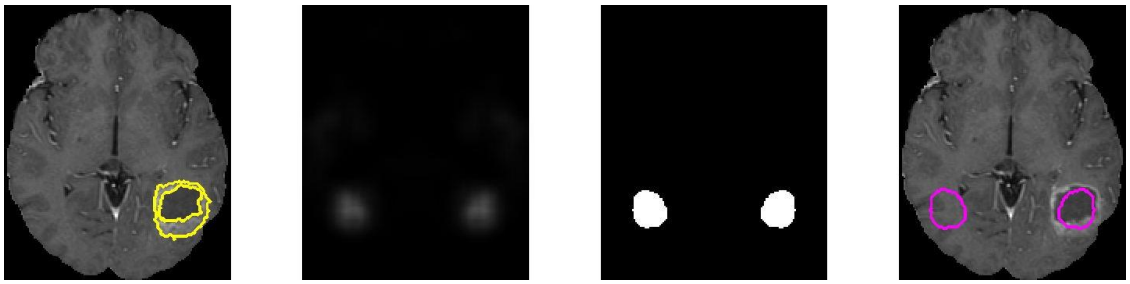

(c)

Fig. 3.7: Instances of thresholding set value in multiresolution in the digital image processing charts by total values. From left to right: input axial slice of digital MRI image with physical annotation (a) entire tumor, (b) tumor core, (c) vigorous tumor and multiresolution irregularity map for the digital image, binary mask after the value of the thresholding is request of the subsequent mask to the input image digital image. (a) Input image which is the FLAIR digital MRI image slice where the threshold value is 0.2 and (b) second input image is the T2w where the threshold value for this image is set as 0.05 and (c) the third input digital image slice is the image with T1w from MRI slice where the value of threshold is set as the 0.05.

Holding the furthermore information that we get is that, they are situated in the entire human brain or cancer patients brain. For human brain tumors the sum of parts sizes may be analogous to the value calculated for vigorous brains, but the number of counties is smaller.
Five dissimilar levels of verge are set for both comparative and complete thresholding foremost to five standards of each feature. Statistical charts of number of areas and their size for both total and comparative thresholding for five dissimilar threshold heights are shown in Fig. 3.10.

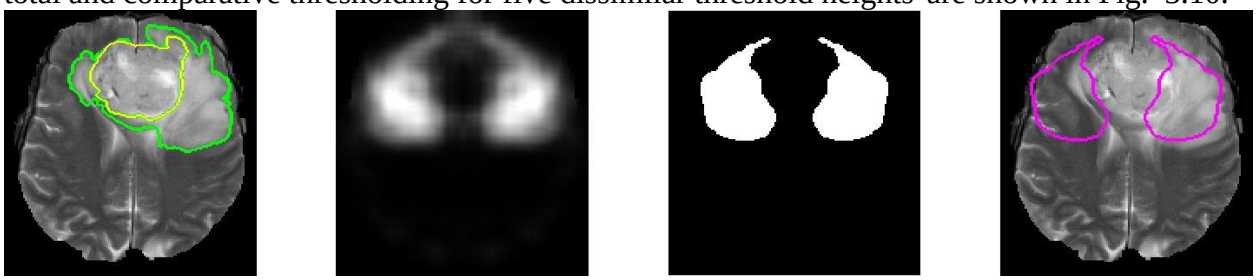

Fig. 3.8: there are certain example of human brain tumor core which is yellow color based and situated on the mid of the sagittal plane in the MRI digital 2D image. Everybody can see that the human brain tumor central positioned was not detected properly from the MRI image using symmetry examination on the images. Nevertheless, edema which contain the green color green which was not located proportionally on the cancer patient's brain was noticed.

(a)

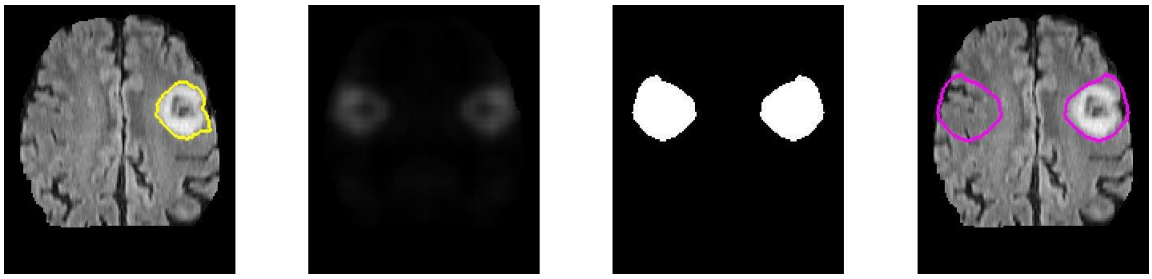

(b)

Fig. 3.9: there is a clear contrast between multiresolution map in the digital human brain image comparative thresholding value which is the 0.2 of the diagram (a) and vigorous human brain and (b) human brain with any kind of tumor resulting from FLAIR MRI digital 2D image slices. From left to right the input axial digital image slice with physical footnote and multiresolution irregularity map for the digital image which is 2D, binary mask after thresholding set value are the request of the subsequent mask to the input digital 2D image.

3.2.4Application to 3D volume

The planned and advance algorithm may also be practical to particular digital image slices in 3D volume capacity. In this case, supplementary set of geographies can be removed. This feature set undertakes that the strengths of the input bulk has been regulated. The pixel strength features are based on the similar multiresolution irregularity map thresholding, but the evidence is extracted from the input share-. For each level of digital image edges four more features are removed from the input 2D digital image after the request of the mask which is created by

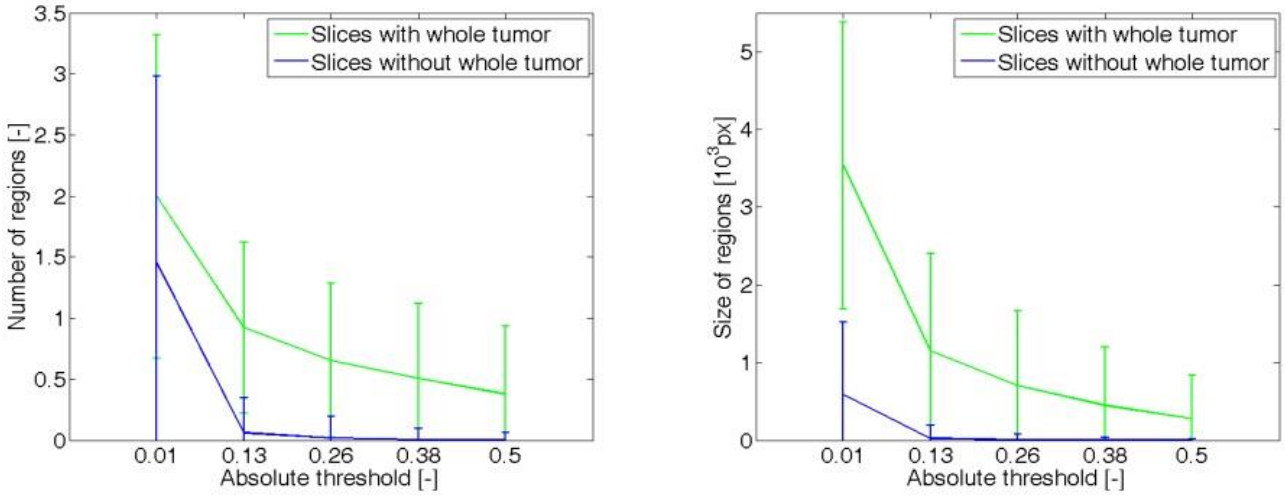

(a) (b)

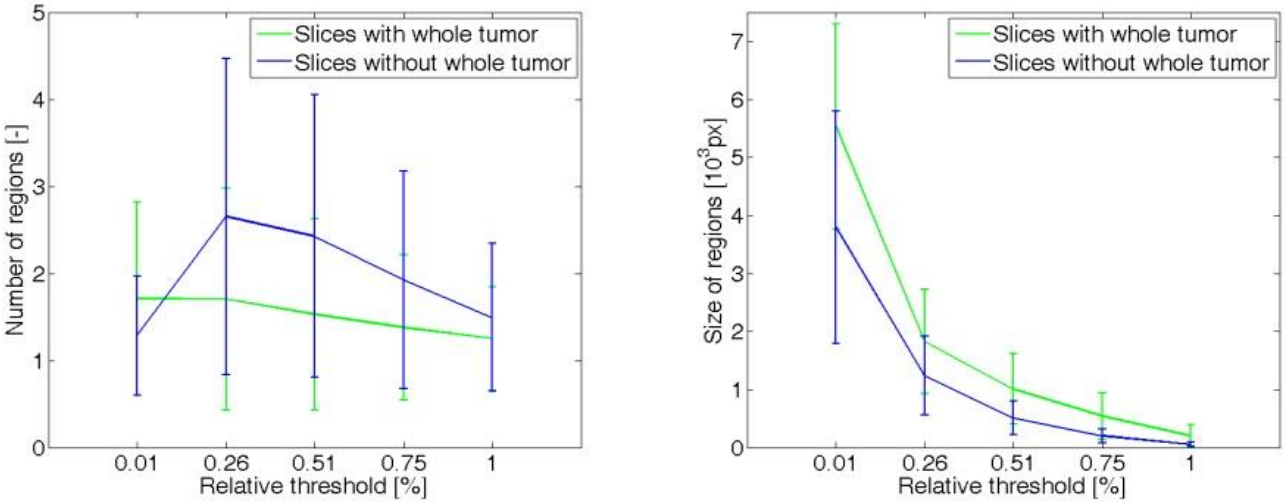

(c) (d)

Fig. 3.10: (a) and (b) shows the number of selected image areas and the sum of their object size for dissimilar absolute threshold set values levels of multiresolution irregularity map in digital 2D images derived from FLAIR MRI digital 2D image slices. (c) And (d) demonstration number of areas in the MRI digital image and the sum of their scope for dissimilar threshold values set and the pixels levels relative to the extreme of a specific pixels multiresolution irregularity map derived from FLAIR MRI 2D digital images slice.

Thresholding. The features are as follows:

- Regular pixel strength in the entire masked area in the MRI images,
- Complete threshold value of the regular pixel strength is alteration in the left and right masked area in the digital MRI images,
- Pixel strength pixel value average deviation in the entire masked digital image 2D area,
- Total value of the total pixel strength is found normal deviation alteration in the left and right masked area in the digital 2D images.

All of these selected features set are calculated for both total and relative value of thresholding calculated value. They are portrayed in Fig. 3.11 and 3.12 where the compulsive digital image slices are signified and show the green color in the graph and vigorous brain slices by blue color in the image.

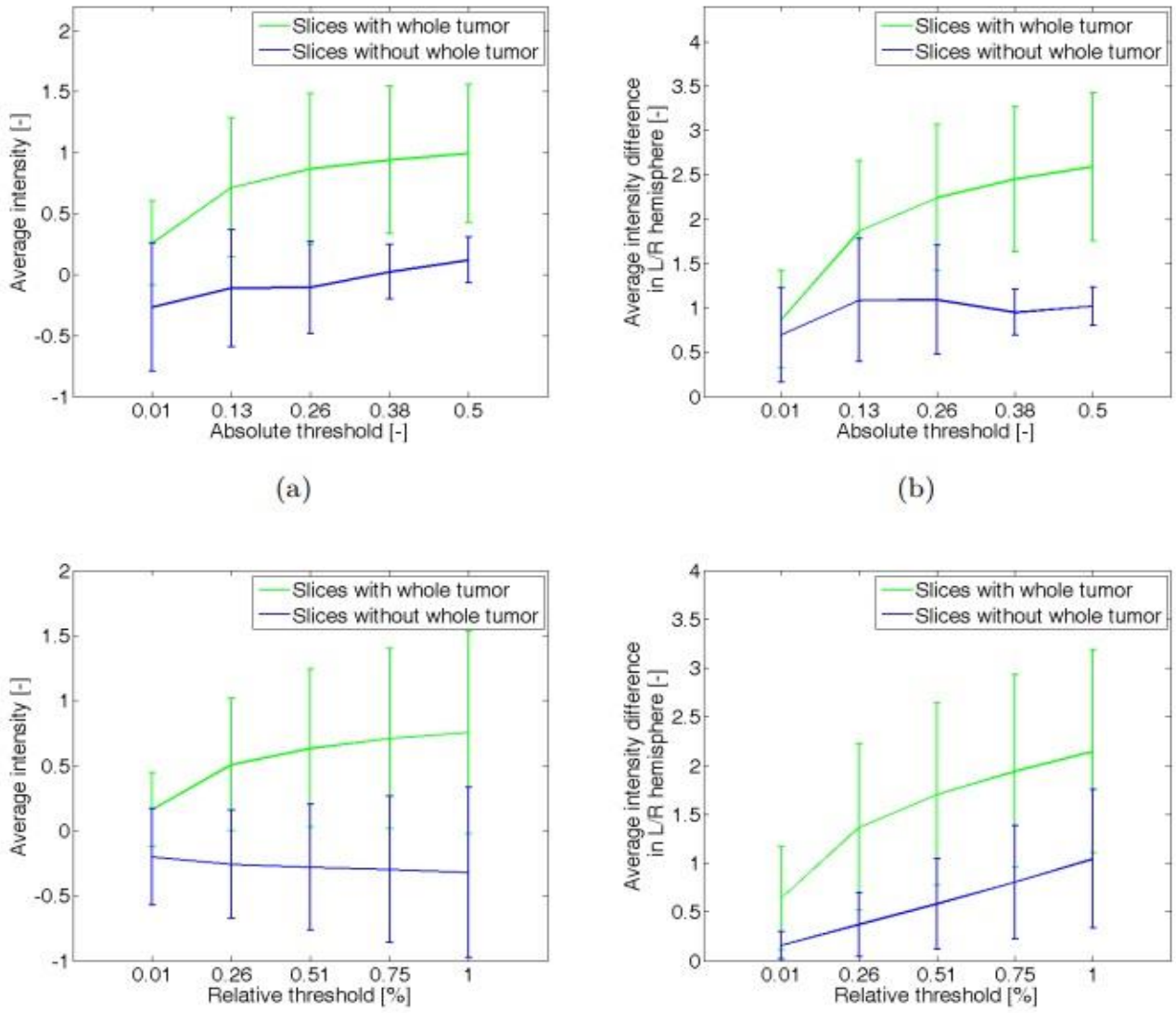

Fig. 3.11: (a) shows the average value strengths of image pixels in the digital image areas of interest within the mask created by total value thresholding of the multiresolution irregularity map for 2D digital MRI image. (b) Demonstrations the absolute total value of the change between average digital image pixel strength in the left and right hemisphere of the cancer patient image. (c) and (d) show the similar results for standards for relative thresholding value as the result.

3.3 Unsupervised brain tumor extraction

The brain tumor type like Gliomas are signified by high level pixel strengths in T2w digital images and FLAIR MRI digital image slice sequences. Though, we are considering the dissimilar measurement of pixels strictures and equipment's the pixels strengths in the resulting MRI of cancer patient's digital image are not recognized by this method. The shared unsupervised learning approach is to regularize the strengths of pixels of MRI images

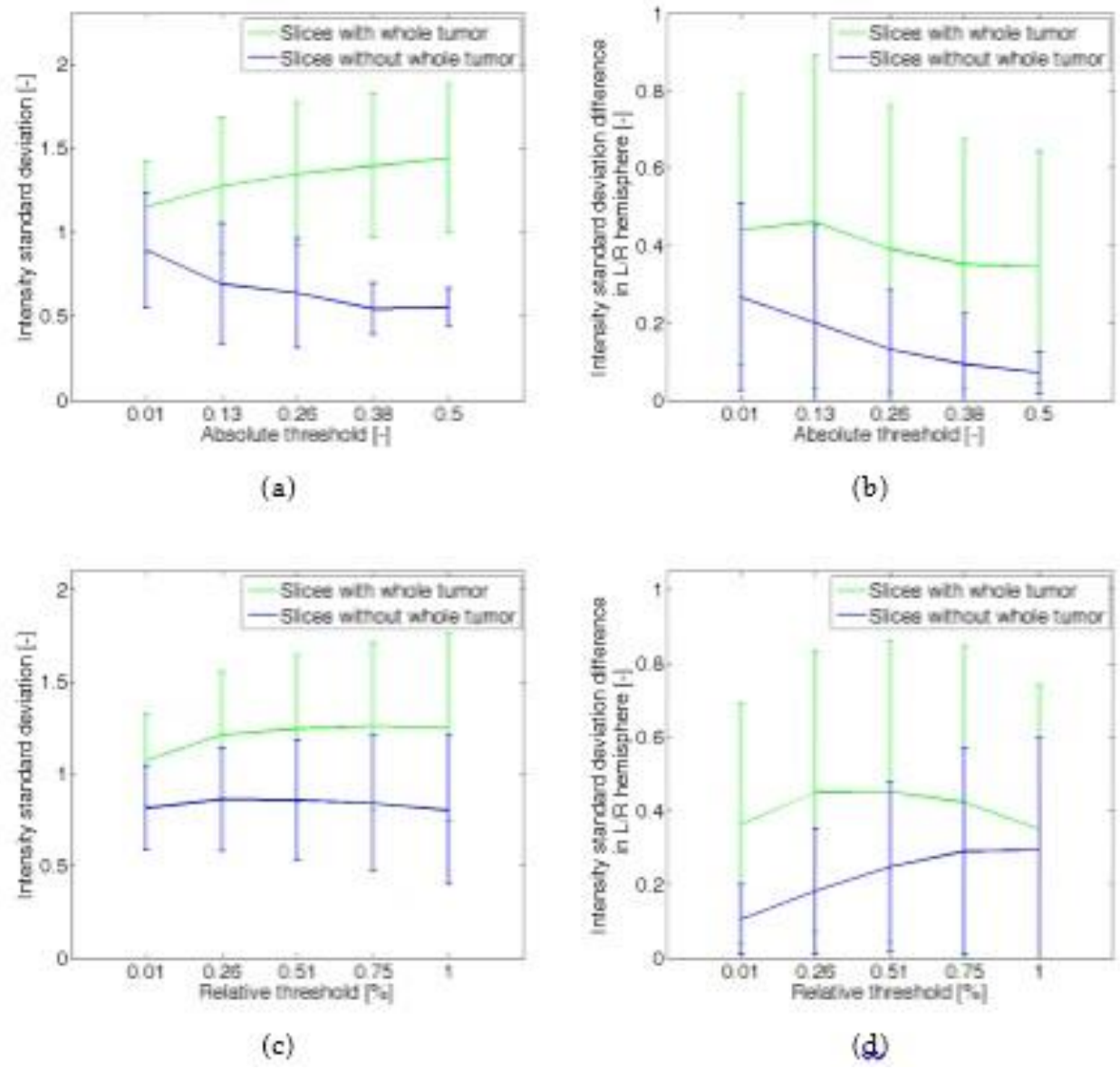

Fig. 3.12: (a) demonstrations the digital image pixel strength in the MRI normal deviation in the digital 2D MRI image areas within the estimated mask created by total value thresholding set of the multiresolution irregularity map used in the digital MRI image. (b) Diagram is demonstrations the total thresholding value of the change between digital image regions pixels and its pixel strength of normal deviation in the left and right hemisphere of the human patient brain. (c) And (d) figures are demonstration the same thresholding values for comparative analysis.

By the calibration or digital image processing histogram matching advance algorithm. As a stand-alone 2D MRI digital image slice sequence, such as the digital 2D image pixels strength in the MRI image standardization is unbearable by machine due to the lack of data and its information about the human brain tumor size in the skull and the part located inside the cancer patients position. Therefore, machine learning methods based on the pixel strength data are not valid here. The planned algorithm avoids the pixel strength standardization by involuntary determination of the pixel strength threshold from the most unequal brain parts. It is based on the same regularity examination labelled in Sec. 3.2. Hence, the system requires the same pre-processing as the scheme projected for the supervised brain tumor recognition. The method can

Be practical for both 2-D image and 3-D volume. Only FLAIR images are used for 2D image request while both orders are used for 3-D volume application. I have previously described this process in detailed in the following papers [116, 128].

3.3.1Pathology extraction

For the medical tests lab molecular pathology or histology of the given samples of human brain tumors got by the biopsy process, its extraction and then resolve. The thresholding of the multi-resolution irregularity map is done by the value of 10% of the extreme irregularity. This charge was set experimentally and confirms that at least small area is removed. The outcome is a both-sided mask that comprises both the tumor on one side and the vigorous tissue on the other side. Since multifocal tumor can seem, the abstraction procedure is not limited to only one area. All areas created by thresholding are measured. As an effect, multi- focal tumors positioned unequally can be properly detected. The perfect area of gliomas can be well detached using FLAIR, since they appear hyper strong in this MRI classification. The insentient thresholding can be done to excerpt these pathological portions. The threshold is firm using the Otsu's system [86] from the points confidential the subsequent mask of irregularity exposure but the thresholding procedure is applied to the entire image. The Rendering to this advance and accurate algorithm projected by Otsu researcher in 1979, the Ideal value of threshold k* for the digital image of MRI is a threshold value with the next stuff is calculated by the following equation as given below

$$\sigma_B^2(k^*) = max_{1 \le k \le L} \sigma_B^2(k) \qquad (3.3)$$

Where L is the amount of 2D digital images pixel strength in MRI standards in the targeted area of the image we get and à2 (k) signifies the between given two classes alteration for the threshold value obtained for the k, which is founded on the next session and its means and is calculated easily by the equation mathematically according to the given equation as follows:

$$\sigma_B^2(k) = \omega_1 \omega_2 (\mu_1 - \mu_2)^2 \qquad (3.4)$$

Where Ω0, Ω1 mean the possibilities of the class rate and Û0, Û1 position for the session mean levels for classes 0 and 1, correspondingly. Morphological erosion and dilation are practical to the subsequent mask to smooth the area limits and distinct regions linked by a thin part. The combination of these masks is then originate. Since some improper zones could be take out, only those, which are located mostly confidential the unequal area, are branded as pathological. Areas with the size smaller than 10% of the largest section are also eradicated. Since the pathological part may range outside the irregularity part edge, the entire area shaped by the thresholding is removed.

3.3.2Extension into 3D

The similar advance algorithm may be applied to 3-D MRI bulk images of human brain tumor as we did for the 2D images in previous sections of this paper. The multi-resolution irregularity map is calculated in the precisely same way but in 3-D instead of 2-D, i.e. cubic chunks are used in its place of square chunks. A sample of a 3-D single-resolution irregularity map is revealed in Fig. 3.13. Figure 3.14 demonstrations an instance of a 3-D multi-resolution irregularity map. I have already defined this 3-D postponement in [122, 148].

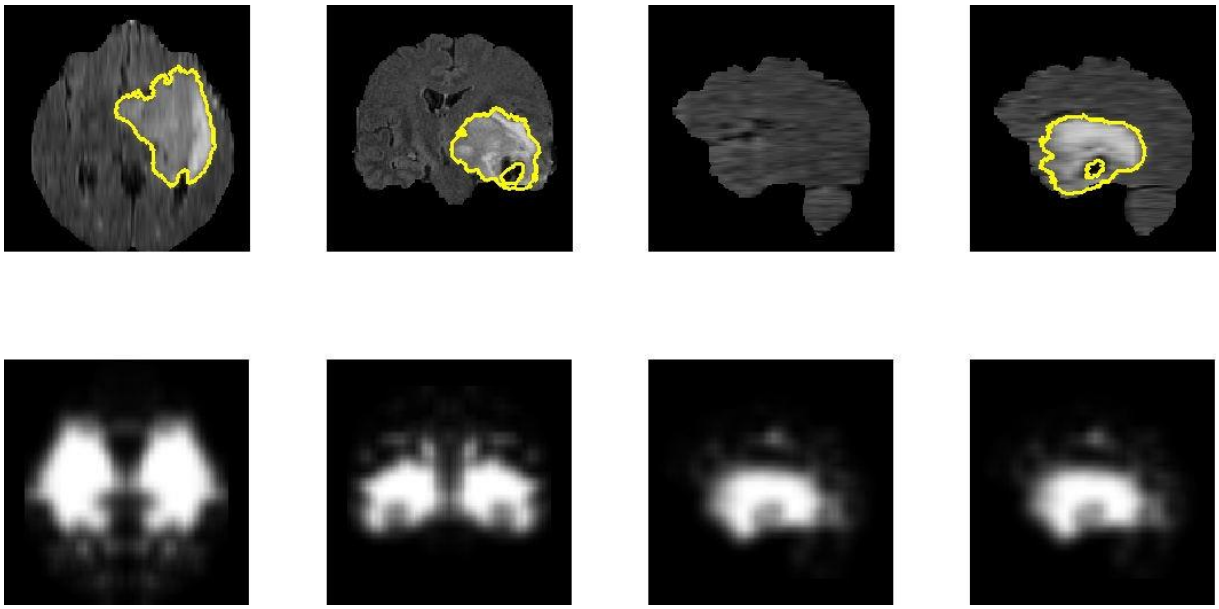

Fig. 3.13: The sample of the human brain tumor types like astrocytoma's irregularity map for the image on real statistics got by the MRI machine of high-grade human brain tumor types like gliomas for the extreme digital MRI image resolution. The higher row demonstrations FLAIR slices with the uppermost AC with ground truth physical comments. The inferior row shows the 3-D irregularity maps in the consistent slices.

The abstraction of features form the digital image for the brain tumor procedure starts in the axial slice portion of the image where the uppermost AC was noticed and it is then spread into the entire 3-D volume. Such tactic is more precise than the abstraction straight from the 3-D irregularity chart. Though, it is somewhat sluggish. For 3-D abstraction determination, T2w volume is used composed with FLAIR image to expand the precision. Since brain tumor looks hyper-intense in both T2w and FLAIR images, the similar algorithm is practical to both sizes and their connection is found. The benefit of the mixture of both orders is portrayed in Fig. 3.15. An sample of the calculated threshold from unequal area in T2-weighted and FLAIR image of the similar portion is depicted in Fig. 3.15(a), where histograms of the full unequal area (blue bar diagram), the factual pathological area (green curve) and the calculated thresholds (red line) are revealed. The grouping of both images and their thresholding is displayed by a sprinkle diagram in Fig. 3.15(b). As it can be understood by the given diagram.

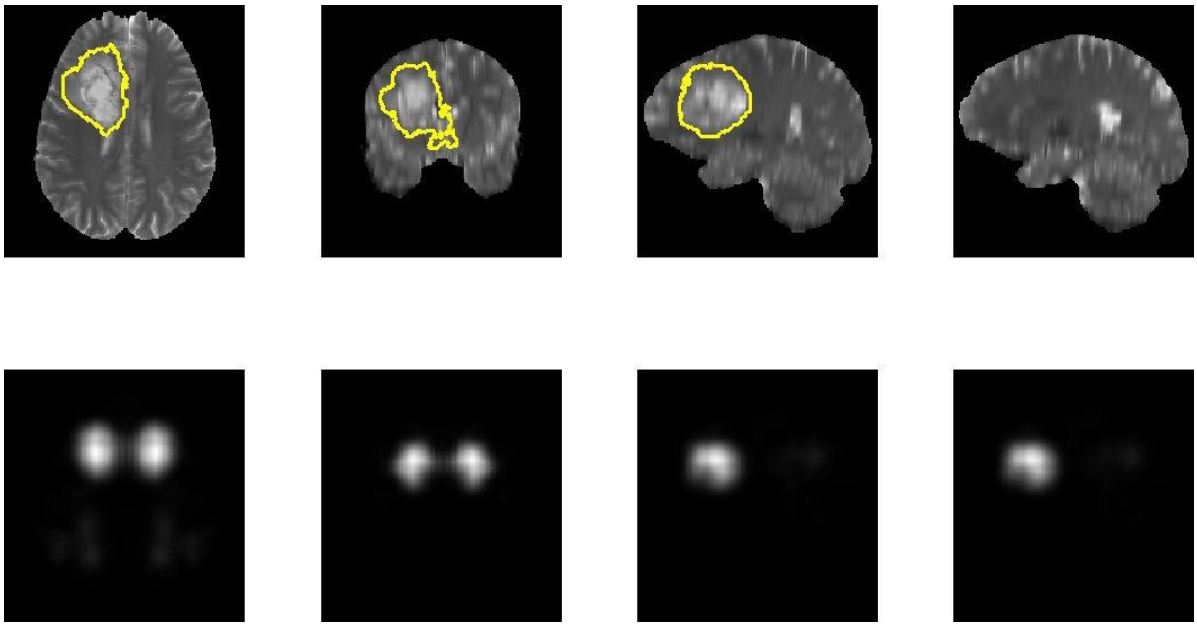

Fig. 3.14: The sample of a the human brain tumor MRI image is possibility map on different sizes of brain tumors from real statistics got from the MRI machine and of the little grade for example grade one or maximum grade two brain tumor type like glioma brain tumor. The higher row shows T2w portions with the uppermost AC and conforming manual explanations. The lower row demonstrations the irregularity charts of the consistent slices in both these facts, the pathology could not be detached correctly in neither of them, but mixture of both brings upgrading. The re subsequent mask M of the abstraction process is formed as M = Mt 2 π M flair, where M*T* 2 and M*F LAIR* signify the thresholding mask of T2-weighted and FLAIR image, correspondingly. This resembles to the pixels with strengths situated in top Right Square in Fig. 3.15(b).

Propagation into Neighbor Slices

Once the medical test like molicular pathology or histology is take out from the axial slice sequence portion of the digital image with the uppermost irregularity coefficient set for the image, it can be spread into other portions. At first both 3-D sizes are thresholded using the precise threshold ideals resolute in the first slice with the maximum irregularity. In order to circumvent abstraction of vigorous zones far from the pathological ones, the spread of mask assessed in neighbor portion is essential. The propagation procedure starts with together neighbor axial slices and remains in both guidelines. The outcome for n-th slice from the digital MRI image can be certain as:

$$M(n) = Mt\ 2\ (n) \cap MFLAIR\ (n) \cap MD\ (n \circ +\text{-}1)\ , \qquad (3.5)$$

where MD (n +- 1) is the opened mask from neighbor slice portion from the digital image where the sign be contingent on the broadcast way.

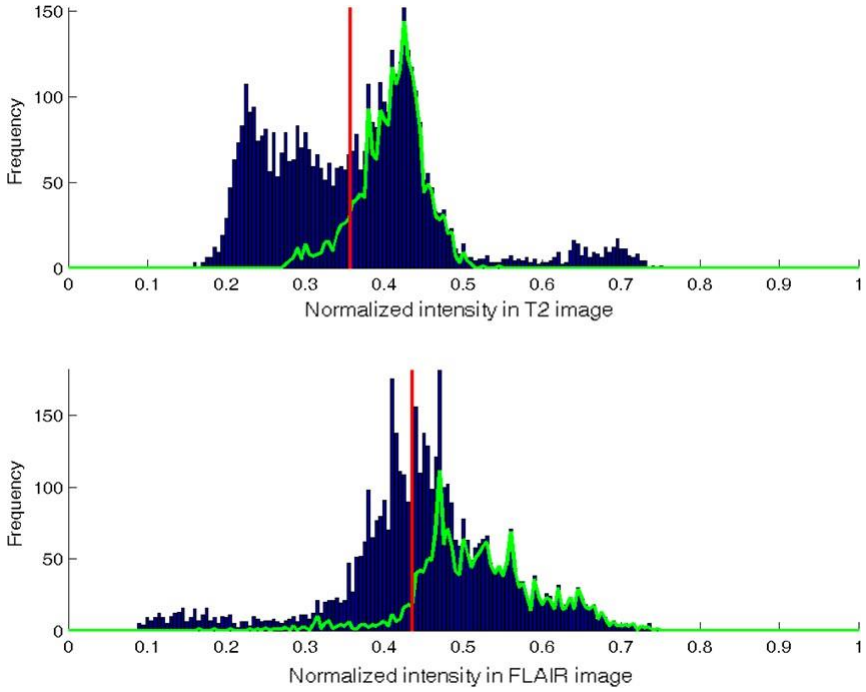

(a)

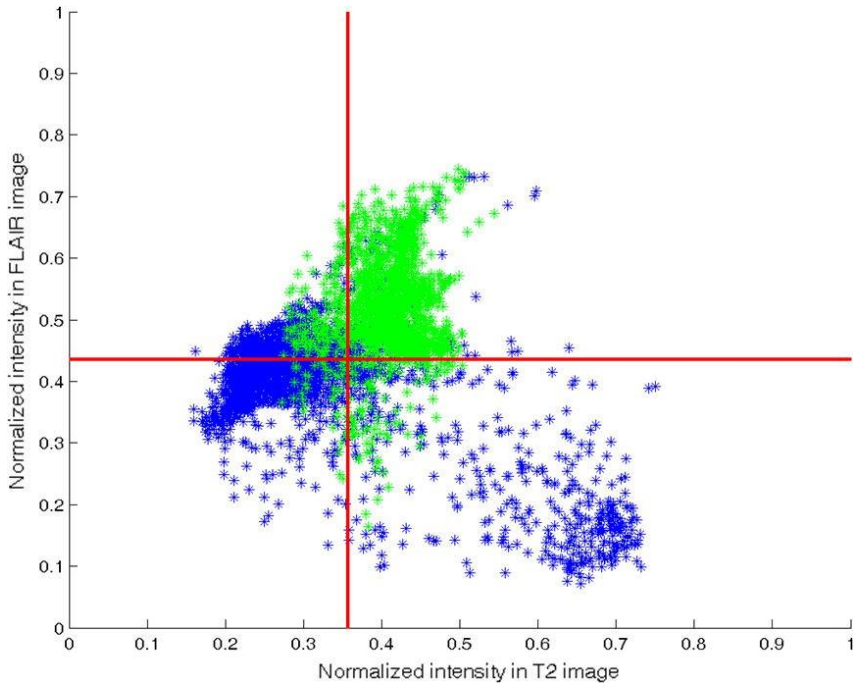

(b)

Fig. 3.15: The sample of tumorous pixels in the cancer patients MRI image is purpose using Otsu's advance algorithm for T2w digital image and FLAIR MRI image of extraordinary grade like the grade 3 and grade 4 brain tumor type like glioma (a) distinctly and (b) together. Blue color is used in the graph the whole unequal area of human brain tumor. Green color is used in the pathological zone in the graph. Red color is used for the calculated thresholds values for the MRI image.

3.4 Brain Tumor Segmentation using Structure Prediction

In spite of the achievement of patch-based classification in medical image explanation, and the extremely tedious local tag construction in many applications, the idea of local assembly forecast as defined in Chapter 3 has not received devotion in the dispensation of 3-D medical image yet.

Nevertheless, methodologies classification super voxels rather than pixels has previously seemed, e.g. hierarchical subdivision by weighted aggregation lengthy into 3-D by Akselrod-Ballin et al. [2] and advanced by Corso et al. [20], or spatially adaptive chance forests presented by Geremia et al. [42]. Numerous structure-based approaches has also been used in medical imaging but only at worldwide level, where the form of the complete segmented structure is measured, e.g. [91, 132]. Here, the offered work will focus on indigenous structure since comprehensive structure is not appropriate for items with some profiles and sites such as brain tumors.

The projected system allocations the impression of local structure prediction [29] by patch-based tag vocabularies to the task of thick tags of pathological erections in multisequence 3-D volumes. Different from Dollar, convolutional neural networks are used for forecasting tag patches as they are well suitable for dealing with local association, also in 3-D medical image explanation tasks [71] [93].

The brain tumor separation unruly comprises of three sub-problems: classifying the entire tumor area in a set of multisequence images, the tumor essential area, and the active tumor area [80]. All three sub-tasks are treated distinctly, which variations the multi-class division task into three binary subdivision sub-tasks. The innovation of this work lies in the righteous mixture of the deep learning style together with local structure forecast in the medical image division
task.

In this chapters section we just overview to the employed clustering technique and the classification method approaches is given below in detail by the followed explanation of the projected technique which is the acknowledged for publication of the research [135].

3.4.1Patch Clustering

The patch clustering technique is used for the group of a tag patch builtin dictionary for the digital image processing. k-means described algorithm is used for this determination process to get our results.

k-means

k-means is an iterative clustering algorithm diminishing the quantity of distances from each facts sample to its allocated centroid. The goal is to divide observed examples into k collections with alike properties, where k has to be selected before the algorithm starts. The algorithm typically starts with k arbitrary centroids designated from the explanations. It is followed by irregular between two steps. In the first step, reserves of all statistics samples to each centroid are calculated followed by transfer all data samples to the adjacent centroid. In the other step, centroids of each group are re- calculated. These two steps are recurrent until no cluster task change occurs, or predefined extreme number of repetition is reached. The labelled algorithm

frequently leads to a local best. This is usually overwhelmed by numerous independent grouping with arbitrary initial centroids.

3.4.2Patch Classification

The convolutional neural network which is known as the CNN as well is used as a organization of described advance algorithm as it has the great benefit of conserving the pixel set for 2D and spatial structure for three dimentional MRI images of the input, for example the 2-D grid is used for the digital MRI images for cancer patients. It is one type of the current Deep learning DL approaches in this research paper.

Deep Learning (DL)

Deep learning (DL) is a new classification style based on Neural Networks. It varies from other classification algorithms such as SVM or RF in the method how features are well-read. In traditional method, features are take out earlier the learning of the classification algorithm starts, and they have to be quantified by the algorithm designer. In DL method, structures are learned and stated by the classification algorithm itself based on assemblies and designs in the training data. The algorithm hunts for significant characteristics of the statistics, which may help in the choice procedure. One of the aim of D-L is to substitute hand-crafted features with programmed feature extraction and unsupervised or semi-supervised feature knowledge algorithms. In image processing, numerous D-L algorithms have been used, such as Deep Belief Network (DBN), Stacked Auto-encoder (SAE), Deep Boltzmann Machine (DBM), or Convolutional Neural Network (CNN). CNN is used in this effort, and hence it will be defined in detail.

Neural Network (NN)

Neural network (NN), sometimes also named Artificial neural network (ANN), is a statistical learning process inspired by the human brain. NN contains of a set of simple artificial neurons which are linked together to create a system. These networks are distinct by adaptive bulks, which are tuned throughout the learning process. NNs were extensively used for classification tasks, nevertheless, they were slowly swapped by simpler approaches such as SVM due to the computational stresses of NNs. Their admiration started to growth again after the overview of the deep learning method and its achievement in numerous international image and speech acknowledgement challenges. A lot of dissimilar varieties of NN sorts exist. Since this work makes use of Convolutional Neural Network, only this kind will be defined in detail.

Convolutional Neural Network (CNN)

The convolutional Neural Network (CNN) is one of the D-L methods styles which was announced by the researcher known as LeCun et al. [96] in 1991. They used it for handwritten number acknowledgement. Excluding input and output layers, it is encompassed of one or more convolutional layers, one or additional combining layers and a completely linked layer. Convolutional and combining layers are typically in irregular order. A pooling layer is frequently called sub- sampling cover since the goal of this layer is to subsample the output of the preceding layer in order to decrease alteration. The back-propagation algorithm is hand-me-down for system weights learning. This architecture is calculated to take the compensations of a 2-D grid input, which is suitable for image dispensation. In numerous current works [93, 122], 3D filters have been anticipated for medical image examination. But, it was revealed by

Prasoon et al. [93] that it is motionless too difficult to be professionally used in today's computers. They planned a dissimilar methodology for 3-D medical images, which they named a triplanar CNN. They used a 2-D system for each orthogonal plane distinctly, i.e. three sovereign networks were trained. Roth et al. [101] announced a so called 2.5D CNN. The process abstracts consistent patches for a given pixel from each orthogonal plane and charts them as parted input eye maps, i.e. input frequencies. Zikic et al. [137] planned a process where 4-channel 3-D patch of size d1 × d2 × d3 × 4 is understood as a 4 ≤d3-channel 2D patch of extent d1 × d2 × d3 ≤ 4. In this case, d3-times extra 2-D convolutions are completed likened to humble 2-D network in its place of 3-D convolutions. The input of the system is a 2-D image patch of a sure size and a number of networks (e.g. three frequencies in RGB case), and the output is a likelihood distribution of patch fitting to each class. An specimen of a CNN architecture, which was used by Krizhevski et al. [60] for image cataloguing., that is portrayed in Fig. 3.16.

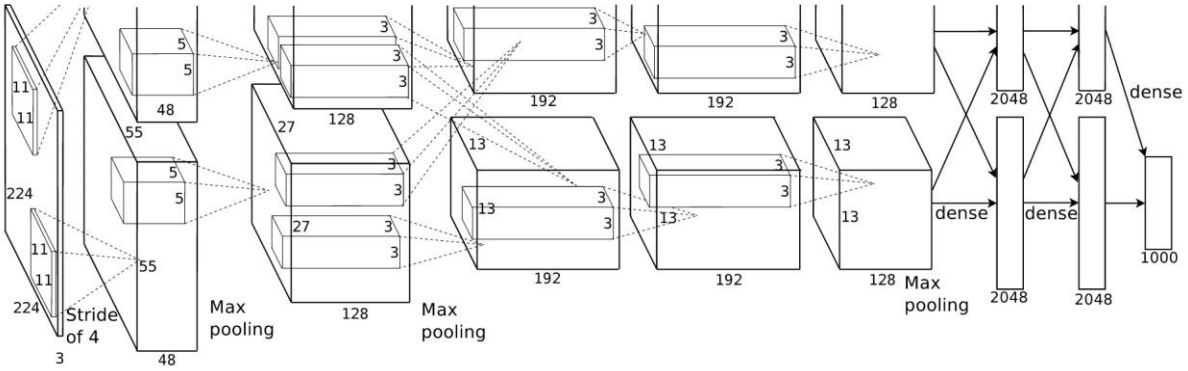

Fig. 3.16: The example of a CNN technique is a style of the deep learning in the image processing. This complete proposed system was used by researcher known as Krizhevski et al. [60] for image grouping in the digital image processing.

Convolutional layer. The critical part of the construction, which also gave the designation to this network type, is a convolutional layer [67]. There can be one or additional layers of this category. An erection block of such layers is a convolutional riddle of a predefined kernel size and measurement. Here, normal 2-D filters are be recycled. The amount of kernels in a given layer and their size is one of the system parameter, which has to be quantified before training. Based on the request, delinquent difficulty and image resolution, this number may meaningfully diverge. Filter kernels are usually haphazardly prepared and they are tuned through the training phase by the back-propagation algorithm. Productions of convolutional layers are also identified as features or feature charts since convolutional filters are de facto feature extractors. The change among common feature extractors and feature extractors used in CNN is the detail that they are learned right from the records instead of being hand-crafted. The activation of a feature chart oℓ, a J-th map in a convolutional layer ℓ, is
Calculated using the equation [10]:

$$\sigma_j^l = f\left(\sum_{i \in M_j^l} \sigma_i^{l-1} * k_{ij}^l + b_j^l\right) \qquad (3.6)$$

Where the described equation function denoted as the f (.) and symbolizes a non-linear beginning function, which is characteristically the sigmoid function (f (x) = (1 + e-x)-1) or the hyperbolic curve function (f (x) = (e2x -1)(e2x + 1) -1), bℓ is a bias, Mℓ signifies a selection of feature maps, and kℓ is a kernel used in the previous layer. A cataract of irregular convolutional and sub-sampling layers produces a hierarchical cascade of feature extractors anywhere first layer extracts low-level topographies while the last layer abstracts high-level features. High-level features are mined from

lower level features, and only features from highest level are used in the final sorting. A specimen of an input and the matching output of a convolutional layer with six filters are portrayed in Fig. 3.17.

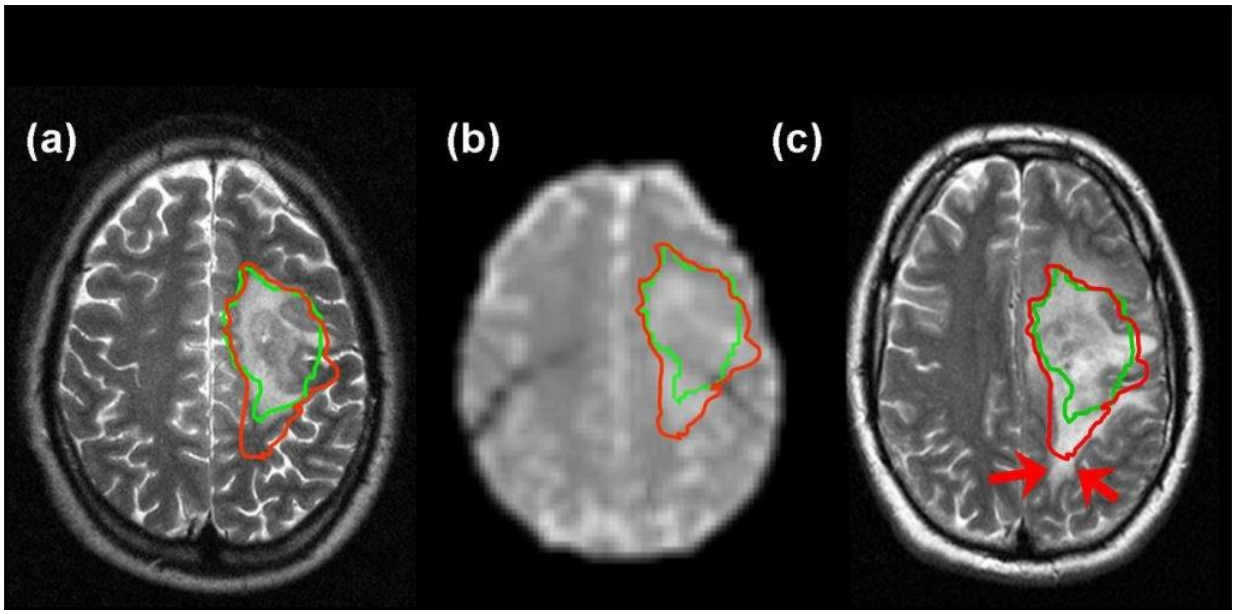

Fig. 3.17: The specimen of figure (a) is an input to the proposed system in the format of 4@24×24 pixels in the digital image that we used for input the designed system and (a) the it is quite suitable output is produced in form of 6@20×20 pixels of a convolutional layer CNN with the seven filters are used of kernel size 5 in the system that produced that output pooling layer.

The combining of pixels clusters that has the same characteristics occasionally called sub-sampling of the image pixels, layers are used for subsampling of the output of the preceding, usually convolutional, layer. This operation makes the network more vigorous to modification. Initial networks used mean-pooling style, where the normal of a receptive field, a non-overlapping squared section used to derive one output worth, was spread to the next layer. In recent years, max-pooling methodology, where the average value is changed by the extreme value, has been familiarized. A given demo of maximum pooling progression in the system that is known as the maximum pooling layer with a rate of pooling is 3 is revealed in Figure. 3.18.

156	150	150	141	138	122	125	125	120
165	155	151	140	135	129	126	124	121
159	152	149	140	128	130	128	127	123
148	145	140	135	131	126	123	125	122
146	142	143	130	130	128	121	120	128
149	140	138	130	129	130	119	118	122
135	135	133	129	134	130	125	128	126
130	135	130	129	135	131	120	130	132
131	130	138	140	138	134	137	131	135

→

165	141	128
149	135	128
138	140	137

Fig. 3.18: The demonstration of the maximum pooling procedure is shown in the above diagram. The Picture of demonstrations procedure and input size and the suitable output for use that we want or we need from the maximum pooling procedure layer system with a pooling rate of 3 is shown in the diagram above.

That is a fully connected with each other in form of layer. The last part of the network, fully associated layer where all neurons of one layer are linked to all neurons of the next layer, is related to a usual NN. All outputs of the preceding layer, either convolutional or pooling, are repositioned to a vector, which performs as an input to a traditional NN architecture. In fact, this is a feature vector take out from the input patch. The output o of the fully linked layer, which is the last network layer L-, is defined as [10]:

$$\sigma = f(W^L \sigma v^{L-1} + b^L) \qquad (3.7)$$

Where the WL parameter used in the equation is the one matrix of different types of masses, ovL-1 is a vectored output of the preceding layer and bL is a bias vector. This portion of the system is occasionally called multi-layer perceptron (MLP) since it may contain of additional layers. Back-propagation. Back-propagation, a shortening for retrograde propagation of faults, is a typical algorithm used for weights approximation throughout the learning phase in NN. It is based on the calculation of a cost function gradient with esteem to the network weights. The cost function procedures the distance between the predictable output and the assimilated output of the network for all training illustrations. Back-propagation algorithm for NN and CNN will be fleetingly designated here, more detailed data can be found in [8, 10, and 65]. The squared-error price function E for C modules and N training samples is well-defined- as in the equation below,

$$E = \frac{1}{2}\sum_{n=1}^{N}\sum_{c=1}^{C}(l_c^m - y_c^n)^2 \qquad (3.8)$$

Where the l cn is signifies the c-th element in the equation or in the image of the label vector of the n-th illustration and the equally yc is the c-th element of the network's output vector for the n-th input.
Let define the output o of a layer ℓ as:

$$o\ell = f(u\ell),\ u\ell = W\ell o\ell\text{-}1 + b\ell, \qquad (3.9)$$

Where function f (.) Signifies again a non-linear beginning function. For fully associated layers, the back-propagated error Óℓ is calculated as:

$$Ó\ell = f(u)lW\ell+11\ Ó(\ell+1)\lfloor \diamond f'\ u\ell\lceil \qquad (3.10)$$

where ◇ stands for the element-wise increase, and f ′(.) is the unoriginal of the start function. For the output layer L, the inaccuracy is intended as:

$$ÓL = f'(u)\ l\ u\ell \diamond (yn - ln) \qquad (3.11)$$

The gradients are calculated for this as:

$$\nabla w\ \ell\ E = o\ell\text{-}1 \qquad (3.12)$$

$$\nabla \ell \, E = \acute{O} \ell. \quad (5.13)$$

The weights and prejudices are updated giving to the instructions:

$$\Delta W \ell = -\curlyvee \ddot{O} \nabla w \, \ell \, E, \quad (5.14)$$

$$\Delta b \ell = -\curlyvee \nabla b \ell \, E, \quad (5.15)$$

Correspondingly where the Ö states the machine or deep learning rate with the help of the DL technique. For the balancing act the convolutional CNN and the subsampling layers for digital image pixels the fault in it is the j-th kernel set in ℓ-th layer is assessed as

$$\delta_j^l = up\left(\left(W_j^{l+1}\right)^T \delta_j^{(l+1)}\right) \circ f(u_j^l) \quad (3.16)$$

Where up is a modest function which up models the input by tiling each pixel in horizontal and vertical way. It's up sampling issue is the same as the sub specimen factor of the present pooling layer. It analyses the fault with respect to the subsampled parts. Gradients are calculated as:

$$\nabla_{k_{ij}^l} E = \sum_{u,v} (\delta_j^l)(\rho_i^{l-1})_{uv} \quad (3.17)$$

$$\nabla_{bj} E = \sum_{u,v} (\delta_i^l)_{uv} \quad (3.18)$$

Where Pℓ-1 signifies a patch from aℓ-1 that was increased element-wise by a kernel

$k\ell$

K throughout the convolution while the component at the location (u, v) of the output Convolution map xℓ was calculated. Since convolutional kernels are practical over the whole input maps, the amount of networks is much advanced than the number of weights. This means that weighs are common and there are less parameters than in regular NNs.

Proposed CNN architecture

The CNN architecture used in this effort is portrayed in Fig. 319. It contains of two convolutional and two mean-pooling layers in irregular instruction. In both convolutional layers, 24 convolutional screens of kernel extent 5 × 5 are used. The input of the system is an image patch of extent 4 × d × d (four MRI orders are present in multisequence capacities) and the output is a vector of distance N representative association to one of the N classes in the tag patch dictionary.

A specimen of patch broadcast through the projected network is portrayed in Fig. 3.20.

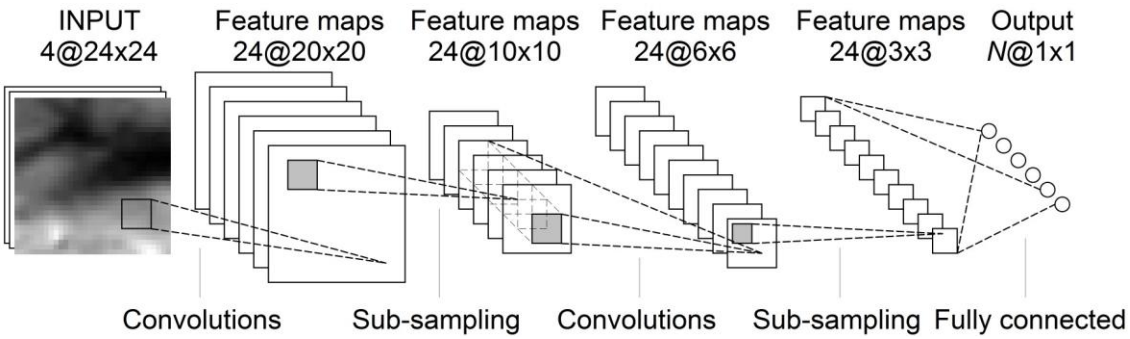

In Figure 3.19 the architecture layers of the CNN for d = 24 and the input size of the network used to process is a multi-sequence MRI generated 2D digital image patch. The output of the proposed system are N possibilities that we get, where N signifies the extent of a label patch dictionary for digital images MRI images.

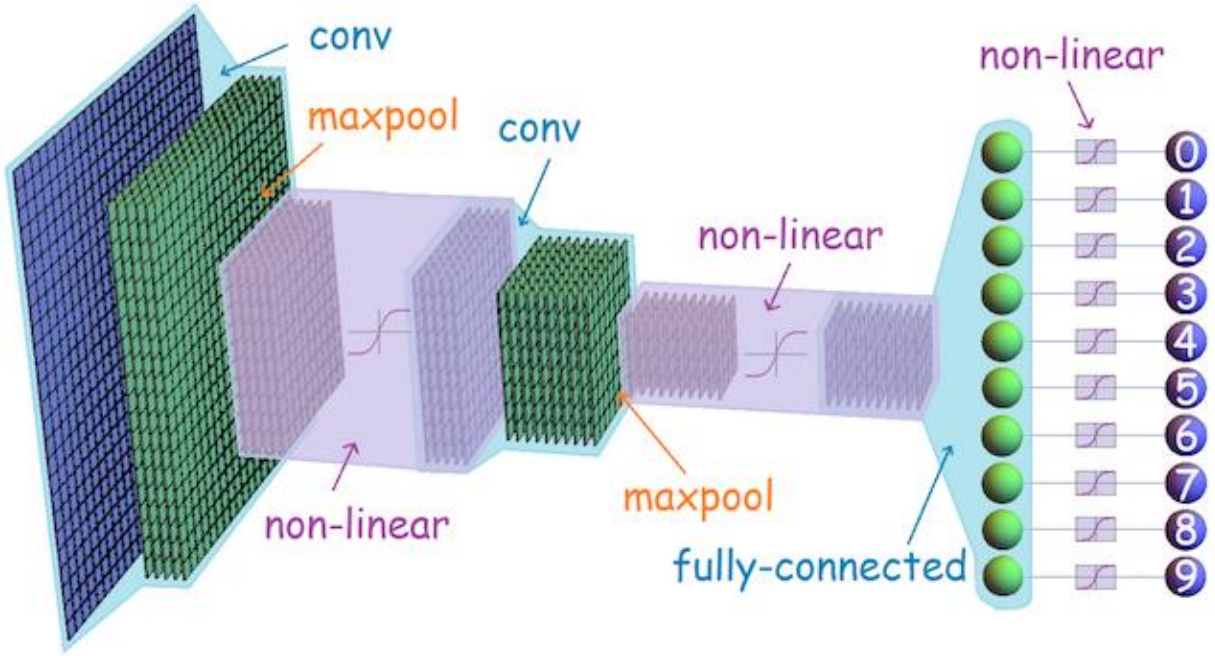

Fig. 3.20: the example of a selected patch spread through the proposed system and the outputs of all network layer is obtained.

3.4.3Local Structure Prediction

This unit defines an original method for classification-based medical image segmentation procedures, which lies in the principled mixture of a deep learning methodology composed with local structure forecast in the medical image segmentation job. This methodology takes the benefit of the fact that greatest medical images feature a great resemblance in the strengths of nearby pixels and a strong association of pixel strength outlines across dissimilar image modalities. One method of dealing with – and even abusing – this association is the use of native image patches. In the same approach, there is a tall correlation between nearby tags in image footnote, a feature that is cast-off in the “local structure prediction” of indigenous tag patches.

Let x be the image patch of extent d × d from the image space $\mathcal{I}$. Concentrating on 2-D patches, a patch x is signified as x(u, v, I) where (u, v) signifies the patch top left corner organizes in a multisequence image I(s, V) where s symbolizes the slice place in a multisequence volume V.

Label Patches

The explanation task for each and every class separately, a tag space $\mathcal{L}$ = ¶0, 1◊, which is given by an expert's physical segmentation of the pathological assemblies, is gotten. The label patch is then a patch p of size d′ × d′ from the organized tag space p, i.e. p = $\mathcal{L}$d ×d . The label size d′ is equal or lesser than the image patch size d. The label patch p is placed on its conforming image patch x (Fig. 3.21), and it is characterized as p(u + m, v + n, L) where L(s, W) is a physical segmentation in a share s of a label volume w and m signifies the boundary defined as m = 1/2 (d - d′). Best standards for d and d′ and, hence, the ratio r = d/d may vary depending on the assembly to be segmented and the image resolution.

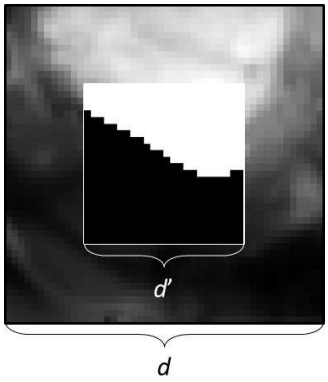

Fig. 3.21: The local infrastructure for the forecast purposes the digital MRI Image feature extraction for patches with the help of side distance described as d are used to patch forecast the greatest probable label patch which is with side distance ′d again in its midpoint that we select manually. Meanwhile the standard patch from the midpoint manual selected based forecast purposes that use the approaches use d′ = 1 which is shows the quantity of pixel taken the projected methodology deliberates all the standards with 1 ≤ d′ ≤ d.

Generating the Label Patch Dictionary

Label patches p are gathered into N groups using k-means foremost to a label patch vocabulary of size N. Next, the label template t of a collection n is recognized as the average tag patch of a given group. In the segmentation procedure, these smooth tag templates t are then used for the segmentation chart calculation rather than strict edge prediction as used in preceding local structure forecast approaches [16][58][135]. The structures are learned straight from the training data instead of using predefined collections as in [135]. A sample of ground truth label patches with their representation by a dictionary of size N = 2 (consistent to mutual segmentation style) and N = 32 is portrayed in Fig. 3.22.

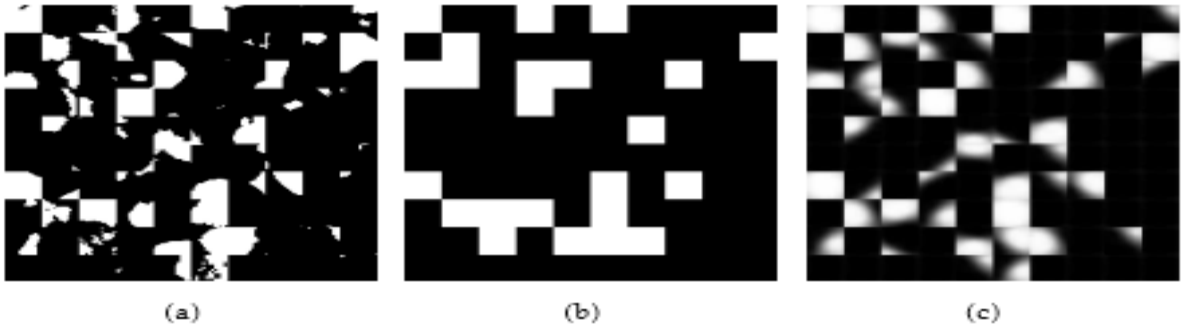

Fig. 3.22: Ground truth tag patches images (a) with the matching binary image (b) and structured images (c) illustration.

The size of the label patch vocabulary N and, later, the amount of classes in the classification tricky, may vary between glitches depending on changeability and shape difficulty of the data. Figure 3.23 demonstrations a sample of gathering training tags patches into 16 modules. The left side of the figure represents the average tags of all cluster, while the right side demonstrations a subset of train labels allocated to a cluster with a given regular patch, i.e. The tags that would be substituted by the same normal label in the unique image.

Defining the N -class prediction problem

After the having gotten the complete set of N clusters that we identified by us, the binary segmentation difficult is transformed into an N class forecast task: Each image patch x is documentation in the training set with the group n that the consistent label patch p has been allocated to during the label patch vocabulary generation. In forecast, the label template t of the forecast group n (size d′ × d′) is allocated to the place of each

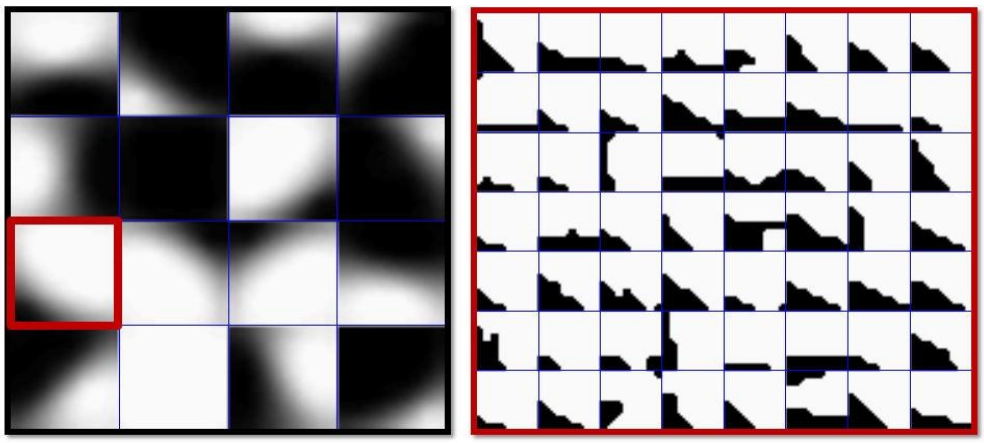

Fig. 3.23: The given example of the clustering technique is the training procedure that tags the patches into 16 different separate clusters. Left: normal labels evaluated for each group. Right: subset of 56 train labels allocated to a collection with the normal patch emphasized by a red bounding box in the left image. Image patch and altogether overlapping forecasts of the

neighborhood are be around. According to the trials, a discrete threshold th = 0.5 was selected for final label forecast.

3.4.4Slice Inference

The digital 2D MRI image of cancer patient's patches from the multisequence MRI bulks images are mapped and scaled into the 2-D digital MRI images input channels of the system proposed network, where m means the number of orders. This is alike to RGB image plotting. Throughout the training phase, patches of a given scope are take out from training capacities. Using the same method for testing is disorganized and therefore dissimilar method used in [89] is employed in its place. The entire input multisequence 2-D slice is sustained to the network style, which clues to a meaningfully earlier convolutional procedure than applying the same convolution numerous times to minor patches. This needs good slice padding to be talented to tag pixels near to the slice edge. The production of the network is a map of tag scores. Though, this label map is lesser than the input slice due to the occurrence of combining layers stealthy the CNN architecture. Two 2×2 pooling layers are present in the upcoming architecture,

Which means that there is only one worth for every 4 × 4 area. Pinheiro and Collobert [89] fed the system by numerous forms of input image removed on X and Y axis and merged the outputs correctly. More shared methodology is to upscale the label map to the scope of the input image. The last method is earlier since only one difficulty per slice is done likened to 16 when using the previous methodology in case of the planned CNN architecture. Though, both of them were verified and associated. One can see the consecutive dispensation of the input multisequence slice in Fig. 3.24.

3.24(b) and 3.24(c) represent 24 outputs of the first and the second convolutional layer of the anticipated CNN architecture. 3.24(d) shows the concluding classification chart of the network. Note the normal labels for all collection in 3.24(e). One can liken them to the ground truth tumor edge in the input image. The final possibility map of the whole tumor area is described in 3.24(f).

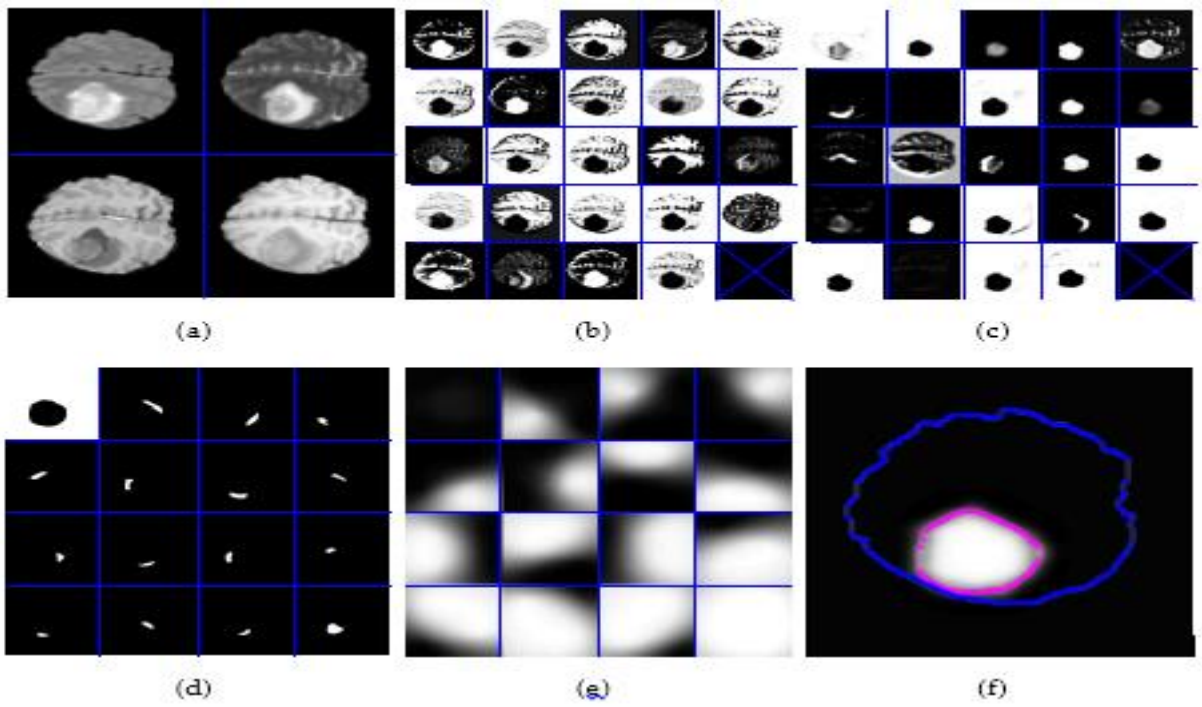

Fig. 3.24: The sequential treatment of multisequence MRI machine digital image single slice (a). (b) And (c) shows all of 24 outputs get from the proposed system of the first digital image slice and the second digital MRI image slice convolutional layer of the anticipated CNN architecture. (d) Represents the output of the entire network for 16 groups with the average patch labels shown in (e). (f) Shows the final possibility map of the whole tumor zone with outlined brain mask (blue) and final segmentation (magenta) gotten by thresholding by th = 0.5.

Since a hierarchy happens between specific segmentation sub-tasks, both tumor essential and active tumor are segmented only confidential the entire tumor area. This makes the segmentation procedure knowingly faster. Although the hierarchy happens between tumor central and active tumor too, this method is not used here since the segmentation of tumor central is the hardest sub-task and it is typically the least precise one

Thesis contribution

This work contribute the brain tumor detection and its segmentation in multisequence MR images successfully with particular focus on high- and low-grade gliomas. Three methods are successfully use for this purpose. The first method deals with the presence detection of brain tumor structures in axial and coronal slices. This method is based on multi-resolution symmetry analysis and it was tested for T1, T2, T1C and FLAIR images. The second method deals with extraction of the whole brain tumor region, including tumor core and edema, in FLAIR and T2 images and is suitable to extract the whole brain tumor region from both 2D and 3D. It also uses the symmetry analysis approach which is followed by automatic determination of the intensity threshold from the most asymmetric parts. The third method is based on local structure prediction and it is able to segment the whole tumor region as well as tumor core and active tumor. This method takes the advantage of a fact that most medical images feature a high similarity in intensities of nearby pixels and a strong correlation of intensity profiles across different image modalities.

Chapter # 04 Results and discussions

4 OUTCOME AND DISCUSSION

This section defines all tests that were done for all three algorithms. The explanation of the research is in the same order as the algorithms explanation in Chapter. 4, i.e. supervised 2-D brain tumor occurrence recognition (Sec. 4.3), unsupervised 2-D and 3-D brain tumor abstraction (Sec. 4.4 and 4.5), and supervised brain tumor subdivision in 3-D volumes using local structure forecast (Sec. 4.6). The assessment standards and experimental setup are defined in Sec. 4.2. The abstraction and segmentation algorithms use the similar standards, while only numerous of them are used to assess the occurrence recognition algorithm. The overall algorithm presentation as well as the enactment for high-grade (HG) and low-grade (LG) gliomas is assessed. For each test, the normal calculating time for the test catalogue is also revealed. These times do not comprise the inhomogeneity alteration, skull stripping and image co-registration since all statistics sets had been preprocessed earlier they were unconfined. All tests were run on 4-core CPU Intel Xeon E3 3.30GHz without GPU speeding up using Matlab. All algorithms were verified on publicly obtainable figures from the MICCAI 2014 Challenge on Multimodal Brain Tumor Image Segmentation (BRATS The explanation of the statistics is assumed in the first section of this chapter (Sec. 4.1).

4.1 Dataset

Brain tumor image data used in this work were attained from the exercise data set of the MICCAI 2014 Challenge on Multimodal Brain Tumor Image Segmentation (BRATS) prepared by Bjoern Menze, TU Munchen; Mauricio Reyes, Bern University; Keyvan Farahani, NIH; and Jayashree Kalpathy-Cramer, Harvard MGH. The experiment daTablease covers fully anonym zed images from the following organizations: ETH Zurich, University of Bern, University of Debrecen, and University of Utah and openly obtainable images from the NIH Cancer Imaging Archive (TCIA). For each patient, T1w, T2w, FLAIR images, and post-Gadolinium T1w MRI volumes are obtainable. All sizes are linearly co-registered to the T1w image, skull stripped, and interpolated to 1mm isotropic determination. No effort was made to put the separate patients in public reference space. Comments comprise the entire tumor, the tumor essential (counting cystic parts), and the enhanced tumor central and are defined in the BRATS orientation paper [80] recently available in IEEE Businesses for Medical Imaging.

All data sets used in this effort initiating from the BRATS2012 and BRATS2013 challenge were segmented physically. Training data from TCIA were marked by combining outcomes of segmentation algorithms that hierarchical high in the BRATS 2012 and BRATS 2013 test. Explanations were reviewed visually and were accepted by knowledgeable raters. A sample of

a manually explained volume is given in Fig. 4.1. The figure demonstrations manual explanations for three tumor structures (full tumor, tumor central, and lively tumor) in dissimilar MRI sequences and their synthesis. Note the hierarchy (lively tumor ⊖ tumor central ⊖ entire tumor) among the structures.

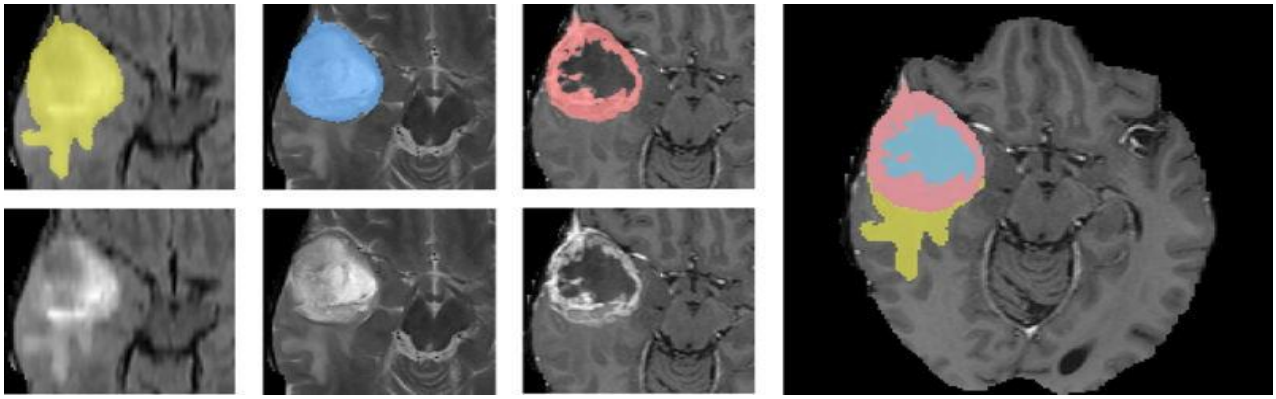

Fig. 4.1: The simple example of a manually marked MRI image on computers with the color marker mark the human brain tumor volume. Left hand side shows the digital images demonstration of human brain tumor image a cut-out with human brain tumor in the cancers patient of the same part in the human brain in three dissimilar MRI 2D digital image orders with three dissimilar interpreted human brain structures which is starts from the left to right hand side the entire tumor, tumor central, and lively tumor is exist in the given image.

The data set used for the assessment of the anticipated algorithm comprises 254 real multisequence volumes of 199 high-grade and 55 low-grade glioma topics. For brain tumor occurrence recognition and brain tumor segmentation using local structure forecast, the data set was separated into three clusters: training, authentication and testing. The training set comprises of 130 high-grade and 33 low-grade glioma topics, the authentication set contains of 18 high-grade and 7 low-grade glioma topics, and the testing set contains of 51 high-grade and 15 low-grade glioma subjects, summing up to 254 multisequence volumes of normal size 240×240×155. For un- supervised brain tumor abstraction, all 254 volumes were used for challenging since no training phase is compulsory there.

4.2 Evaluation criteria

The segmentation procedure advance algorithms are typically assessed by the Dice score (DS). Dice score, sometimes named Dice similarity coefficient, is calculated according to the equation

$$DS = \frac{2|A \cap B|}{|A| + |B|}$$

Where A and B represent the ground truth and the abstraction outcome masks, correspondingly. The variety of the DS standards is [0;1], where DS = 1 states the exact correspondence. Other actions widely employed for segmentation precision are Correctness, which is occasionally named Positive predictive value (PPV), and Sensitivity, from time to time named Recall. They are both established on the Confusion matrix, a 2×2 (in case of binary grouping) matrix:

		Truth	
		True	False
Prediction	True	TP	FP
	False	FN	TN

where TP , FP , FN and TN position for True Positive, False Positive, False Negative, and True Negative, respectively. The occurrence recognition performance is assessed by the confusion matrix, which, for easier clarification, is adapted to:

		Truth	
		True	False
Prediction	True	TPR	FPR
	False	FNR	TNR

where TPR, FPR, FNR and TNR position for True Positive Rate defined as

$$\text{precision} = TP/\ TP+FP \qquad (6.2)$$

Which dealings the proportion of the true positives in the possibility of all positive forecasts. Compassion, on the other hand, actions the proportion of the true positives in the scope of all real positives and is well-defined as:

$$\text{Sensitivity} = TP/TP + FN \qquad (6.3)$$

Which the resembles to the TPR. Correctness, which is clear as:

$$\text{Correctness} = TP + TN/\ TP+FP+\ TN + FN \qquad (6.4)$$

Only used for the human brain digital image tumor occurrence recognition advance algorithm is used. This quantity is not appropriate for brain tumor segmentation assessment, which is actual imbalanced task for the amount of negatives is much advanced than the number of positives. Correctness is always spreads high rate identification from the digital image here.

4.3 Brain Tumor Presence Recognition

In this chapter number four the human brain presence identification method proposed for recognition and its identification in the digital image of particular structures of human brain tumor identification for example the entire tumor, central tumor, and lively tumor, is evaluated here. This proposed method is the based on a simple novel approach by using the multiresolution symmetry analysis of digital 2D image as described in previous Section 4.2.

4.3.1Experimental setup

This simple and advance proposed algorithm was verified for all these four MRI 2D digital image classifications procedures such as FLAIR MRI images, T2w digital image, and T1w 2D digital image and T1C simple high contrast images. Since brain regularity occurs in two planes,

axial and coronal, together of them were measured and tested distinctly during the algorithm assessment. Note that slices with tumor central and lively tumor are also comprised in the set of slices with complete tumor; therefore the total amount of slices is equivalent to sum of complete tumor and well slices. The statistics of pathological slices (with a pathology of size of 100px, i.e. A pathology of magnitude of 1cm2 seeing the 1mm isotropic resolution) and fit slices (with no tumor area) in axial and coronal planes are potted in Table. 4.1 And Table. 4.2, correspondingly. This Table demonstrations the distribution of the data set in exercise, validation and testing subsections. The distribution follows the separation labelled in Sec. 4.1 but it shows the careful figures of slices used throughout the algorithm assessment. The total quantity of extracted features for stand-alone images was 24 per sequence, i.e. an extreme from multiresolution irregularity chart and three most from each single-resolution chart, five complete thresholding levels, and five comparative parameters are thresholding levels.

Table. 4.1: New setup of brain tumor occurrence recognition in axial plane.

	Entire tumor	Central	**Livelytu1nor**	Healthy	Overall
Train	10572	6741	4910	9820	20392
Validation	1553	1057	708	1639	3192
Te-st	4335	3099	2442	4268	8603
Overall	16460	10897	8060	15727	32187

Table. 4.2: The experimental setup of human brain tumor digital 2D image occurrence in the human brain revealing in coronal plane.

	Entire tumor	Central	**Lively tu1nor**	He<llthy	Overall
Train	9887	4369	1922	11323	21210
Validation	1449	758	307	1883	3332
Te-st	4176	**2353**	1079	4859	9035
Overall	15512	7480	3308	18065	33577

Each value of thresholding digits are leads to two following features number of areas and scope of all areas. In 3D application, four more strength features were calculated for each threshold: normal strength in created areas, complete value of the alteration between regular strength in areas in the left and the right hemisphere, standard deviation of strengths in created areas, and complete value of the variance between strength average deviation in areas in the left and the right hemisphere. This calculations that we had made up to 64 image features or extracted from image which is digital for portions in 3-D volume bulk.

4.3.2Application to the Test Set

Stand-alone Slices

According to the axial plane, the correctness of complete human brain tumor of the cancer patient tumor, tumor central, and lively tumor recognition and identified by axial multisequence digital image slices is revealed in Table. 6.3. In this Table, one can see that in axial plane, the best correctness for the entire tumor area is touched in FLAIR images, for the tumor central and lively tumor areas in FLAIR or T2 images. When all MRI sequences are joint, the correctness is enhanced for all perceived structures.
Confusion matrices for multisequence recognition of a given part of the brain tumor are revealed in Table. 4.4, 4.5 and 4.6.

Table. 4.3: The accurateness of specific human brain tumor structures finding in the axial plane of digital 2D image slices of dissimilar MRI of cancer patient sequences.

Correctness (in	Entire tumor	Central	Lively tu1nor
FLAIR	90	*89*	83
T2	88	*89*	83
TIC	83	84	81
TI	81	80	78
multisequence	90	90	88

Table. 4.4: The confusion matrix is used for the lively human brain tumor type occurrence recognition in multisequence MRI digital image stand-alone axial plane slices of digital image.

	Tumor present	Tumor absent
Test positive	91	11
Test negative	09	89

Table. 4.5: The confusion matrix of human brain tumor MRI central occurrence finding in multisequence MRI digital image stand-alone axial plane digital image slices.

	Tumor present	Tumor absent
Test positive	88	08
Test negative	12	92

Table. 4.6: The confusion matrix of lively human brain tumor occurrence in the patient brain finding in multisequence MRI digital image stand-alone 2D digital image axial plane slices.

	Tumor present	Tumor absent
Test positive	83	10
Test negative	17	90

When the Coronal plane is concerned. The accurateness of complete tumor, tumor central, and lively tumor finding in coronal slices is revealed in Table. 4.7. In this Table, one can see that in axial plane, the finest exactness for the entire tumor and lively tumor regions is reached in FLAIR images, for the tumor central region in FLAIR images. When all sequences are mutual, the accurateness is enhanced for all spotted structures.

Table. 4.7: Accurateness of specific human brain tumor specific structures finding in coronal digital image slices of changed MRI sequences.

Correctness (in	Entire tumor	Central	Lively tu1nor
FLAIR	90	88	86
T2	85	*89*	86
TIC	80	83	81
TI	76	77	75
multisequence	91	91	88

The confusion matrices for the specific multisequence brain tumor finding of a given digital MRI slice of the human brain tumor are revealed in Table. 4.8, 4.9 and 4.10.

Table. 4.8: The confusion matrix of complete human brain tumor occurrence recognition and its identification in multisequence MRI stand-alone coronal digital MRI slices.

(in %)	Tumor pre-sent	Tu1nor absent
Test positive	87	07
Te.st negative	11	93

Table. 4.9: The confusion matrix of human brain tumor central occurrence recognition and its identification in multisequence MRI stand- alone coronal digital image slices.

(in %)	Tumor pre-sent	Tu1nor absent
Test positive	87	07
Te.st negative	13	93

Presence recognition in 3D volume

According to the axial plane is concerned. This examination used the similar new setup as the assessment of occurrence finding in stand-alone images. Though, image features are take out together with the irregularity features used in stand-alone image, because strengths.

Table. 4.10: The confusion matrix of lively human brain tumor occurrence recognition and its identification in multisequence stand-alone coronal digital image slices.

(in %)	Tumor pre-sent	Tu1nor absent
Test positive	81	19
Te.st negative	11	91

The confusion matrix can be regularized in whole 3-D human brain tumor volumes. The accurateness of complete tumor, tumor central, and lively tumor recognition in axial slices are revealed in Table. 4.11. One can see that in axial plane, the finest accurateness for the complete tumor areas as well as for the tumor central area is reached in FLAIR images. Lively tumor is greatest precisely noticed in T1C slices.

Table. 4.11: The correctness of specific human brain tumor the structures finding in human axial digital slices of dissimilar MRI sequences are available here.

Correctness (in	**Entire tumor**	Central	Lively tumor
FLAIR	94	92	88
T2	89	90	88
TIC	83	87	89
TI	80	80	78
[multis-equence	93	93	92

The confusion matrices for multisequence human brain tumor MRI imaging finding of a given part of the human brain tumor are revealed in Table. 4.12, 4.13 and 4.14.

Table. 4.12: The confusion matrix of human brain lively tumor occurrence recognition in multisequence MRI digital MRI images axial slices in 3-D volume.

(in %)	Tumor pre-sent	Tu1nor absent
Test positive	95	9

Te.st negative	05	91

Coronal plane.

The correctness of complete tumor, tumor central, and lively tumor recognition in coronal slices are revealed in Table. 4.15. In this Table, one can see that in

Table. 4.13: Confusion matrix of tumor central occurrence finding in multisequence axial slices in 3D volume.

(in %)	Tumor pre-sent	Tu1nor absent
Test positive	92	06
Te.st negative	08	94

Table. 4.14: Confusion matrix of lively tumor occurrence recognition in multisequence axial slices in 3D volume.

(in %)	Tumor pre-sent	Tu1nor absent
Test positive	92	08
Te.st negative	08	92

Axial plane, the finest accurateness for the complete tumor region as well as for the tumor central area is reached in FLAIR images. Lively tumor is most exactly noticed in T1C slices.

Table. 4.15: Accurateness of specific brain tumor structures recognition in coronal slices of dissimilar MRI sequences.

Correctness (in	**Entire tumo:r**	Central	**Lively tu1nor**
FLAIR	93	91	87
T2	86	90	87
TIC	80	87	88
TI	77	80	77
i'vfultisequence	94	93	92

The confusion matrices is mentioned in the table for the multisequence finding of a given portion of the human brain brain tumor are revealed in Table. 4.16, 4.17 and 4.18.

Discussion

In this portion, the supervised process for brain tumor occurrence recognition was tested. It was assessed for two dissimilar cases, the discovery in stand-alone 2-D images and slice-wise recognition in 3-D volumes. The previous used only features take from
Table. 4.16: Confusion matrix of complete tumor occurrence finding in multisequence coronal slices in 3-D volume.

Table 4.16

	Tumor present	**Tumor absent**
Test positive	91	06
Test negative	09	94

Table. 4.17: Confusion matrix of human brain tumor tumor central occurrence recognition and its identification in multisequence coronal slices in 3-D volume.

Table. 4.17

	Tumor present	**Tumor absent**
Test positive	91	06
Test negative	09	94

Table. 4.18: Confusion matrix of lively human brain tumor tumor occurrence recognition and its identification in the digital image in multisequence coronal slices in 3D volume.
Table. 4.18

	Tumor present	**Tumor absent**
Test positive	91	09
Test negative	09	91

The irregularity charts, while the latter additional the asymmetry-based image strength features. Figure 4.2 demonstrations Precision-recall arcs for axial plane examination set for all tumor fragment discovery using dissimilar MRI sequences in both stand-alone slices and slices in 3-D capacity. Recall is equal to compassion. Green dashed arcs portray is level lines of F-measure, which is equal to the Dice total. Charts for the coronal plane are absent since they are very comparable to the diagrams for the axial plane. As it can be decided from the consequences, the strength features bring significant data, which in most tests better the finding correctness, e.g. the presentation amplified from 90% to 94% using axial FLAIR slices for complete tumor discovery, or from 81% to 88% using coronal T1w slices for lively tumor recognition.

Giving to the consequences, it can be specified that in stand-alone images all portions can be automatically perceived with the maximum correctness in FLAIR. In 3D volume slices, including intensity-based features recovers the outcomes and lively tumor is than noticed with uppermost accurateness in T1w slices. Yet, using all MRI sequences.

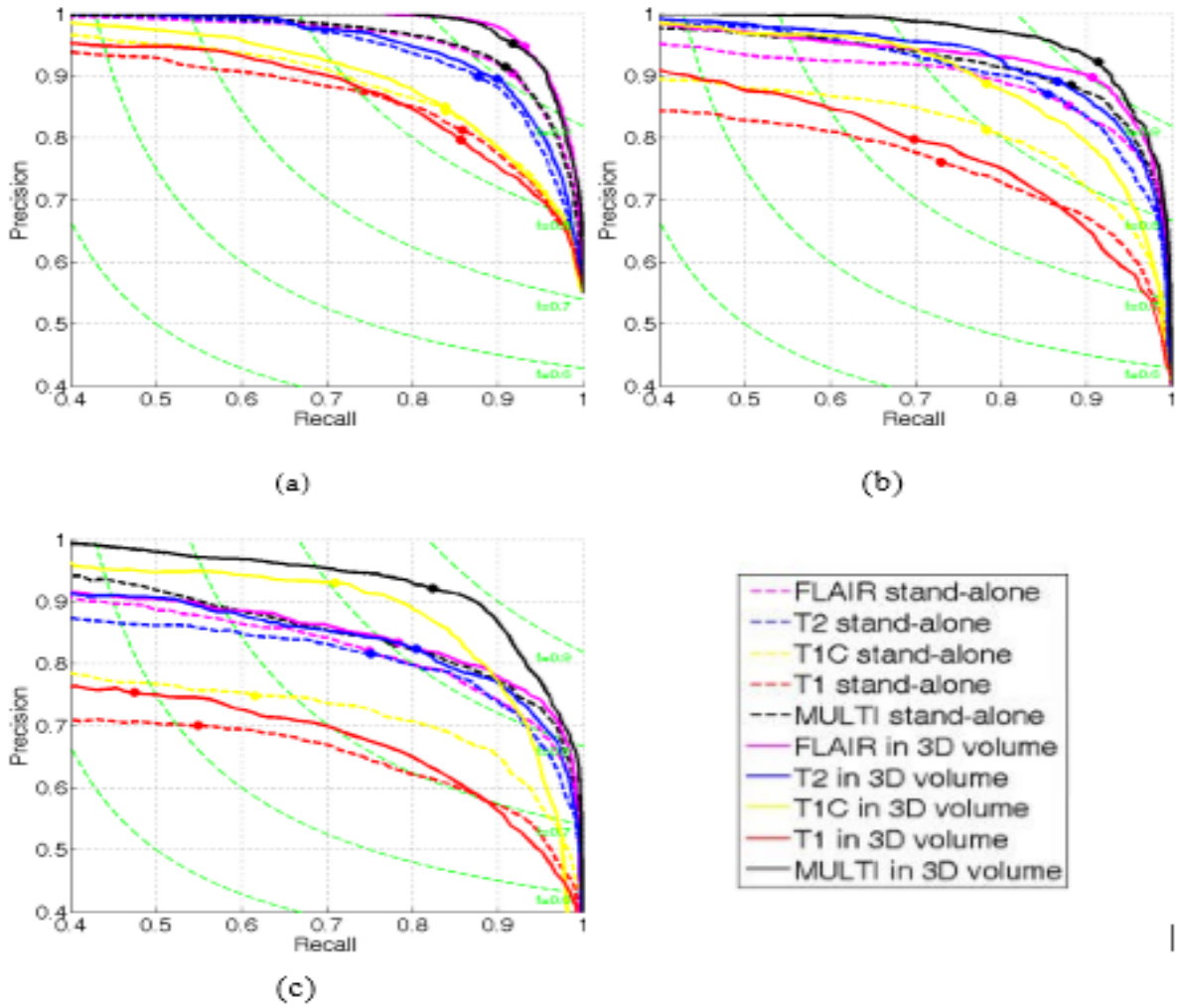

Fig. 4.2: Precision-recall arcs for (a) entire tumor, (b) central tumor and (c) lively tumor occurrence recognition in both stand-alone slices (dashed arcs) and slices in 3-D volume (solid arcs) for the axial plane examination set. Loops on each arc signify the real achieved outcome. Green dashed arcs portray is level lines of F-measure, which is equal to the Dice score.

Increases the presentation in nearly all recognition tasks. It was revealed that the algorithm spreads high accurateness in both axial and coronal planes. Since, giving to the finest information of the writer, there are no procedures for the fast brain tumor occurrence recognition task, it is not likely to associate the outcome with state-of-the-art algorithms. The computing time of 0.11s per slice and classification, where 90% of the time is spent by regularity examination and the rest by feature extraction and grouping, displays that this scheme can be used either for fast conclusion, whether an image

Comprises a tumor, or in the division procedure as a pre-processing step to govern the slices to be segment or examined. Many state-of-the-art approaches based on deep learning architectures use slice-wise approach, and, therefore, this scheme can also be used in channels of such algorithms.

4.4 Unsupervised 2D brain tumor extraction

After the entire human brain tumor occurrence inside the human brain is spotted in 2-D in the MRI, it can be extracted using the novel unsupervised 2-D brain tumor extraction scheme

labelled in Sec. 4.3. This system is intended for FLAIR images only, therefore, other MRI classifications will not be considered now.

4.4.1Experimental setup

Since the planned advance algorithm is followed the unsupervised technique, i.e. No exercise phase is obligatory; it was verified on the entire set of 254 FLAIR volumes. Axial and coronal slices comprising entire tumor part of at least 6cm2 were taken out from each volume since the scheme cannot deal with lesser pathologies. The general statistics of axial and coronal slices involved in the test are 22213 (18445 of HG and 3768 of LG) and 28078 (23401 of HG and 4669 of LG), correspondingly.

4.4.2Application to the test set

The outcome of the proposed algorithm is the application to axial and coronal slices are potted in Table. 4.19. The Table comprises the general outcome as well as the outcome attained for high- and low-grade gliomas assessed by the Dice score, accuracy and compassion. In the Table, one can see advanced compassion values than exactness. This points to the fact that the subsequent area is typically superior to the true tumor part, in other words, more false positives than false negatives are existing. The compassion standards demonstration that in normal 87% of positive pixels were originate, while the accuracy values show that in normal 64% of positive tags were truly positive. The regular calculating time per slice is 0.13 seconds, where 75% of the time is spent by the regularity examination. Examples of the contrast of a physical explanation and a programmed abstraction in both axial and coronal planes are revealed in Fig. 4.3. Three positive and one unsuccessful (the maximum right) involuntary segmentations are revealed for each plane. The unsuccessful subdivision in axial plane demonstrations the disappointment of the scheme in case of an unimportant pathology. The algorithm was not intelligent to appropriately regulate the threshold due to the small quantity of tumorous pixels. The ineffective segmentation in coronal plane demonstrations a disappointment of the system for table. 4.19: Division consequence reporting normal and median Dice score, exactness and sensitivity. Revealed are outcome for axial and coronal slices. std and mad signify normal deviation and median total deviance. HG and LG stand for high- and low-grade gliomas, correspondingly.

Table 4.19

	Axial		Coronal	
		HG ! LG		HG ! LG
Dice Score (in %)				
mean	**63030**	63•30 / 59•32	63•29	63•29 / 60•30
median mad	77•27	77•27 *I* 76•30	76•26	78•26 / 70•28
Precision (in %)				
mean	64•37	64•37 *I* *51*•39	**63037**	65•37 / 58•38
median mad	**85035**	85•35 / 71•37	81•34	84•34 / 65•36
SensitMty (in %)				
mean	**87031**	87•16 / 91•12	87•15	*86•151* 91•12
median mad	92•11	91•12 / 96•09	91•11	91•12 / 95•09

A digital human brain image where the strengths of the clinical molecular pathology or the histology are very alike to the intensities of vigorous human brain tissues.

Discussion

The perseverance of this algorithm was to cutting a tumor zone (including edema) from a stand-alone FLAIR image. The outcome are not similar to the state-of-the-art procedures used for multisequence 3-D brain tumor abstraction, which are typically based on machine learning practices using the strength data. Such methodology is likely for 3-D volumes where the strength standardization can be performed. Yet, this is not appropriate for a stand-alone axial or coronal slice with unidentified data about the tumor scope and the slice directs. This system was calculated to deal with such images and reached capable outcome with ordinary and median Dice scores of 63∘30 and 77∘27 and calculating time of only 0.13 seconds.

4.5 Unsupervised 3D brain tumor extraction

In this chapter the concerning section is, the scheme anticipated for unsupervised brain tumor finding and take out is assessed. This scheme is based on a novel unsupervised algorithm linking 3-D multiresolution regularity analysis designated in Sec. 4.2 and reflex thresholding.

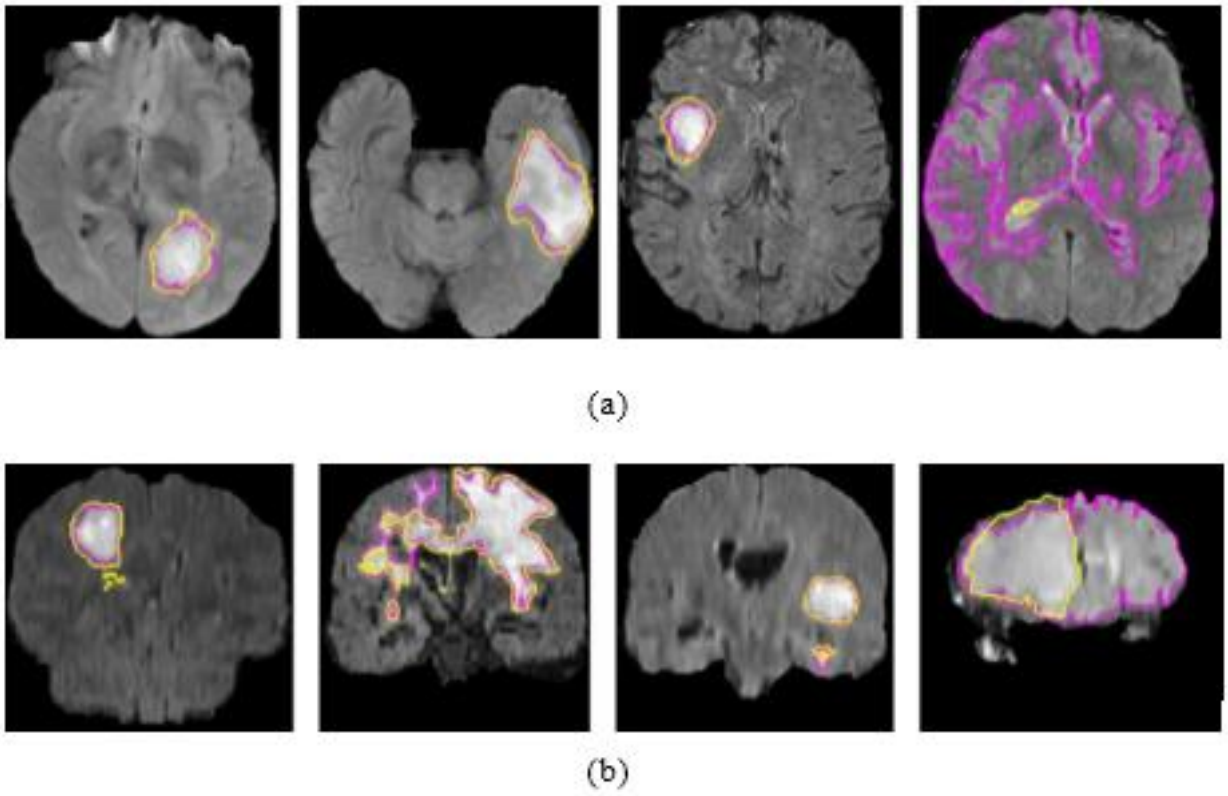

Fig. 4.3: For the instances of the human brain tumor features abstraction using the unsupervised way of advance algorithm in 2-D (a) axial plane in digital image and (b) coronal plane in the FLAIR MRI image slices. A huge contrast of manual explanation which is expressed in the yellow color in the MRI images and the programmed features extraction is expressed in the magenta color is illustrated in above diagrams.

4.5.1Experimental Setup

The 3-D unsupervised method of human brain tumor features abstraction advanced designed algorithm was also verified on the whole brain tumor images database of 254 multisequence MRI volumes since it does not need any training phase, and, hence, statistics partitioning is not needed. This algorithm needs only T2w and FLAIR images, consequently other MRI sequences

are not careful in these tests. During challenging, the precision of the automatic tumor finding using the regularity examination is assessed together with the involuntary whole tumor abstraction. The tumor position is resolute by the supreme of the multiresolution irregularity diagram. This point demonstrations the uppermost likelihood of the tumor site and, from now, it is talented to notice slices in all three planes where there is the supreme probability of the tumor occurrence. If this point lies within the area of a tumor, it is considered as a correct locating. Since the irregularity map is regular according to the mid-sagittal plane, i.e. two most exist, either of them is careful. The second test assesses the precision of the entire tumor area abstraction. This is assessed by the Dice score, exactness and sensitivity.

4.5.2Application to the test set

Brain Tumor Locating

This test was done distinctly for each and every human brain tumors type MRI slices sequence, i.e. T2w and FLAIR. Consequence for both MRI sequences are potted in Table. 4.20. The normal calculating time for one sequence is 6.7∘0.8 seconds per size. Table. 4.20: Brain tumor finding using irregularity acknowledgement. The Table present the proportion of properly situated brain tumors.

Table 4,20

	Overall	HG/LG
T2	90	90/90
FLAIR	95	96/95

As everyone can see in this Table which is contains the correctness of T2w and FLAIR images, the anticipated algorithm can repeatedly find a tumor and demonstration slices with a tumor within fewer than 7 seconds with a precision of 95% in FLAIR image volumes and 90% in T2w size of 1mm isotropic resolution. Mixture of T2 and FLAIR capacities, where the time essential for the asymmetry acknowledgement is double higher, did not bring any development, and, hence, it can be quantified that FLAIR volume is more appropriate for brain tumor finding, at least in case of using the regularity prior and the planned method.

A specimen of the tumor finding algorithm is exposed in Fig. 4.4 where slices with the extreme irregularity of all three planes are exposed. The coordinates of this extreme are portrayed by blue circle. The figure demonstrations four dissimilar slices per topic. Two slices are revealed in sagittal plane. The determination is to show both slices with the supreme irregularity, i.e. one slice from the left and one slice from the right hemisphere.

Brain Tumor Extraction

The presentation of the human brain tumor various features abstraction proposed algorithm based on the regularity of human brain examination is evaluated here by mean and median standards of Dice score, accuracy and sensitivity. All outcome are potted in Table. 4.21. The overall presentation as well as the performance for high-grade (HG) and low-grade (LG) gliomas is revealed. The average calculating time is 13.8∘1.3 seconds per volume with the former symmetry examination in both volumes, which reaches about 93% of the calculating time. Somewhat lower performance was attained by applying regularity examination only. To one volume, e.g. FLAIR. Yet, the calculating time reduced to 7.7∘0.9 seconds in this case.

Table. 4.21: Brain tumor extraction using asymmetry recognition.

Precision (in %)	Whole	HG/LG	Core	HG/LG	.. ctive
Validarion set					
1ne.an o Ms!	78•16	77•1 I 81•07	92•06	91•0 I 93•03	90•10
1ne-diano 1nad	84•08	83•0 I 84•08	93003	93•0 I 92•01	92•04
Test set					
me.a.n o	81•16	83•1 I 71•25	87013	88•1 I 86•12	85•18
1ne-diano 1nad	86•04	87•0 I 82•07	92•04	92•0 I 89•09	91•05

Examples of the contrast between the automatic abstraction and the manual explanation are given in Fig. 4.4 Where manual explanations are portrayed by yellow color, and the outcome of the automatic abstraction procedure are publicized by magenta color. The figure demonstrations four dissimilar slices per topic. Two sagittal slices are exposed. The determination is to display both slices with the extreme unevenness, i.e. one slice from the left and one slice from the right hemisphere.

Discussion

In this digital image segmentation process, the unsupervised algorithm for fast brain tumor finding and extraction was verified. The unsupervised tactic for the brain tumor finding and delineating was confirmed on FLAIR and T2w volumes of 254 topics. The proposed scheme used a style dissimilar from other state-of-the-art algorithms. Likened to them, it is not supervised and, so, it does not need any training phase. It cannot spread the top three state-of-the-art consequence stated in [80] with 79%-82% (here: 64%), but it still stretched relative outcome with other means defined in that paper. But, the benefit of the proposed algorithm is its rapidity since it is not that difficult as other approaches. With 13.8 seconds, it is faster than the dissolute scheme reported in [80], where only 3 procedures out of 16 consecutively on CPU were intelligent to extract brain tumor in fewer than 8 minutes. Therefore, the planned algorithm is appropriate for fast preliminary estimated tumor extraction rather than precise segmentation. The first portion of the proposed algorithm for brain tumor detection from the image.

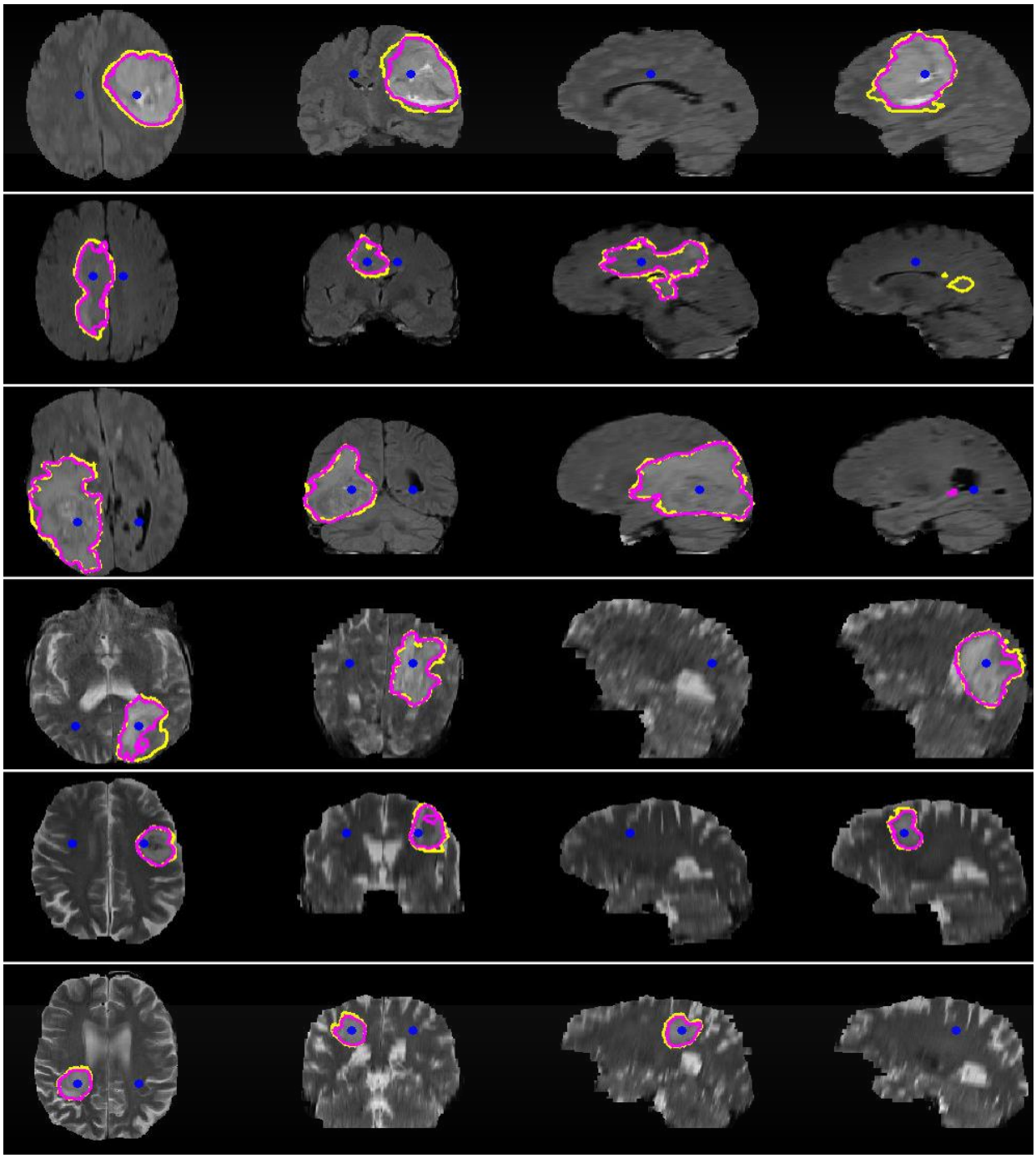

Fig. 4.4: Examples of the unsupervised technique or procedure which is the human brain tumor feature abstraction based on the multiresolution of human brain and regularity of human brain examination. The outcome are established on three FLAIR (up- per rows) and three T2w (lower rows) volumes. The images demonstration slices where the extreme asymmetry was noticed with corresponding manual explanation (yellow) and automatic extraction (magenta). Blue circles point to the voxel with the peak asymmetry. Together sagittal slices with the maximum asymmetry are presented. Finding, is appropriate for fast brain tumor detecting for pre-analysis of a single-sequence capacity since it may pre-analyze a solitary volume in less than 8 seconds.

Table 4.22a Critical Evaluation of the Automated MRI Techniques

Reference	Algorithm/ Technique	Focus Area/ Features Used	Strengths	Limitations	Experimental Results
[11]	• 2D Continuous Wavelet Transformation (CWT). • Incremental Supervised Neural Network (ISNN). • Zernike Moment by Vector Representation. • Euclidean Distance.	• Unified the Mid-sagittal plane extraction method and segmentation process for the detection of Tumors and asymmetry.	• The Physical implementation of ANN is simple. • The ANN can map complex class distributions easily. • Generalization property of ANN produces accurate result.	• The small asymmetric differences increases the value of ND2 and the Algorithm take wrong decisions. • Calculation of Zernike moments is complex.	• The system has shown 100% segmentation performance for 20 tumors and 50 Normal brain images.
[13]	• Fuzzy Filters. • Type-II Probabilistic C-Mean (T2PCM). • Type-II Fuzzy Logic. • Thresholding. • Fuzzy Clustering.	• White Matter (WM). • Gray Matter (GM). • Cerebrospinal Fluid (CSF). • Abnormal Brain Tissue (Brain Tumor).	• The Type-II fuzzy proved to be more robust than Type-I.	• The model has shown less accuracy. • The Type-II Fuzzy expert system for pre-processing needs further perfection.	• The total of 95 images were considered. • The system identified 79 images correctly and 16 incorrectly with accuracy of 78.94%.
[17]	• Internet Brain Segmentation Repository (IBSR). • Anisotropic Diffusion Filter. • Stationary Wavelet Transform (SWT). • Spatial Filters. • Self-Organization Map (SOM). • Learning Vector Quantization.	• Multiresolution information for distinguishing different tissues. • Multidimensional feature vector is formed by combining SWT coefficients and their statistical features.	• The SWT is very effective for splitting texture information into different frequency channels. • SOM is very effective for dividing M x N dimensional data into multiple segments.	• The division of image into channel increases execution time. • The accuracy rate of the Technique is not mentioned in the paper.	• Highly robust than manual segmentation but the Accuracy rate has is not properly mentioned.
[19]	• Principal Component Analysis (PCA). • Artificial Neural Network (ANN). • Gradient Descent with Momentum Weight and Bias Learning Function. • Feed Forward ANN. • Liebenberg Marquardt Algorithm.	• Linear Regression. • Linear Correlation Coefficient. • Four Classes of images i.e. normal class, Edema class, cancer class, and Not classified class.	• ANN is very easy and Simple for classification. • The technique is fast in execution, efficient in classification and is easy to implement.	• The train used as Training function for ANN, is very fast, but it requires a lot of memory to run.	• First Training (time consuming = 43.3839 sec). • Third training (time consuming = 40.5603 sec). • The average time consumed is 0.2434 sec. • The technique has accuracy Of 96.33%.

[20]	• Thresholding. • K-Means Clustering Algorithm. • Color Converted Segmentation.	• Color converted images. • Distinguish exact lesion size and region.	• Easy and fast for small data. • The method Has higher accuracy with reasonable computation time.	• Not effective for large data. • K-means clustering is sensitive to the initial cluster assignment and the choice of distance measure.	• For MRI T2-weighted 100% accuracy and 30s. • For MRI T1-weighted 8% accuracy and 30s. • For Spin density 75% accuracy and 30s computation time.
[21]	• Short Time Fourier Transform. • Principal Component Analysis (PCA). • Back Propagation Neural Network (BPNN). • Scaled Conjugate Gradient (SCG). • Wavelet Transform.	• Level-3 decomposition via Haar Wavelet. • Time analysis. • Minimum possible features utilization for the classification.	• Neural Network (NN) is simple approach. The Scaled Conjugate Gradient (SCG) is powerfuland designed to avoid line search. • The features were reduced by PCA and only 19 principle components, i.e. 1.86% of original features were used.	• Training time of the Neural Network is very high with large amount of data. The Fourier Transform (FT) has Drawback of losing the time information of the signal. • The computation time can be accelerated by using lift-up wavelet.	• Total of 66 images were considered. • The time consumption for feature extraction is 0.023s, for feature reduction 0.0187s and classification by NN is 0.0035s. • 100% accuracy with the execution time for each image processing 0.0451s is satisfactory.
[23]	• Simple Filtering. • Gaussian Mixture Model (GMM). • Low Pass and High Pass Filters. • Three Dimensional Fluid Attenuation Inversion Recovery (FLAIR) Images. • WMH Segmentation Method. • Probability Density Function.	• Cerebrospinal Fluid (CSF) • White matter (WM) • Gray matter (GM) • Intensities information.	• The other methods uses two MR modalities but the proposed method uses only FLAIR images. • The method has general applicability because it just uses intensities information. • Better processing than manual segmentation. • Performs closer to the Human observer.	• Two steps for pre-processing used i.e. Skull skipping from the brain MRI and the bias field correction that takes extra time. • The bias field correction need to be incorporated into the segmentation process.	• 30% training and 70% testing criteria is used. • Total40 images were used. 12 for training and 28 for testing. • The method has attained an overall score of 82.0055.

[26]	• Binary Masking. • Fast Volume Image Segmentation (HFS). • Entropy Gradient Segmentation (EGS). • Self-Organization Map (SOM). • K-Means Clustering Algorithm.	• Segmentation of MRI images. • Voxel intensities. • Statistical Features. • First order features from gray level of a specific voxel and its neighborhood. • Second order features derived from the spatial relationship among different voxels.	• Fully unsupervised method is used for the MRI image segmentation. • Self-Organization map (SOM) is fast and efficient approach. • Resolution/so immunity.	• Computational complex. • Computation cost and precision trade-off.	• Two methods have been compared. • EGS has better sensitivity and specificity than the HFS.
[27]	• Anisotropic Diffusion Filter. • Improved Fuzzy Connectedness Algorithm. • Similarity Index (SI). • Extra Fraction (EF). • Overlap Fraction (OF). • Gaussian Variable Coefficient. • Canny Algorithm.	• Seed points. • Calculating Scale as a homogeneity region radius. • To improve the general fuzzy algorithm for proper segmentation of images.	• The algorithm is independent of the tumor type in terms of pixels intensity. • The direct relation between fuzzy connectedness and affinity. • The algorithm's sensitivity to noise decreased. • The boundary information of the tumor tissue reduced the error.	• The tumors in the sequence of slices and surrounded by tissues reduces the accuracy of the algorithm. • Tumors with vague borders and low contrast cannot be segmented well. • The false-negative results lead to the lower SI and OF.	• The data of 10 patients has been used. • The result is 17.8% better than the general fuzzy using similarity index (SI), • 21.1% better than the general fuzzy using overlap fraction (OF) • 6.8% better than the general fuzzy using the extra fraction (EF).
[29]	• Artificial Neural Network. • Fuzzy C-Means Algorithm. • Low Pass and High Pass Filters. • Mean and Standard Deviation.	• Detection of volume changes in the brain tissues.	• Minimizes the number of iterations and predictably classifies a pixel into one group.	• The training of Neural Network requires a huge amount of data and time. • Accuracy of fuzzy classification depends upon fuzzy rule base. • Computation is complex	• The computation time for the method is between 177 and 259 seconds.

[30]	• Fractal Dimension, Level Set Based Method. • KLD Method. • Graph Cut Procedure. • Expectation Maximization Algorithm. • Laplacian Matrix.	• Fractal Dimension (FD). • mBm texture features. • Probability Distribution.	• Can be applied to different Modalities. • The technique perform better for segmentation of tumor.	• The time for normalization, Feature extraction, feature selection and segmentation are very high. • Not providing accuracy for different modalities.	• Total of 249 real MRI Images were considered. • The mBm feature in multimodality T1, T2, and FLAIR MRI offered 100% tumor segmentation.
[31]	• Median Filter. • Arithmetic Mean. • Standard Deviation. • Region Growing Algorithm.	• Seed point. • The intensity of different pixels. • Standard Deviation. • Arithmetic Mean of Neighboring pixels.	• The results are satisfactory due to the simplicity and easiness of the method. • The median filter retains and preserves the edges of the images that enhance the accuracy.	• The pre-processing and post- processing techniques increase execution time. • The method is prone to Leakage into skin area.	• Total execution time is less than the 20s. • The execution time of Segmentation stage is only 2.9s.
[32]	• Discrete Wavelet Transform (DWT). • Principal Component Analysis (PCA). • K-Nearest Neighbor (KNN). • Artificial Neural Network (ANN). • Levenberg-Marquardt Learning Rule.	• Wavelet Coefficients. • Eigen Vector. • Asymmetry in an axial MR brain images.	• ANN simple and KNN good for smaller data. • The proposed method has shown better accuracy than the other methods. • The PCA has removed the complexity.	• The features reduced from 1024 to 7 only which are not enough and the increase in features may reduce the performance of the system.	• 90% with Artificial Neural Network (ANN). • 99% with K-Nearest Neighbor (KNN).
[33]	• Bhattacharya Coefficient. • Fast Bounding Box (FBB). • Score Function. • Ellipse Fitting Technique. • Mean Shift Clustering (MSC).	• 2D MR slices. • Region based global change. • The tumor region considered as a change in the original image.	• The FBB does not need image registration. • The unsupervised technique does not require any prior parameter distribution. • A training set of labelled images is not required. • Intensity standardization in MR slices is not required.	• The noise reduces the performance of FBB. • Performance of FBB depends upon the asymmetry among the two halves of the MRI images. • The method generates box on an MR slice even in the absence of tumor or Edema.	• The method has shown the accuracy of 92% for Tumor detection and 89% for Edema.

[34]	• K-Mean Clustering. • Fuzzy C-Mean Algorithm. • Median Filter. • Euclidean Distance.	• Detection of range and shape of tumor in Brain. • Mass tumor detection.	• The Fuzzy C-Mean algorithm is More powerful and accurate than K-Means Clustering.	• The addition of noise and then removing By applying median filter is not properly explained. • The accuracy of the system is not provided.	• The results are not properly Mentioned.

4.6 Brain tumor segmentation using structure prediction

In this segment of this research paper the scheme planned for human brain image segmentation of specific human brain structures of the brain tumor type for example complete tumor, central tumor, and lively tumor, is assessed. This process is based on a method, whose innovation lies in the principled mixture of the deep approach composed with the local structure forecast in medical image segmentation task. The algorithm was labelled in Sec. 4.4.

4.6.1Experimental setup

The algorithm is calculated for a binary segmentation difficult and it was applied disjointedly to three brain tumor segmentation sub-problems: segmentation of entire tumor, central tumor and lively tumor.

As it has been exposed in [93], the computational difficulties of 3-D CNN are still out of scope for today's processers. Therefore the volume is treated sequentially in 2-D in the plane with the uppermost resolution, the axial plane now. Image patches from each multisequence volume are mapped into four 2-D input channels of the system. This methodology gives a good chance for parallelization of this task to diminish the calculating time.

Replacements to this basic methodology have been projected: slice-wise 3-D segmentation methodologies using CNN were offered used in [93] and [101]. The former disclosed non-feasibility of using 3-D CNN for larger cubic patches and anticipated using of a 2-D CNN for each orthogonal plane distinctly. The later planned abstraction of analogous patches for a given pixel from all orthogonal plane and plotting them as whole feature maps. In this work, both of these methods were verified and associated to the single slice methodology that was selected here.

From each training topic, 1500 arbitrary 2-D multisequence image patches with matching label covers were extracted summing up to 244 500 training image patches. To safeguard approximate balance of the record, higher probability of patch abstraction was about the pathological part.

The parameters of the algorithm, i.e. the image patch scope, the tag patch dictionary scope, and the label patch scope were enhanced distinctly for each subtask on the authentication set and the consequence of the optimization procedure are labelled

4.6.2Parameter Optimization

Besides the parameters of the convolutional architecture, there are constraints of the anticipated model: the image patch magnitude d, the label patch extent d′, and the size of the label patch vocabulary N. These parameters were verified with a pre-optimized secure network architecture represented in Fig. 4.19, which contained of two convolutional layers, both with 24 convolutional filters of kernel magnitude 5 × 5, and two mean-pooling layers in broken order.

The values certain for following experimentations are highlighted in charts with a red vertical line.

Image patch size

The human brain tumor type containing MRI image patch size of let's suppose d is a significant parameter since the segmented structures have dissimilar sizes and therefore less or more data is essential for the label structure forecast. Figure 4.6.2 demonstrations the Dice total standards for dissimilar patch sizes with their finest label patch size. Rendering to the charts, d = 8 was selected for the lively part segmentation and d = 24 for the segmentation of central tumor and entire tumor. All three tests were done for N = 32, which giving to the earlier tests is adequately enough for all patch sizes. The best outcome were in all cases realized for $d' \geq 1/2d$. The values particular for following experiments are specified by a red vertical line.

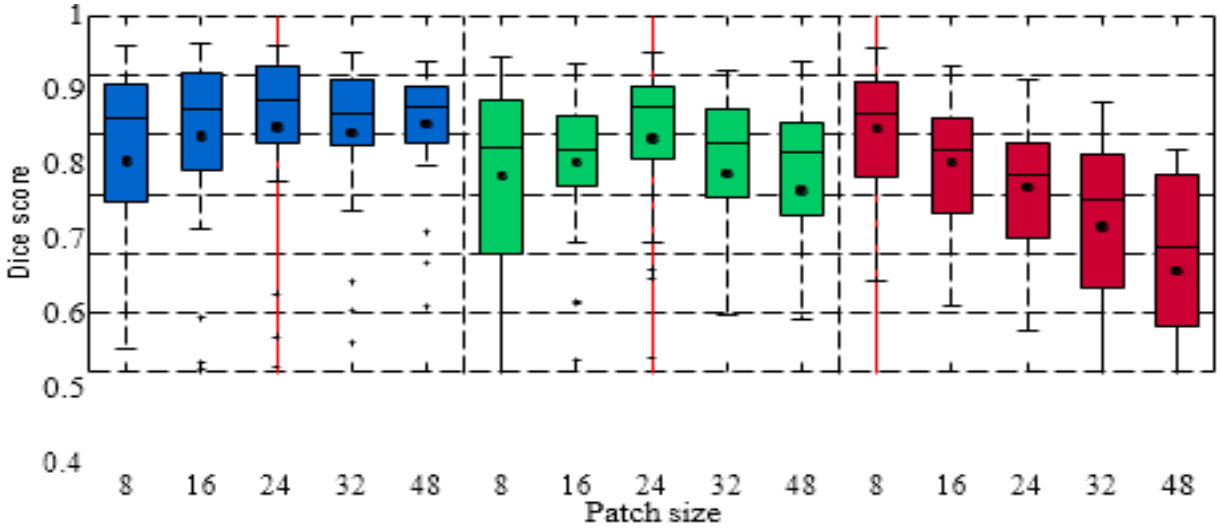

Fig. 4.5: Dice total as the size function of the human brain tumor digital 2D image patch size d with its finest tag patch size is d′ as well and the label patch vocabulary size for the image is N = 32 for entire human brain tumor is shown in the figure with blue color, central tumor is shown as the green color and lively tumor shown as in red color.

Size of the Label Patch Dictionary

The size of the label patch dictionary N effects alterations between each label template t as well as the changes between fitting image patches x in each collections n. Outcome for numerous values of are shown in Fig. 4.6.2. Normally the best outcome were attained for N = 16. The outcome were assessed in similar way as in the earlier test, i.e. The best d′ is used for all value of N. The values particular for subsequent tests are indicated by a red vertical line.

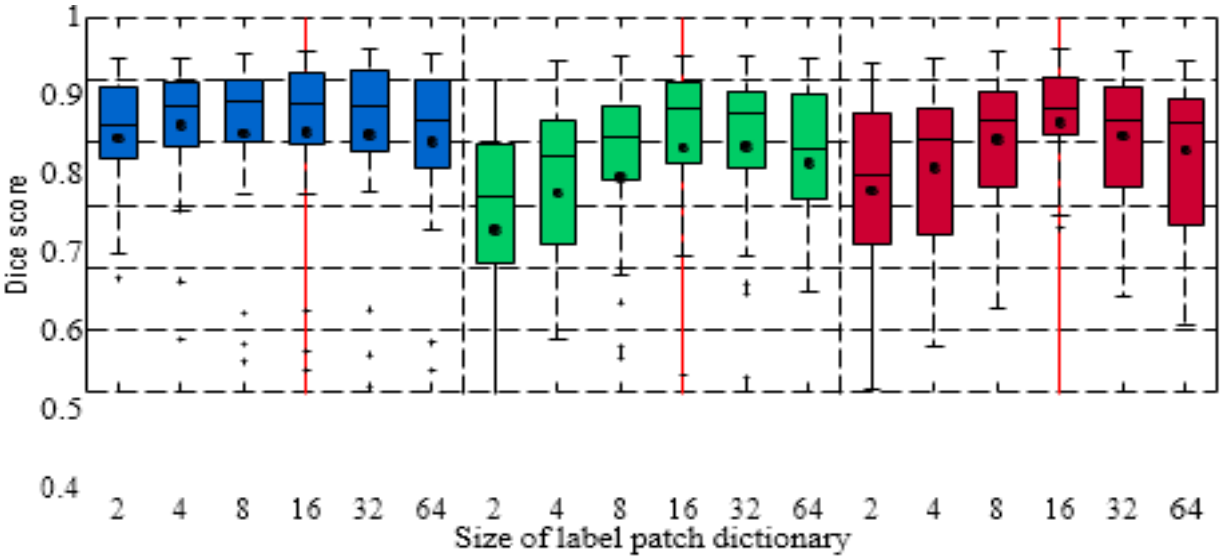

Fig. 4.6: Dice score as a function of the tag patch dictionary size using the optima of Fig. 4.6.2: d = 24 for entire tumor (blue), d = 24 for central tumor (green),
d = 8 for lively tumor (red).

Label patch size

The label patch size d′ effects the size of structure forecast as well as the number of forecasts for each voxel. Figure 4.6.2 shows the growing performance with growing d′. The values designated for following tests are indicated by a red vertical line.

2D versus 3D

Together the triplanar and 2.5D deep learning DL technique or methods for 3-D data segmentation processed as anticipated in [83] and [102], correspondingly, were tested and associated to the single slice-wise segmentation method. It was discovered that both tactics even reduced the performance of the planned scheme by 2% and 5%, individually

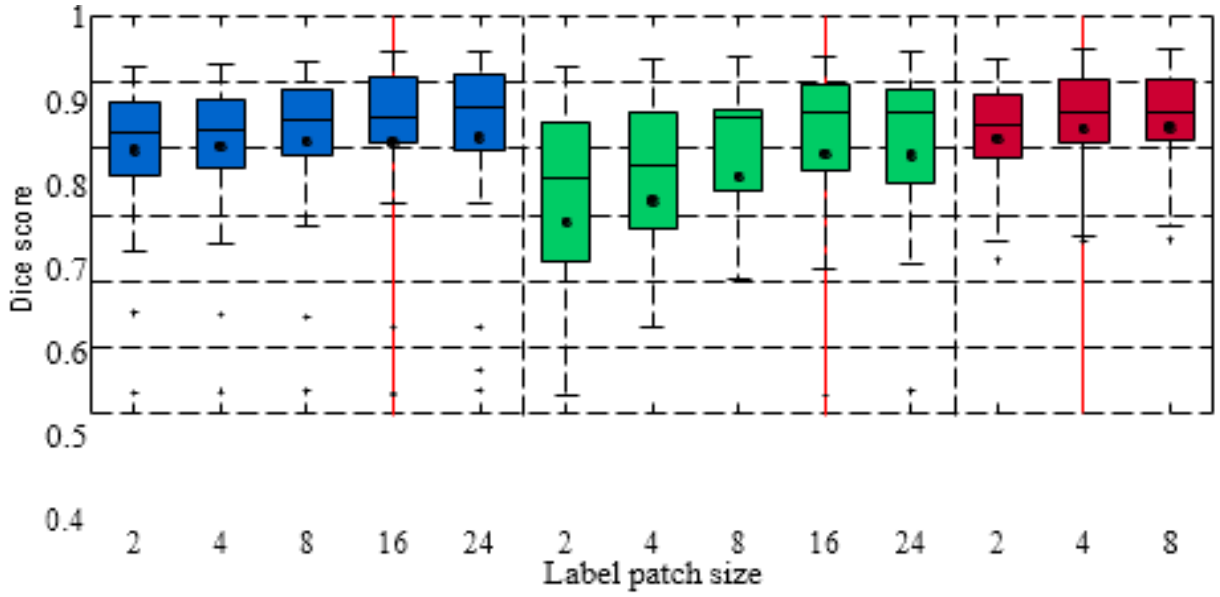

Fig. 4.7: Dice spot as a function of the tag patch size d′ for entire human brain tumor shown in the blue color with d = 24, central tumor shown in the green color with d = 24, and lively tumor presented in red color with d = 8, with tag patch vocabulary size N = 16.

4.6.3Application to the test set

After the optimization of the restrictions using the validation set, the algorithm was verified on a new set of 66 topics arbitrarily chosen from BRATS 2014. The presentation for both authentication and test set of all three segmented structures is shortened in Table. 4.22. For the test set, the achieved normal Dice scores are 83% (entire tumor), 75% (central tumor), and 77% (lively tumor).

Table. 4.22: Segmentation outcome on authentication and test data sets, reporting regular and median Dice scores. Revealed are the outcome for all three segmented structures, i.e., entire tumor, central tumor and lively tumor. Scores for lively tumor are considered for high-grade cases only. “std” and “mad” signify normal deviation and median absolute deviance. HG and LG stand for high- and low-grade gliomas, separately.

Table 4.22

Dice Score	Whole	HG/LG	Core	HG/LG	Active
ılidation set					
me.a.n o	81•15	80•1 I 85•06	79013	85•0 I 65•15	81•11
me-dian omad	86•06	86•0 I 85•05	85•06	85•0 I 73•10	83•08
Test set					
1ne.an o Ms!	83013	86•0 I 76•2I	75•20	79•1 I 61•29	77•18
me-dian omad	88•04	s8•o I 87•05	83•08	82•0 I 72•14	83•09

Table 4.23 and 4.24 review accuracy and sensitivity of the projected algorithm for all three segmented structures. As it can be resulting from the outcome in these two table, the process

has higher sensitivity than exactness for the complete tumor region, which incomes that there are less false negatives than false positives, in other arguments the resulting area is usually superior than the true section. In average, 89% of the entire tumor part is branded as pathological, while 81% of the resulting zone is truly pathological. For central tumor and lively tumor, the state is contradictory. High standards of accuracy demonstration that high fraction of voxels labeled as tumorous were designated as tumorous by skilled too, i.e. 87% for central tumor and 85% for lively tumor in regular. However, the standards of sensitivity are lower, particularly for central tumor in case of low-grade gliomas. This means that there are less false positives than false negatives. In other arguments, the subsequent area is slighter than the region designated manually by a skilled.

Table. 4.23: Segmentation outcome on validation and test data sets, reporting regular and median accuracy. Revealed are the outcome for all three segmented structures, i.e., entire tumor, central tumor and lively tumor. Totals for lively tumor are calculated for high-grade cases only. “std” and “mad” signify standard deviation and median absolute deviance. HG and LG stand for high- and low-grade gliomas, separately.

Table 4.23

Precision (in %)	Whole	HG/LG	Core	HG/LG	**.. ctive**
Validarion set					
1ne.an o Ms!	78•16	77•1 I 81•07	92•06	91•0 I 93•03	90•10
1ne-diano 1nad	84•08	83•0 I 84•08	93003	93•0 I 92•01	92•04
Test set					
me.a.n o	81•16	83•1 I 71•25	87013	88•1 I 86•12	85•18
1ne-diano 1nad	86•04	87•0 I 82•07	92•04	92•0 I 89•09	91•05

The examples of digital image segmentations procedure created by the anticipated system and corresponding the manual segmentations procedure of 2D human brains digital image for processing for the three segmented image brain structures on illustrative test cases are revealed in Fig. 4.8.

Compute time vs. correctness

The opportunity of subsampling the volume in order to diminish the computational stresses was verified here. The trade-off between accuracy and calculating time per volume is examined in Table. 4.25 By running numerous experiments with dissimilar resolves of the CNN output before final calculation of the local structure (fi column). Table. 4.24: Segmentation outcome on authentication and test data sets, reporting regular and median sensitivity. Revealed are the outcome for all three segmented structures, i.e., entire tumor, central tumor and lively tumor. Marks for lively tumor are intended for high-grade cases only. std and mad signify standard deviation and median complete deviance. HG and LG stand for high- and low-grade gliomas, correspondingly.

Table 4.25

Sensitivity (in %)	Whole	HG/LG	Core	HG/LG	Active
Validarion set					
1ne.an o Ms!	87•10	84•1 I 93•04	58•26	66•2 / 35025	71•17
1ne-diano 1nad	89•06	88•0 I 95•02	66•17	71•1 I 25•11	73012
Test set					
me.a.n o	89•09	89•0 I 89•08	66•24	71•2 I 47•27	72•23
1ne-diano 1nad	92•03	9200 I 90•06	71•16	78•1 I 53•17	80•12

i.e., subsampling in x and y, as well as dissimilar distances amid segmented slices (second column), i.e., subsampling in z way. All trials were run on 4- core CPU Intel Xeon E3 3.30GHz. As one can see in the counter, the state-of-the-art outcome can be realized in an order of size shorter time than in case of most approaches contributed in BRATS test. Cheers to the fast application of the CNN classification algorithm, all three structures can be segmented in the complete volume in 13 seconds without using GPU employment. Dispensation by the CNN is about 80% of the overall calculating time, while the task final labels using local structure forecast needs only 17%. The rest of the time are other processes counting exclamation?

Discussion

In this unit, it has been shown that manipulating local structure through the use of the tag patch vocabularies recovers segmentation performance over the normal approach forecasting voxel wise tags. It has also been revealed that local structure prediction can be shared with, and improves upon, typical prediction approaches, such as CNNs. When enhanced for a given segmentation problematic it also performs a spatial regularization at the local level. On the position benchmark set, the planned methodology achieved state-of-the-art presentation even without post-processing through Markov arbitrary fields which were part of most finest performing methods in the tumor segmentation test. Besides, all three structures can be take out from the total volume within only 13 seconds using CPU finding state-of-the-

Table. 4.25: Trade-off among spatial subsampling, computing time, and division accuracy. First two columns express dissimilar CNN output resolution, i.e., after subsampling in x and y, and steps among segmented portions, i.e., after subsampling in z direction.

Table 4.25

C:NN output	Slice step	Computing time	Dice Score (illl:9)		
1/4	4	19s	83	75	73
1/4	2	22s	84	75	74
1/4	⌶	74s	84	75	75
112	4	24s	83	75	74
112	2	41s	83	75	76
112	⌶	142s	84	75	76
111	4	47s	83	75	75
111	2	80s	83	75	77
111	⌶	280s	83	75	77

Art outcome is provided by the proposed algorithm that simply means, for instance, to do online informs when aiming at a communicating segmentation. The subsequent Dice scores are similar to intra-rater resemblance that had been reported for the three explanation responsibilities in the BRATS data set [80] with Dice scores 85% (entire tumor), 75% (central tumor) and 74% (lively tumor) and to the best outcome of automated segmentation algorithms with Dice notches of the top three in between 79%–82% (here: 83%) for the entire tumor division task, 65%–70% (here: 75%) for the segmentation of the central tumor area, and 58%–61% (here: 77%) for the segmentation of the lively tumor area.

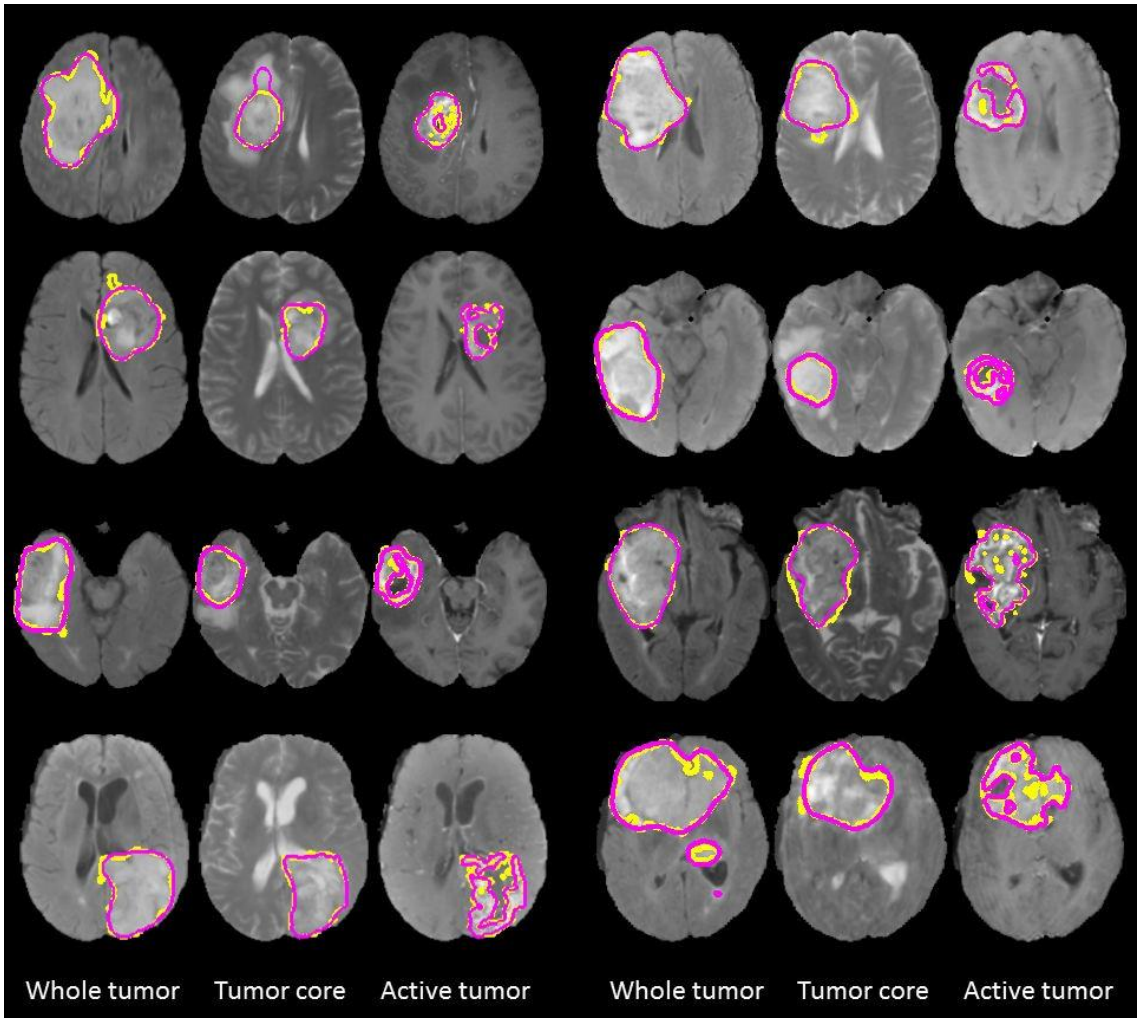

Fig. 4.8: The example of agreement skilled explanation in the yellow color in the given diagram and reflex segmentation procedure is shown in the magenta color and the size functional to the test digital 2D image data set. Each row expressions two cases. From left to right: segmentation of entire human brain tumor is shown in FLAIR images, central tumor is shown in T2w digital images and lively tumor is shown in T1contrast images.

Chapter # 5 Conclusion

Conclusion

This thesis presented numerous methodologies for brain tumor detection and segmentation in 2-D or 3-D single- and multi order MRI. The consideration was paid to high- and low-grade gliomas. Three algorithms dealing with this subject were presented. All three algorithms were verified and assessed on a large public BRATS test database of 254 3D multisequence topics. It confined co-registered and skull- stripped FLAIR, T2w, T1w and T1-contrast improved volumes with isotropic resolution 1mm. So, the work did not deal with such pre-processing stages. All data sets comprised manual explanations provided by specialists and they were used for the assessment of the planned approaches.

The first two methods sightseen the appropriateness of using prior brain anatomy information to perceive and abstract brain tumors. The first process used this data for supervised acknowledgement of a specific brain tumor structure occurrence in 2-D single and multisequence images in together stand-alone slices and portions in 3-D volume of planes anywhere the left-right regularity occurs, i.e. axial and coronal. When functional slice-wise to 3-D volumes, more data was used and higher accuracy was completed. For stand-alone multisequence slices, where only the data take out from irregularity maps was used, the recognition accuracy of each structure of size ⊙1cm2 was about 90%. When practical to the same slices with the use of Irregularity data together with image strength data, which is only valid in 3-D volume, the precision amplified to 93%. A slice was treated in only 0.11 seconds in normal, which makes it appropriate for either brain tumor finding in 3-D volumes using the slice-wise forecast tactic, or in a channel of any brain tumor segmentation procedures.

The second scheme applied similar approach to find a brain tumor in a single sequence 2-D and 3-D MRI trailed by its abstraction from a multisequence MRI in an unsupervised way. In 2-D MRI, the calculating time of the complete abstraction procedure was 0.13 seconds with grasped normal and median Dice score of 63∘30 and 77∘27, correspondingly. In 3-D, the planned scheme was able to find the tumor in less than 8 seconds and abstract it in about 13 seconds with stretched regular and median Dice score of 66∘21 and 74∘17, correspondingly. Associated to other state-of- the-art algorithms, both planned approaches are not unfair by the accuracy of the strength standardization algorithm since they are sovereign on the strength range.

The third process, focused on the division of entire tumor, central tumor, and lively tumor, presented that manipulating local structure through the use of the tag patch vocabularies better segmentation presentation over the normal methodology forecasting voxel-wise tags. It was exposed that local structure forecast can be mutual with, and recovers upon, normal forecast approaches, such as CNN. When the tag patch size is enhanced for a assumed segmentation job, it is accomplished of accumulating local sign for a given tag, and also does a spatial regularization at the local equal. The planned methodology attained state-of-the-art presentation even without classy post-processing step which are part of greatest best performance methodologies in brain tumor segmentation. Furthermore, all three structures can be take out from the complete volume within only 13 seconds using CPU procurement state-of-the-art outcome if means, for instance, to do online updates when aiming at an communicating segmentation. Most medical image statistics contain of 3-D volumes. So, one of the likely future instructions in the expansion of the local structure forecast algorithm can be an examination of natural 3-D implementation in its place of slice-wise methodology.

Bibliography

[1] Q. Ain, I. Mehmood, S. M. Naqi, et al. Bayesian Classifcation Using DCT Features for Brain Tumor Detection. In: Proc KES. 2010.
[2] A. Akselrod-Ballin, M. Galun, M. J. Gomori, et al. An Integrated Segmentation and Classifcation Approach Applied to Multiple Sclerosis Analysis. In: Proc CVPR. 2006.
[3] R. D. Ambrosini, P. Wang, and W. G. O'Dell. Computer-aided detection of metastatic brain tumors using automated three-dimensional template matching. In: J. Magn. Reson. Imaging 31 (2010), pp. 85–93.
[4] T. S. Armstrong, M. Z. Cohen, J. Weinbrg, et al. Imaging techniques in neuro oncology. In: Seminars in Oncology Nursing 20 (2004), pp. 231–239.
[5] R. Ayachi and N. B. Amor. Brain Tumor Segmentation Using Support Vector Machines. In: Symbolic and Quantitative Approaches to Reasoning with Uncertainty. 2009, pp. 736–747.
[6] S. Bauer, L. P. Nolte, and M. Reyes. Fully automatic segmentation of brain tumor images using support vector machine classifcation in combination with hierarchical conditional random feld regularization. In: Proc MICCAI. 2011, pp. 354–361.
[7] A. Bhattacharyya. On a measure of divergence between two statistical populations defned by their probability distribution. In: Bulletin of the Calcutta Mathematical Society 35 (1943), pp. 99–110.
[8] C. Bishop. Neural Networks for Pattern Recognition. Oxford University Press, 1995.
[9] A. Bleau and L. Leon. Watershed-based segmentation and region merging. In: Comput Vis Image Under 77(3) (2000), pp. 317–320.
[10] J. Bouvrie. Notes on convolutional neural networks. Tech. rep. MIT, 2006.
[11] A. Capelle, O. Alata, C. Fernandez, et al. Unsupervised segmentation for automatic detection of brain tumors in MRI. In: Proc ICIP 2000. 2000.
[12] V. Caselles, F. Catte, T. Coll, et al. A geometric model for active contours. In: Numerische Mathematik. Vol. 66. 1993, pp. 1–31.
[13] J. Cates, R. Whitaker, and J. G. Case study: an evaluation of user-assisted hierarchical watershed segmentation. In: Medical Image Analysis (2005), pp. 566–578.
96[14] J. E. Cates, A. E. Lefohn, and R. T. Whitaker. GIST: An interactive GPUbased level-set segmentation tool for 3D medical images. In: Med Image Anal 8(3) (2004), pp. 217–231.
[15] S. Chaplot, L. M. Patnaik, and N. R. Jagannathan. Classifcation of magnetic resonance brain images using wavelets as input to support vector machine and neural network. In: Biomedical Signal Processing and Control 1 (2006), pp. 86–92.
[16] L.-C. Chen, G. Papandreou, and A. Yuille. Learning a Dictionary of Shape Epitomes with Applications to Image Labeling. In: Proc ICCV 2013. 2013, pp. 337–344. doi: 10.1109/ICCV.2013.49.
[17] M. Clark, L. Hall, D. Goldgof, et al. Automatic tumor segmentation using knowledge-based techniques. In: TMI 17(2) (1998), pp. 187–201.
[18] L. Clarke. MR image segmentation using MLM and artifcial neural nets. In: Med Phys 18(30 (1991), pp. 672–682.
[19] D. Cobzas, N. Birkbeck, M. Schmidt, et al. 3D variational brain tumor segmentation using a high dimensional feature set. In: Proc ICCV 2007.

2007.
[20] J. J. Corso, E. Sharon, S. Dube, et al. Efcient Multilevel Brain Tumor Segmentation with Integrated Bayesian Model Classifcation. In: TMI 27(5) (2011), pp. 629 –640.
[21] J. J. Corso, E. Sharon, and A. Yuille. Multilevel Segmentation and Integrated Bayesian Model Classifcation with an Application to Brain Tumor Segmentation. In: Medical Image Computing and Computer Assisted Intervention. 2006, pp. 790–798.
[22] C. Cortes and V. Vapnik. Support-Vector Networks. In: Mach. Learn. 20.3 (Sept. 1995), pp. 273–297. issn: 0885-6125. doi: 10.1023/A:1022627411411. url: http://dx.doi.org/10.1023/A:1022627411411.
[23] A. Criminisi and J. Shotton. Decision Forests for Computer Vision and Medical Image Analysis. Springer, 2013.
[24] E. Dam, M. Loog, and M. Letteboer. Integrating automatic and interactive brain tumor segmentation. In: 17th International Conference on Pattern Recognition (ICPR 2004). Vol. 3. 2004, pp. 790–793.
[25] A. Davy, M. Havaei, D. Warde-Farley, et al. Brain Tumor Segmentation with Deep Neural Networks. In: Proc MICCAI-BRATS. 2014.
97[26] B. M. Dawant, S. L. Hartmann, S. Pan, et al. Brain atlas deformation in the presence of small and large space-occupying tumors. In: Comput. Aided Surg. 7(1) (2002), pp. 1–10.
[27] A. Dempster, N. Laird, and D. Rubin. Maximum Likelihood from Incomplete Data via the EM Algorithm. In: Journal of the Royal Statistical Society 39(1) (1977), pp. 1–38.
[28] S. Dickson and B. Thomas. Using neural networks to automatically detect brain tumours in MR images. In: Int J Neural Syst 4(1) (1997), pp. 91–99.
[29] P. Dollar and C. L. Zittnick. Structured Forests for Fast Edge Detection. In: Proc ICCV 2013. 2013, pp. 1841–1848.
[30] W. Dou, S. Ruan, Y. Chen, et al. A framework of fuzzy information fusion for the segmentation of brain tumor tissues on {MR} images. In: Image and Vision Computing 25.2 (2007). <ce:title>Soft Computing in Image Analysis</ce:title>, pp. 164 –171. issn: 0262-8856. doi: http://dx.doi.org/10.1016/j.imavis.2006.01.025. url: http://www.sciencedirect.com/science/article/pii/S0262885606000734.
[31] M. Droske, B. Meyer, M. Rumpf, et al. An adaptive level set method for medical image segmentation. In: Proceedings IPMI. 2001, pp. 416–422.
[32] E. Eisenhauer, P. Therasse, J. Bogaerts, et al. New response evaluation criteria in solid tumours: Revised RECIST guideline (version 1.1). In: European Journal of Cancer 45 (2) (2009), pp. 228–247.
[33] R. Farjam, H. A. Parmar, D. C. Noll, et al. An approach for computer-aided detection of brain metastases in post-Gd T1-W MRI. In: Magn. Reson. Imaging 30 (2012), pp. 824–836.
[34] C. Fennema-Notestine, I. B. Ozyurt, C. P. Clark, et al. Quantitative Evaluation of Automated Skull-Stripping Methods Applied to Contemporary and Legacy Images: Effects of Diagnosis, Bias Correction, and Slice Location. In: Human Brain Mapping 27(2) (2006), pp. 99–113.
[35] J. Festa, S. Pereira, J. A. Mariz, et al. Automatic Brain Tumor Segmentation of Multi-sequence MR images using Random Decision Forests MICCAI Grand Challenge: BRATS 2013. In: Proc MICCAI-BRATS. 2013.
[36] L. M. Fletcher-Heath, L. O. Hall, D. B. Goldgof, et al. Automatic segmentation of non-enhancing brain tumor in magnetic resonance images. In: Artifcial Intelligence in Medicine 21 (2001), pp. 43–63.

[37] V. S. Fonov, A. C. Evans, K. Botteron, et al. Unbiased average ageappropriate atlases for pediatric studies. In: NeuroImage 54(1) (2011).
98[38] B. J. Frey and D. Dueck. Clustering by Passing Messages Between Data Points. In: Science 315 (2007), pp. 972–976. url: www.psi.toronto.edu/affinitypropagation.
[39] C. Garcia and J. Moreno. Kernel based method for segmentation and modeling of magnetic resonance images. In: LNCS, 3315. 2004, pp. 636–645.
[40] E. Geremia, O. Clatz, B. H. Menze, et al. Spatial Decision Forests for MS Lesion Segmentation in Multi-Channel Magnetic Resonance Images. In: Neuroimage 57(2) (2011), pp. 378–390.
[41] E. Geremia, D. Zikic, O. Clatz, et al. Decision Forests for Computer Vision and Medical Image Analysis Advances in Computer Vision and Pattern Recognition. In: Springer, 2013. Chap. Classifcation Forests for Semantic Segmentation of Brain Lesions in Multi-channel MRI, pp. 245–260.
[42] E. Geremia, B. H. Menze, and N. Ayache. SPATIALLY ADAPTIVE RANDOM FORESTS. In: Proc ISBI. 2013.
[43] D. T. Gering. Recognizing Deviations from Normalcy for Brain Tumor Segmentation. PhD thesis. Massachusetts Institute of Technology, 2003.
[44] P Gibbs, D. L. Buckley, S. J. Blackband, et al. Tumour volume determination from MR images by morphological segmentation. In: Physics in Medicine and Biology 41 (1996), pp. 2437–2446.
[45] M. Goetz, C. Weber, J. Bloecher, et al. Extremely randomized trees based brain tumor segmentation. In: Proc MICCAI-BRATS 2014. 2014.
[46] M. Havaei, A. Davy, D. Warde-Farley, et al. Brain Tumor Segmentation with Deep Neural Networks. In: (2015), pp. 1–29.
[47] M. Havaei, P.-M. Jodoin, and H. Larochelle. Efcient interactive brain tumor segmentation as within-brain kNN classifcation. In: Proc ICPR. 2014.
[48] S. Ho, E. Bullitt, and G. Gerig. Level-Set Evolution with Region Competition: Automatic 3-D Segmentation of Brain Tumors. In: Proc ICPR.
ICPR '02. Washington, DC, USA: IEEE Computer Society, 2002, pp. 10532–.
isbn: 0-7695-1695-X. url: http://dl.acm.org/citation.cfm?id=839290.
842671.
[49] C.-W. Hsu and C.-J. Lin. A comparison of methods for multiclass support vector machines. In: Neural Networks, IEEE Transactions on 13(2) (2002), pp. 415–425.
[50] J. E. Iglesias, E. Konukoglu, D. Zikic, et al. Is Synthesizing MRI Contrast Useful for Inter-modality Analysis? In: Proc MICCAI 2013. 2013, pp. 631–638.
99[51] A. Islam, S. M. S. Reza, and K. M. Iftekharuddin. Multifractal Texture Estimation for Detection and Segmentation of Brain Tumors. In: IEEE Trans Biomed Eng. 60 (11) (2013), pp. 3204–3215.
[52] M. Kaleem, M. Sanaullah, M. A. Hussain, et al. Segmentation of Brain Tumor Tissue Using Marker Controlled Watershed Transform Method. In: Emerging Trends and Applications in Information Communication Technologies. Vol. 281. 2012, pp. 222–227.
[53] M. R. Kaus, S. K. Warfeld, A. Nabavi, et al. Segmentation of meningiomas and low grade gliomas in MRI. In: Proc MICCAI. 1999, pp. 1–10.
[54] M. R. Kaus, S. K. Warfeld, A. Nabavi, et al. Automated Segmentation of MR Images of Brain Tumors. In: Radiology 218(2) (2001), pp. 586–591.
[55] N. E. A. Khalid, S. Ibrahim, and P. N. M. M. Haniff. MRI Brain Abnormalities Segmentation usingK-Nearest Neighbors. In: International Journal on Computer Science and Engineering 3(2) (2011), pp. 980–990.

[56] O. Khotanlou H. Colliot and I. Bloch. Automatic brain tumor segmentation using symmetry analysis and deformable models. In: Conf. on Advances in Pattern Recognition ICAPR, Kolkata, India, (2007).
[57] J. Kong, J. Wang, Y. Lu, et al. . A novel approach for segmentation of MRI brain image. In: IEEE MELECON (2006), pp. 525–528.
[58] P. Kontschieder, S. Rota Bulo, H. Bischof, et al. Structured class-labels in random forests for semantic image labelling. In: Proc ICCV 2011. 2011, pp. 2190–2197. doi: 10.1109/ICCV.2011.6126496.
[59] P. Kontschieder, S. R. Bulo, M. Donoser, et al. Semantic Image Labelling as a Label Puzzle Game. In: Proceedings of the British Machine Vision Conference (BMVC). 2011, pp. 111.1–111.12. doi: http://dx.doi.org/10.5244/C.25.111.
[60] A. Krizhevski, I. Sutskever, and G. E. Hinton. ImageNet Classifcation with Deep Convolutional Neural Networks. In: NIPS 2012. 2012.
[61] D Kumar and A Halder. Automatic brain tumor detection and isolation of tumor cells from MRI images. In: Int J Comput Appl 39(16) (2012), pp. 26–30.
[62] S. K. Kyriacou, C. Davatzikos, S. J. Zinreich, et al. Nonlinear Elastic Registration of Brain Images with Tumor Pathology Using a Biomechanical Model. In: TMI 18(7) (1999), pp. 580–592.
100[63] S. Lakare. 3D segmentation techniques for medical volumes. , state university of NY; 2000. Stony Brooks: Center of Visual Computer, State university of NY, 200.
[64] A. Law, F. Lam, and F. Chan. A fast deformable region model for brain tumor boundary extraction. In: Int Conf EMBS. Vol. 2. 2002, pp. 1055–1056.
[65] Y. LeCun, B. Boser, J. Denker, et al. Back-propagation applied to handwritten zip code recognition. In: Neural Computation 1(4) (1989).
[66] Y. LeCun, B. Boser, J. S. Denker, et al. Advances in neural information processing systems 2. In: Morgan Kaufmann Publishers Inc., 1990. Chap. Handwritten digit recognition with a back-propagation network, pp. 396–404.
[67] Y. LeCun and Y. Bengio. The Handbook of Brain Theory and Neural Networks. In: ed. by M. A. Arbib. Cambridge, MA, USA: MIT Press, 1998. Chap. Convolutional Networks for Images, Speech, and Time Series, pp. 255–258. isbn: 0-262-51102-9. url: http://dl.acm.org/citation.cfm?id=303568.303704.
[68] C. Lee, S. Wang, A. Murtha, et al. Segmenting brain tumors using pseudoconditional random felds. In: Proc MICCAI 2008. 2008.
[69] A. Lefohn, J. Cates, and R. Whitaker. Interactive GPU-based level sets for 3D brain tumor segmentation. Tech. rep. University of Utah, 2003.
[70] M. Letteboer, O. Olsen, E. Dam, et al. Segmentation of tumors in magnetic resonance brain images using an interactive multiscale watershed algorithm. In: Academic Radiology 11(10) (2004), pp. 1125–1138.
[71] S. Liao, Y. Gao, A. Oto, et al. Representation Learning: A Unifed Deep Learning Framework for Automatic Prostate MR Segmentation. In: Proc MICCAI 2013. 2013, pp. 254–261.
[72] Y. Liu, R. T. Collins, and W. E. Rothfus. Robust midsagittal plane extraction from normal and pathological 3-D neuroradiology image. In: IEEE Transactions on Medical Imaging 20(3) (2003), pp. 175–192.
[73] S. Luo. Automated medical image segmentation using a new deformable surface model. In: Int J Comput Sci Netw Secur 6(5A) (2006), pp. 109–115.
[74] S. Luo, R. Li, and S. Ourselin. A new deformable model using dynamic

gradient vector flow and adaptive balloon forces. In: APRS Workshop on Dig Image Comp. 2003, pp. 9–14.
101[75] M. Mancas and B. Gosselin. Toward an automatic tumor segmentation using iterative watersheds. In: Medical Imaging 2004: Image Processing (SPIE2004). Vol. 5370. 2004, pp. 1598–1608.
[76] D. Mattes, D. R. Haynor, H. Vesselle, et al. Nonrigid multimodality image registration. In: Medical Imaging 2001: Image Processing (2001), pp. 1609–1620.
[77] T. McInerney and D. Terzopoulos. Deformable models in medical image analysis: a survey. In: Med. Image. Anal. 1 (1996), pp. 91–108.
[78] R. Meier, S. Bauer, J. Slotboom, et al. A Hybrid Model for Multimodal Brain Tumor Segmentation. In: Proc MICCAI-BRATS 2013. 2013.
[79] R. Meier, S. Bauer, J. Slotboom, et al. Appearance- and Context-sensitive Features for Brain Tumor Segmentation. In: Proceedings MICCAI-BRATS 2014. 2014.
[80] B. Menze, A. Jakab, S. Bauer, et al. The Multimodal Brain Tumor Image Segmentation Benchmark (BRATS). In: IEEE Transactions on Medical Imaging (2014), p. 33. doi: 10.1109/TMI.2014.2377694. url: https: //hal.inria.fr/hal-00935640.
[81] B. Menze, K. van Leemput, D. Lashkari, et al. A Generative Model for Brain Tumor Segmentation in Multi-Modal Images. English. In: Proc MICCAI 2010. 2010, pp. 151–159. isbn: 978-3-642-15744-8. doi: 10.1007/978-3-642-15745-5_19. url: http://dx.doi.org/10.1007/978-3-642-15745-5_19.
[82] B. H. Menze, K. V. Leemput, A. Honkela, et al. A Generative Approach for Image-Based Modeling of Tumor Growth. In: Proc MICCAI 2011. 2011, pp. 735–747.
[83] J. Mikulka and E. Gescheidtova. An Improved Segmentation of Brain Tumor, Edema and Necrosis. In: Progress in Electromagnetics Research Symposium. 2013, pp. 25–28.
[84] N. Moon, E. Bullitt, K. van Leemput, et al. Model-Based Brain and Tumor Segmentation. In: Proc ICPR 2002. 2002.
[85] S. Murugavalli and V. Rajamani. An improved implementation of brain tumor detection using segmentation based on neuro fuzzy technique. In: J Comput Sci 3(110 (2007), pp. 841–846.
102[86] N. Otsu. A Threshold Selection Method from Gray-Level Histograms. In: IEEE Transactions on Systems, Man and Cybernetics 9.1 (1979), pp. 62–66. doi: 10.1109/TSMC.1979.4310076. url: http://dx.doi.org/10.1109/TSMC.1979.4310076.
[87] M. Ozkan, B. Dawant, and R. Maciunas. Neural-network-based segmentation of multi-modal medical images: a comparative and prospective study. In: TMI 12(3) (1993), pp. 534–544.
[88] W. Phillips, R. Velthuizen, S. Phupanich, et al. Application of fuzzy Cmeans segmentation technique for tissue differentiation in MR images of a hemorrhagic glioblastoma multiforme. In: Magn Reson Imag 13(20 (1995), pp. 277–290.
[89] P. H. O. Pinheiro and R. Collobert. Recurrent Convolutional Neural Networks for Scene Labeling. In: International Conference on Machine Learning (ICML). 2014.
[90] A. Pinto, S. Pereira, H. Dinis, et al. Random decision forests for automatic brain tumor segmentation on multi-modal MRI images. In: Proc ENBENG 2015. 2015.
[91] K. M. Pohl, S. Bouix, M. Nakamura, et al. A Hierarchical Algorithm for

MR Brain Image Parcellation. In: TMI 26(9) (2007), pp. 1201–1212.
[92] K. Popuri, D. Cobzas, M. Jagersand, et al. 3D variational brain tumor segmentation on a clustered feature set. In: SPIE Med Imaging. 2009.
[93] A. Prasoon, K. Petersen, C. Igel, et al. Deep feature learning for knee cartilage segmentation using a triplanar convolutional neural network. In: MICCAI. 2013, pp. 246–253.
[94] M. Prastawa, E. Bullitt, S. Ho, et al. A brain tumor segmentation framework based on outlier detection. In: Med Image Anal 8 (2004), pp. 275–283.
[95] M. Prastawa, E. Bullitt, N. Moon, et al. Automatic Brain Tumor Segmentation by Subject Specifc Modifcation of Atlas Priors. In: Academic Radiology 10 (12) (2003), pp. 1341–1348.
[96] F. Prior, S. J. Fouke, T. Benzinger, et al. Predicting a multi-parametric probability map of active tumor extent using random forests. In: Proc EMBC 2013. 2013.
[97] W. Reddick, J. Glass, E. Cook, et al. Automated segmentation and classifcation of multispectral magnetic resonance images of brain using artifcial neural networks. In: TMI 16(6) (1997), pp. 911–918.
103[98] J Rexilius, H Hahn, J Klein, et al. Multispectral brain tumor segmentation based on histogram model adaptation. In: SPIE Conf Med Image Comp. 2007.
[99] S. Reza and K. M. Iftekharuddin. Multi-class Abnormal Brain Tissue Segmentation Using Texture Features. In: Proc MICCAI-BRATS 2013. 2013.
[100] S. Reza and K. M. Iftekharuddin. Multi-fractal texture features for brain tumor and edema segmentation. In: Proc SPIE Medical Imaging 2014. 2014.
[101] H. R. Roth, L. Lu, A. Seff, et al. A new 2.5D representation for lymph node detection using random sets of deep convolutional neural network observations. In: MICCAI 2014, Part I. 2014, pp. 520–527.
[102] S. Ruan, S. Lebonvallet, A. Merabet, et al. Tumor segmentation from a multispectral MRI images by using support vector machine classifcation. In: Proc ISBI. 2007, pp. 1236–1239.
[103] G. C. S. Ruppert, L. Teverovskiy, C. Yu, et al. A New Symmetry-based Method for Mid-sagittal Plane Extraction in Neuroimages. In: International Symposium on Biomedical Imaging: From Macro to Nano. 2011.
[104] B. N. Saha, N. Ray, R. Greiner, et al. Quick detection of brain tumors and edemas: A bounding box method using symmetry. In: Computerized Medical Imaging and Graphics 36.2 (2012), pp. 95 –107. issn: 0895-6111. doi: http://dx.doi.org/10.1016/j.compmedimag.2011.06.001. url: http: //www.sciencedirect.com/science/article/pii/S0895611111000796.
[105] Y Salman. Modifed technique for volumetric brain tumor measurements. In: J Biomed Sci Eng 2 (2009), pp. 16–19.
[106] Y. Salman and A. Badawi. Validation techniques for quantitative brain tumor measurements. In: Int Conf IEEE EMBS. 2005, pp. 7048–7051.
[107] Y. Salman, A. Badawi, M. Assal, et al. New automatic technique for tracking brain tumor response. In: 2005, pp. 1–4.
[108] M Sato, S Lakare, M Wan, et al. A gradient magnitude based region growing algorithm for accurate segmentation. In: Int Conf Image Process. 2000, pp. 448–451.
[109] K. Shanthi and M. Kumar. Skull stripping and automatic segmentation of brain MRI using seed growth and threshold techniques. In: Intelligent and Advanced Systems, 2007. ICIAS 2007. International Conference on. 2007, pp. 422–426. doi: 10.1109/ICIAS.2007.4658421.
104[110] E. Sharon, A. Brandt, and R. Basri. Segmentation and boundary detection using multiscale intensity measurements. In: Proc CVPR. 2001, pp. 469–

476.
[111] S. Shen, W. A. Sandham, and M. H. Granat. Preprocessing and segmentation of brain magnetic resonance images. In: IEEE Conf. on Information Technology Applications in Biomedicine. 2003, pp. 149–152.
[112] F. Y. Shih and S. Cheng. Automatic seeded region growing for color image segmentation. In: Image and Vision Computing 23.10 (2005), pp. 877 –886. issn: 0262-8856. doi: http://dx.doi.org/10.1016/j.imavis.2005.05.015. url: http://www.sciencedirect.com/science/article/pii/S0262885605000673.
[113] P. P. Singhai and S. A. Ladhake. Brain Tumor Detection Using Marker Based Watershed Segmentation from Digital MR Images. In: International Journal of Innovative Technology and Exploring Engineering 2(5) (2013), pp. 201–204.
[114] J. Solomon, J. A. Butman, and A. Sood. Segmentation of brain tumors in 4D MR images using the hidden Markov model. In: Computer Methods and Programs in Biomedicine 84 (2006), pp. 76–85.
[115] A. Stadlbauer, E. Moser, S. Gruber, et al. Improved delineation of brain tumors: an automated method for segmentation based on pathologic changes of 1H-MRSI metabolites in gliomas. In: NeuroImage 23.2 (2004), pp. 454 –461. issn: 1053-8119. doi: http://dx.doi.org/10.1016/j.neuroimage.2004.06.022. url: http://www.sciencedirect.com/science/article/pii/S1053811904003313.
[116] R. Stupp, W. Mason, M. van den Bent, et al. Radiotherapy plus concomitant and adjuvant temozolomide for glioblastoma. In: New England Journal of Medicine 352(10) (2005), pp. 987–996.
[117] L. Szilagyi, S. Szilagyi, and Z. Benyo. A modifed fuzzy C-means algorithm for MR brain image segmentation. In: Image Analysis and Recognition. 2007.
[118] S. Taheri, S. Ong, and V. Chong. Level-set segmentation of brain tumors using a threshold-based speed function. In: Image and Vision Computing 28(1) (2010), pp. 26–37.
[119] K. Thapaliya, J.-Y. Pyun, C.-S. Park, et al. Level set method with automatic selective local statistics for brain tumor segmentation in MR images. In: Computerized Medical Imaging and Graphics 37 (2013), pp. 522–537.
105[120] T. Tong, R. Wolz, P. Coupe, et al. Segmentation of MR images via discriminative dictionary learning and sparse coding: Application to hippocampus labeling. In: NeuroImage 76 (2013), pp. 11–23.
[121] N. Tustison, B. Avants, P. Cook, et al. N4ITK: Improved N3 Bias Correction with Robust B-Spline Approximation. In: Proc. of ISBI. 2010.
[122] G. Urban, M. Bendszus, F. Hamprecht, et al. Multi-modal brain tumor segmentation using deep convolutional neural networks. In: Proc MICCAIBRATS. 2014, pp. 31–35.
[123] C. Vijayakumar, G. Damayanti, R. Pant, et al. Segmentation and grading of brain tumors on apparent diffusion coefcient images using self-organizing maps. In: Comput Med Imaging Graph 31 (2007), pp. 473–484.
[124] F. Vincent, H. Chong, J. Zhou, et al. Tongue carcinoma: tumor volume measurement. In: International Journal of Radiation Oncology, Biology, Physics 59(1) (2004), pp. 59–66.
[125] S. Vinitski, T. Iwanaga, C. Gonzalez, et al. Fast tissue segmentation based on a 4D feature map: Preliminary results. In: Proc ICIAP. 1997, pp. 445–452.
[126] T. Wang, I. Cheng, and A. Basu. Fully automatic brain tumor segmentation using a normalized Gaussian Bayesian Classifer and 3D Fluid Vector Flow.

In: Proc ICIP. 2010, pp. 2553–2556.
[127] T. Weglinski and A. Fabijanska. Brain tumor segmentation from MRI data sets using region growing approach. In: Perspective Technologies and Methods in MEMS Design (MEMSTECH), 2011 Proceedings of VIIth International Conference on. 2011, pp. 185–188.
[128] C. Xu, D. L. Pham, and J. L. Prince. Handbook of Medical Imaging. In: SPIE Press, 2000. Chap. Medical Image Segmentation Using Deformable Models: Medical Image Processing and Analysis, pp. 129–174.
[129] J. G. Zhang, K. K. Ma, M. H. Er, et al. Tumor segmentation from magnetic resonance imaging by learning via one-class support vector machine. In: Proc IWAIT 2004. 2004.
[130] N. Zhang. Feature Selection based Segmentation of Multi-Source Images: Application to Brain Tumor Segmentation in Multi-Sequence MRI. PhD thesis. INSA de Lyon, 2011.
[131] N. Zhang, S. Ruan, S. Lebonvallet, et al. Multi-kernel SVM based classifcation for brain tumor segmentation of MRI multi-sequence. In: Proc ICIP. 2009.
[133] L. Zhao, W. Wu, and J. J.Corso. Brain tumor segmentation based on GMM and active contour method with a model-aware edge map. In: Proc BRATS 2012. 2012.
[134] L. Zhu, Y. Chen, Y. Lin, et al. Recursive Segmentation and Recognition Templates for 2D Parsing. In: NIPS. 2009, pp. 1985–1992.
[135] L. Zhu, Y. Chen, Y. Lin, et al. Recursive segmentation and recognition